University of Zurich[UZH]

Multi-Method Investigation of the Hydrological and Glaciological System of Griess Glacier on Klausenpass

GEO 511 Master's Thesis

Author
Andrin Livio Hauser
18-116-897

Supervised by
Dr. Martin Lüthi
Boris Ouvry

Faculty representative
Prof. Dr. Andreas Vieli

31.01.2024
Department of Geography, University of Zurich

Table of contents

List of tables

List of figures

Abstract

Background: As glaciers are melting in times of climate change, future water availability management is part and parcel of today's challenges not only for the Alpine communities but also for the lowlands, which depend on the water from the mountains. The valley of Klausenpass and Urnerboden, the largest mountain pasture of Switzerland, is characterized by large karstic aquifers in the limestone of the Griessstock nappe. These karst conduits are widely unexplored, and the water origins of the springs are currently unknown.

Aims: The object of this study is to gain more insight into the hydrological network and its functioning. This study also investigates how Griess Glacier and Griesssee develop and behave over the summer of 2023 and how they potentially impact the karst aquifer discharge of Urnerboden. Additionally, this study aims to find deeper knowledge about the water origins of the major springs of Urnerboden, such as Chlus and Waldhüttli.

Methods: Therefore, eight tracer studies were conducted around Klausenpass, in addition to the recording of water pressure and temperature at two different springs on Urnerboden. Furthermore, the Griess Glacier situated beneath the Clariden north wall was observed during the ablation season using ablation stakes, time-lapse photography, and drone-based aerial surveys.

Results: Griess Glacier lost 1.8±0.4 meters of ice thickness in 96 days of analysis. The positive degree day factor (PDDF) determined for the glacier is $1.82\,\frac{\mathrm{mm}}{^{\circ}\mathrm{C}*\mathrm{d}}$. The tracer studies revealed a karst aquifer connecting Chlaridenbödmeli to the Chlus spring. Surprisingly, this was the only discovered connection from the Griess basin to the Chlus spring. Furthermore, links between the Griessfirn Chammli and the Waldhüttli Waterfall, as well as between Gämschplanggen and the Waldhüttli Bach, were discovered. Additionally, a connection from the Griessloch (cave situated in the Clariden north wall) also to Waldhüttli Waterfall was exposed. Also, different general origins for the water at Chlus and Waldhüttli could be determined, as the Waldhüttli p&T logger recorded clear indications of glacier melt, while the p&T logger at Chlus displays behaviour of precipitation-fed catchments.

Conclusion & implications: Overall, the study showed that waterways do not strictly follow the surface topography and can possibly be directed to another valley. Moreover, the main springs Chlus and Waldhüttli revealed information on the origins of their water supply. This has major implications for the community of Urnerboden, as the catchment of Fätschbach is larger than initially expected and more water is directed into the valley. Moreover, the generated data on Griess Glacier can be used in further studies as basis for melt and ablation modelling regarding future changes of climatic weather pattens.

1. Introduction

1.1. Motivation

Climate impacts the environment. And the climate is changing. The influence of climate change is drastically noticeable in the landscape. Climate change influences not only the climate of polar regions, but also the intermediate zones of central Europe and the tropics. And with time, the impacts of Climate change are projected to increase in severity (IPCC, 2023). For example, the cryosphere around the world is decreasing, and glaciers are showing negative mass balances (Rossini et al., 2018; WGMS, 2024). Glaciers are confirmed to be proxies for the extent estimation of global climate change (Bhardwaj et al., 2016). Glacier melt is of major importance for many Alpine valleys and Alpine forelands, especially as they store water supplies during periods with low precipitation, as it is estimated that one-sixth of the global population depends on snow and glacier melt to survive (Hock et al., 2006). The reference glaciers of the World Glacier Monitoring Service (WGMS) have lost globally on average almost -1.2 meter water equivalent (m w.e.) in 2022 compared to 2005, when the global mass balance was below -0.5 m w.e. the last time. However, this loss is dependent on the location since glaciers strongly differentiate in mass loss. For instance, Glaciers in central Europe are leading in cumulative mass change since 1950, as they have cumulatively lost on average almost 40 m w.e. (WGMS, 2024). Consequently, continuous excessive glacier mass loss will on the long-term result in water scarcity (Huss & Hock, 2018) and the increased ice melt rates around the world let the sea level rise (Zemp et al., 2019).

Monitoring glaciers is a valuable practise to keep track of their response to climate change (Haeberli et al., 2000; WGMS, 2024). The mass balance data collected worldwide is summarized and published by WGMS (2024) which classifies glaciers according to distinct melting characteristics. For example, debris covered glaciers may show reduced melt of ice (ablation) compared to a bare ice glacier. The reduced ablation is due to an insulating effect of the debris cover, given that it exceeds a certain threshold thickness (Moore, 2018; Nicholson & Benn, 2006; Østrem, 1959). The threshold for the insulating effect of the debris cover varies between glaciers but is estimated to be below 5cm of debris cover as illustrated by Østrem (1959). Scientific studies of debris covered glaciers have increased lately. A detailed examination is essential for future water availability modelling since the area of debris covered glaciers has increased globally (Herreid & Pellicciotti, 2020). Furthermore, debris cover thicknesses vary significantly between glaciers. This, in addition to elevation differences across the glacier, impacts the melting rate of the ice. In short, debris covered glaciers pose various challenges but are often studied in an oversimplified manner (Huo et al., 2021). However, one method to model debris covered glacier's ablation is to use the Positive Degree Day Factor (PDDF) according to debris cover thickness. The PDDF is derived from the measured ablation

in combination with the sum of the positive mean daily temperatures. The described method is applied frequently, previously in studies by Juen et al. (2014), Wu et al. (2011) or Mihalcea et al. (2006).

Also important for alpine ecological systems are their hydrological aspects, whether their flow paths are surface or subsurface. While surface water bodies mostly follow topography, subterranean water flow paths alter their flow direction depending on the underlying stratigraphy and geology. According to Lauber et al. (2014) “Groundwater flow and contaminant transport in karst aquifers are difficult to predict because of the unknown configuration and geometry of the conduit network. However, the sustainable use and protection of karst groundwater resources requires detailed knowledge of the underground flow paths and spring catchment areas” (Lauber et al., 2014, p. 435). A logistically easy and minimally time-consuming way to assess a subterranean water network is by the use of hydrological colour tracers (Goldscheider et al., 2008; Jeelani et al., 2017), which are non-toxic and environmentally friendly (Goldscheider et al., 2008).

1.2. Research gap

Very little is known about the catchment characteristics “Im Griess” on Klausenpass and Urnerboden. The area has neither been targeted by scientific studies in recent years nor are there any further analyses of the region. The Griess Glacier below the north wall of Clariden is the major water supplier of the Urnerboden Valley, the largest mountain pasture in Switzerland (Verkehrsverein Urnerboden, n.d.). Additionally, the glacier serves as water reservoir to its proglacial lake (Griesssee). The Griess Glacier has not been under observation for a while, even though it presents interest to glaciologists. The Griess Glacier persists at an elevation of only 2050 m. a.s.l., which is very low for Alpine glaciers. Therefore, it came to interest for Buri et al. (n.d.) in the mid-2010s. They initiated further analyses on lake development and glacier area reduction, but they never officially published their result.

Furthermore, by diverting water to Limmernsee, the discharge of Griesssee feeds the important hydroelectric power production plant of the company AXPO (Appenzeller Kalender, 1967).

The Griesssee is also of touristic importance for the Klausenpass region, as it provides several ecosystem services to the public. Ecosystem services are aspects of nature that positively influence humans or increase welfare (Johnston, 2024). It is a destination frequently visited by hikers during summer, providing recreational value and outdoor activities (Pfau, 2023). Furthermore, often during summer, little icebergs float on the water surface due to the lake’s direct connection to the glacier. Icebergs on Swiss Alpine lakes may attract a lot of daily tourists in the summer months.

The interest in a thorough investigation of the hydrological network was initiated by OGH member (Ostschweizerische Gesellschaft für Höhlenforschung) Yvo Weidmann. He found

remains of detonated army grenades and ammunition deep within the Chlus cave. These unexpected findings lead to the question how these artifacts reached the cave, since it is not possible for them to have entered from the Chlus spring entrance below. There are three siphons between the entrance and the finding place (Weidmann, n.d.). This concludes that there must be an unknown connection from the area above to the Chlus cave, which lies indeed directly underneath the lake and the Griess Glacier.

1.3. Aim and research questions

The aim of this master's thesis is to document, investigate, and analyse the Griess Glacier at Klausenpass as well as the lake development of Griesssee over the course of the summer of 2023. Further, this study seeks to provide insight into the catchment, which is characterized by the debris covered Griess Glacier, the proglacial Griesssee and a wide-ranging karst network. This will help to further understand the system's processes and make inferences for future water availability in the area.

In this study, several different glaciological and physical measuring techniques are applied, as well as several hydrological parameters like temperature, tracer concentrations and water flow are measured.

This thesis is divided into a glaciological and hydrological part, which leads to two categories of research questions. The goal for the glaciological part is to gain knowledge about the following characteristics of the glacier:

RQ 1. How will the glacier surface develop over the course of the melting season?

RQ 2. Is the ice still moving, or did it come to a halt? How does it differ between the eastern and western side of the glacier?

RQ 3. What is the PDDF of the glacier in the melting season 2023?

The research questions for the hydrological section are of different interest. They will rely on various experimental techniques as well as half year timeseries of distinctive basic water flow characteristics:

RQ 4. Do the lake's area and surface height vary over the course of the summer?

RQ 5. Can all water sinks be traced to a source and all sources to a sink?

RQ 6. Do some tracers vanish or lead to a spring in an unexpected location, for example another valley?

RQ 7. Where is the lake discharge water channelled through, and where is the underground drainage system of the lake?

RQ 8. For how long is the snow and ice melt observable in the water pressure and temperature data?

RQ 9. How much of the discharge is rainwater, snow, and ice?

RQ 10. How strong are the daily variations in the area of interest?

RQ 11. How long does it take for the water to flow through the karst system?

RQ 12. Where are the possible entrances to the cave system for the ammunition remainders and is the Chlus connected to the Griess Basin, which used to be a practise target for the Swiss Army?

By addressing these research questions, it is aimed to fill existing gaps in knowledge and advance the understanding of the hydrological network of Klausenpass and Urnerboden. From these research questions the following hypotheses are put forward:

H 1. The glacier still shows measurable signs of downward movement.

H 2. Most of the water discharge takes place underground through the karst conduits.

H 3. Lake formation has changed the area's hydrological functioning by making the karst system more accessible for discharged water.

H 4. The lake water has several outflows leading to different springs on both sides of the Klausenpass.

H 5. The Griess basin drains to Urnerboden, as surface topography and geological stratigraphy suggest

2. Scientific background:

In this chapter, several important topics are concisely explained and discussed. This specific information is necessary to fully comprehend the concepts applied in this study.

2.1. Terminology

For illustrative purposes, some major terms are explained here. Furthermore, geographical locations are referred to in the same way as in the local language for example ‘Griesssee’ or ‘Griessseeli’ instead of Lake Griess.

Table 1: Commonly used names and abbreviations are put to display for better understanding.

Names of the lake	Griesssee, Griessseeli, Griesslisee, Claridensee,Glacier lake
Names of the glacier	Griess Glacier, Clariden Nordfirn
PDD	Positive Degree Days
PDDF	Positive Degree Days Factor
DEM	Digital Elevation Model
Uranine, Ur	Yellowish-green water tracer colour
Rhodamine WT, Rh	Red water tracer colour (WT = Water Tracer)

2.2. Karst landscape and cave formation

Karst landscapes are characterized by subterranean water flow within soluble rock strata. Karst systems are bound to occur in limestone but may additionally also appear in dolomites (Zepp, 2011). Naturally occurring chemical reactions are corroding the limestone and dissolve the calcium-rich rocks to calcium and hydrogen carbonate-ions (Zepp, 2011).

There are several unique structures indicating the presence of a karst system. Karren or dolines on smaller, and poljes on larger scales are exemplary features characterizing the geomorphology of karst landscape (Zepp, 2011). A constant discharge and depth drainage are necessary to form these iconic features. Therefore, karst systems are always elevated above the general groundwater level (Zepp, 2011). Water permeable cracks and fissures enable water movement along the rock strata. The karstification is initiated by the extension of said cracks, fissures, and the resulting water flow. Without the latter, the water would stay in the rocks, locally developing limestone-saturated solutions, which would inhibit further corrosion of the limestone. Thus, the diversion of saturated water enables continuous dissolution processes along the waterways (Zepp, 2011). Despite the predisposition of mountains for gravitational water flow and by extension for optimal conditions for karst system development, the alpine conditions are not particularly in favour of such developments. The climatic differences between the lowlands and the alpine environments lead to lower denudation rates and slower development of karst

systems (Gunn, 2003). An exception are karst networks possessing substantially higher run-off or additional sources of acid, promoting increased dissolution rates (Gunn, 2003).

Karst springs are directly linked to the cave systems and therefore provide quick access to water discharge. Thus, the resurgences react strongly to variation in subterranean flow. Karst networks display instant reactions to changes in discharge and show for example less delay during dry phases (Zepp, 2011). Additionally, strong climatic gradients prevail in the alpine environment. On average, the temperature in mountainous areas drops by 6° Celsius per kilometre of altitude increase. Furthermore, mountain ranges capture a surplus of precipitation since they build an orographic barrier, a large part of which is snow (Gunn, 2003).

2.3. Glacier lakes

A proglacial lake is defined as a lake which either has physical contact with the ice, is fully detached or right beyond the current ice margin. These lakes are of major importance for trapping meltwater and glacial sediments and preventing their transportation to the proglacial zones as well as further down to the lowlands. They are commonly dammed by moraine or landslide debris, ice or bedrock. Proglacial lakes control glacier ice dynamics in several different ways. Among others, they raise the water table and temperature, promote floatation and calving of the terminus, may intensify ice flexures and fractures by quick filling and draining. Hence, a proglacial lake impacts the stress balance of a glacier, which influences mass balance and ice velocity. Additionally, the lakes hold a greater heat capacity than the surrounding land due to their ability to absorb during summer and reflect short-wave solar radiation in winter when frozen. Therefore, leading to a cooling effect on the air temperature in summer and a warming effect during fall (Carrivick & Tweed, 2013).

Glacier lakes also play an important role in storing water during warmer periods. Glacier-fed lakes in the alps delay the release of meltwater and sustain lowland farmers with water for irrigation. This water supply becomes crucial when there is insufficient precipitation to provide the necessary water to dependent communities as glaciers modulate the discharge seasonally (Biemans et al., 2019).

2.4. Debris covered glaciers

Debris covered glaciers are glaciers in alpine environments partially or for a major part covered by rock debris. The debris cover influences the albedo of the glacier surface and therefore modulates the mass balance of the glacier. When the debris cover is less than a few centimetres, the debris gets warmed by the sun and transfers more heat into the ice, therefore increasing the ablation in comparison to bare ice glaciers (Moore, 2018; Nicholson & Benn, 2006; Østrem, 1959). The thicker the debris cover becomes, the higher the insulating effect is through the

increase in heat absorption. Thus, sub-debris ablation is reduced. Uneven distribution of debris covers increases challenges in ablation modelling and therefore raises uncertainty in future water resource availability calculations (Scherler et al., 2011). Ice cliff back wasting is described to be one of two major surface ablation processes and occurs where debris-free ice cliffs retreat horizontally (Lawson, 1982). Glacier surface morphology evolution is characterized by patterns of debris cover and locally concentrated melt water (Mölg et al., 2020). The surface melt rate of debris covered glaciers is often highest in the middle, as it is limited by debris thickness in the terminus region and by elevation in upper glacier areas. Further, slope aspect or the formation of crevasses and fissures may increase melt rates as well (Fyffe et al., 2014).

2.5. Processes of snow melt and glacier ablation

Water plays an important role in the mountains not only for the environment but also for surrounding communities. Water is crucial for energy production by filling the dammed mountain lakes which are an essential component of hydro energy storage. Mountain water is also important for irrigation purposes, not only within the mountain range but also in the lowlands. Therefore, many different stakeholders rely on water coming from the mountains. Alpine cave water mostly is a combination of several different types of water. One possible source is either rain, another is melted snow (Liu & Brancelj, 2014) melted ice from a glacier (Gremaud & Goldscheider, 2010). Whether this respective share of origin of the water is noteworthy depends on the time of the year. Water contains a distinguishable composition depending on its origin. Glacial water is characterized by a higher turbidity than snow melt water, since glaciers are erosive, and the melt water channels the sediments downstream. The content of turbidity produces distinctive hydrological patterns as well as influences biological and chemical processes (Slemmons et al., 2013). Locating the water flow is relatively easy if it is all surface drainage. However, as water travels underground through a karst network and resurfaces through sources and springs, it gets more difficult to determine a place of origin. Additionally, lakes in the catchment influence water flow, by serving as temporary storage for snow and glacier melt water, and as a sink for sediments transported by the glacial streams.

Furthermore, glacially characterized streams show a specific behaviour of discharge which increases with the start of the ablation period in July – August. It then declines again when the temperatures decrease. Snow melt-fed catchments present a similar behaviour, but the peak rises earlier in the year starting in May. The snow discharge reduces once all the snow is melted. Therefore, it is possible that a stream will not carry any water in August while it was a bubbling stream two months earlier.

In addition to the outflow amount, the creeks also show temperature-specific behaviour depending on whether they contain melt water. The temperature of a stream lowers when melt water starts to contribute to the discharge (Bastiancich et al., 2022). It also differs whether the

water was below, or above ground being exposed to solar radiation. Further, creeks fed by meltwater or influenced by solar radiation are also characterized by diurnal temperature variations (Brown et al., 2006).

2.6. Glaciological method

A complete set up of the glaciological method consists of several different practices. It is a scientific study on measuring and quantifying the surface mass balance of glaciers and ice sheets by assessing the ablation and accumulation of a glacier. By combining data acquired through practical measurements on site, remote sensing data and mathematical modelling, this method is suitable not only for shorter periods like one year but also for projects of extended durations (Cogley, 2021).

The fieldwork is important to gain additional information on existing data from for example snow or ice cores, ground-penetrating radar or GPS, snow layer thickness, ice ablation through ablation stakes and snow pits. Furthermore, satellite or drone data is vital to measure three dimensional and voluminal changes of the ice surface.

Snow pits are commonly used to acquire information on accumulation, snow density and layer sizes. They are dug above the equilibrium line of a glacier where snow mostly persists throughout the year. Hence, the snowfall on the glacier of interest needs to remain to apply this method. As this is not the case on Griess Glacier, a snow pit analysis was not performed. Similarly to the snow pits, probing the snow cover thickness is used to measure the top snow cover depth. However, probing can be performed in shallower snow fields and on a much higher spatial frequency than the pits.

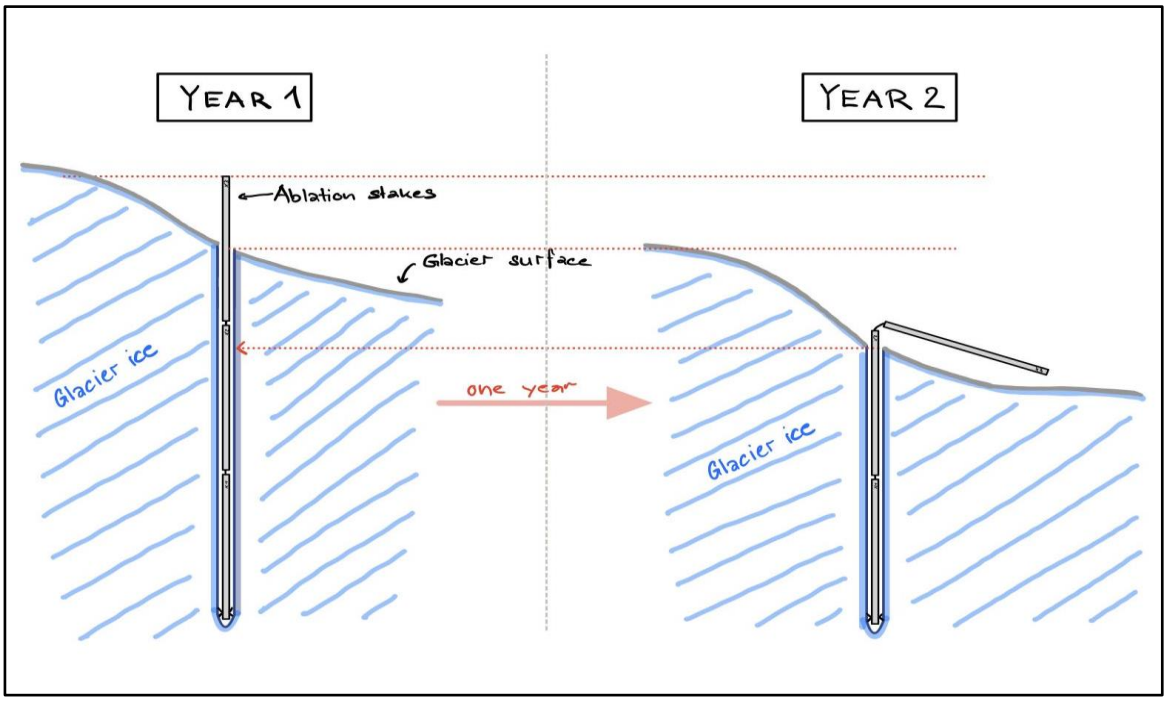

Figure 1: Graphical depiction of the way how the appliance of ablation stakes is working practically in the field.

Another, vital part of the glaciological method is the measurement of ablation stakes. Ablation stakes are PVC-stakes drilled and fixed into the ice to trace the local ice melt. They are evaluated manually to see how much of the stake is sticking out of the ice (Figure 1). Sometimes ablation measuring projects on a glacier or ice shield may last several years. To extend the measurements duration capacity holes of several meters are drilled. Multiple stakes of approximately 2 meters are then wired together to prevent losing an individual stake once the surrounding ice has melted. In this case, as illustrated in Figure 1, the stake tips over and lays on the ice bound to the chain. The ablation can be measured with high precision in the range of a centimetre by this method.

To further investigate the data acquired in the field the contour line method is a commonly used follow up in the glaciological mass balance analysis. This method interpolates the ablation stake and snow pit measurements to the whole glacier area. The measurements are used to differentiate ablation and accumulation areas to their elevation. Then the contour lines of same elevation are used to expand the mass balance per elevation level (Cox & March, 2004; Zemp et al., 2013).

According to Zemp et al. (2013), the glaciological method has three main sources of systematic and random errors which can lead to uncertainties in the data:

- The measurements which are only taken at point locations
- The averaging of these results across the entire glacier in terms of spatial distribution
- Alterations in the extent and height of glaciers.

Additionally, the field measurements are potential sources of errors:

- determining the height (influenced by measurement precision; sinking, tilting and floating of ablation stakes; challenges to identify the surface of last year in the snowpack)
- Errors in density measurements and related assumptions (with larger errors anticipated for snow and firn compared to ice).

The spatial averaging to point measurements are also subject to errors due to

- The local representativeness of the point measurements
- The method used for spatial averaging (interpolation and extrapolations to the whole glacier)

A problem prevailing for all mass balance series is the issue of changes in glacier elevation and area. Coordinates and elevation of reference points can be measured using a GPS, while the most recent geodetic survey of the area is used as reference for the calculation of specific glaciological balances (Zemp et al., 2013).

2.7. Geodetic method

Geodetic methods in glaciology are performed using aerial and satellite images. While There are several different tools used in geodetic methods, the most relevant methods for this study are photogrammetry and GPS measurements. Photogrammetry involves deriving information about the physical properties of the ice surface usually done by aerial images from satellites or drones. Depending on the optical sensor the resolution of the surveyed zones varies significantly. Based on the survey's scale, different approaches are used. For example, if an investigation studies the complete Greenland ice sheet, the resolution will be lower than the one of a study on ice cliffs development on Griess Glacier, when there is strong reliance on high data precision. Commonly, the "geodetic observation method determines volume change by repeated mapping and differencing of glacier surface elevations" (Zemp et al., 2013, p. 1229). Ideally, geodetic surveys should be conducted at the end of the ablation season in fall. They are best repeated every 10 years to acquire a good overview of the ablation over the decade. The timeframe of 10 years is enough to reduce the impacts of interannual meteorological processes and to accentuate the signal of climatic changes (Zemp et al., 2013).

There are two potential sources of errors:

- Sighting: Errors related to the measurement process. They originate from the platform, the sensor and atmospheric interferences.
- Plotting: Errors related to the representation of the sighting results. They include geo-referencing, projection, co-registration and sampling density.
- Other potential systematic errors in geodetic surveys may originate from alterations in the reference areas through gravitational processes.

2.8. Positive degree days and positive degree days factor

A method often used for ablation modelling is the positive degree day method, also known as temperature Index modelling. It was first applied in the Alps by Finsterwalder & Schunk (1887). This method analyses the relation between ice melt rates and temperatures. Specifically, the melt of ice or snow is often regarded at proportionally to the summed up mean daily temperatures above the melting point in the same period (Braithwaite, 1995; Braithwaite & Olesen, 1989)

Previous studies have emphasized the use of the positive degree day method for melt modelling of ice glacier without a debris cover since the debris layer has a strong impact on heat fluxes and transfer into the ice (Braithwaite & Olesen, 1989). Very thin layers of debris or individual grains and lapilli absorb more heat than ice due to a lower albedo. Ablation rates are therefore increased because of the energy transfer into the ice below. Thicker supraglacial debris covers act as protection against the heat, and are therefore insulating the ice, which reduces ablation

significantly (Østrem, 1959). A specific application on debris covered glaciers was pushed forward through the indispensable contribution by Østrem (1959).

In positive degree day modelling, the daily average temperature above the melting temperature gets summed up over a predefined interval. These models are based on the assumed relationship of ablation and air temperature, "usually expressed in the form of positive temperature sums" (Hock, 2003, p. 105). This method is valid for both snow and ice. The most basic formulation connects the ice melt, M $[mm]$, to the summed-up air temperatures values $[T^+]$ during a specific period of n intervals. The formula also includes a proportionality factor DDF, which is called the *degree day factor* (Hock, 2003). The DDF (also referred to as PDDF) describes the amount of melt which happens per degree per day and is therefore expressed in $\frac{mm}{d*°C}$. A reference PDDF for Switzerland has been provided by Lang et al. (1976) for Snow on Grosser Aletschgletscher with $5.4\frac{mm}{°C*d}$ (Lang et al. (1976) cited by Braithwaite, (1995, p. 155))

$$\sum_{i=1}^{n} M = \mathrm{DDF} \sum_{i=1}^{n} T^{+} \Delta t$$

Figure 2: Formula of the degree day method. It calculates the ablation of a glacier over a defined period in a specific interval, based on the positive temperature values.

The degree day factor can be calculated by the help of several different means, like snow lysimeter outflow measurements or ablation stake measurements. Hock (2003) agrees with Singh et al. (2000) and Arnold & MacKay (1964) on the sensitivity of the DDF to the derivation technique. The PDDF varies according to the temporal average that is used or the way the mean daily temperature is calculated. However, the application of daily average temperatures can be misleading, especially if temperatures fluctuate around the freezing point (Hock, 2003).

Since the PDD-Method strongly relies on temperature and climatic conditions, this method is for modelling future changes in ablation rates. Additionally, using the PDD method, it is possible to investigate the response of debris covered glaciers to global warming. These glaciers respond differently to climate change compared to bare ice glaciers, as highlighted by previous research (Bolch et al. (2008), Scherler et al. (2011)). Using the PDDF, an equation can be obtained which connects empirically determined debris cover thickness to the degree day factor. Additionally, measured ablation, debris thickness and extrapolated temperatures are assessed (Juen et al., 2014). Juen et al. (2014) suggest different PDDFs which are valid for the debris covered Koxkar Glacier in northern China, for example $\frac{5.2mm}{d*°C}$. It is important to note that this guide value is an approximated average of a debris covered glacier facing westwards in the Himalayan Mountains. Also, the glacier is located at an elevation between 3000 and 3500 meters above sea level. Another Himalayan PDDF is $\frac{4.1mm}{d*°C}$ for debris covered glaciers, provided by Romshoo et al. (2023).

Kääb et al. (2012) emphasize that debris layers exceeding a critical thickness have insulating properties on local scales but do not have a general effect on larger scale on the glacier

terminus. However, the results presented by Juen et al. (2014) show an opposite effect than proposed by Kääb et al. (2012), as melt is considerably reduced on a debris covered glacier according to their study. They underline that the prediction of debris covered glacier melt water availability must be seriously considered in the future. Therefore, the prediction of future water availability is of major importance in current research (Benn et al., 2012; Bolch et al., 2011; Scherler et al., 2011).

2.9. The use and benefit of unmanned aircrafts in glaciology

Unmanned aerial vehicles (UAV) are part and parcel of today's research in various fields. According to (Bhardwaj et al., 2016) the application in research studies increased significantly after the 2010s, including glaciological studies. They recorded the rising numbers since 2013 for this field of research.

UAVs are remotely controlled and motorized vehicles that can transport different equipment such as cameras or specific sensors designed for different purposes. There are various types of UAVs, for example fixed-wing mapping drones, like the eBee X (AgEagle Aerial Systems Inc, 2024) or Quadrocopters (Figure 3), like the DJI Phantom 4 Pro (DJI, 2024)

Figure 3: DJI Phantom 4 Pro V2 during take-off on Griess Glacier on the 1st of October 2023 (Image by Andrin Hauser (2023)).

Before UAV were used for glaciological data collection, it was commonly done through satellites. However, this method poses various challenges. Firstly, satellite data is bound to the dates when the satellite crosses the region of interest. Therefore, the specific date of the dataset might not be available. Secondly, if a satellite does not operate at microwave lengths, clouds will obstruct the imaging process. Thirdly, the high detail precision on a large-scale monitoring by a satellite costs enormously. However, year-round glacier monitoring in the field is limited by various factors, such as hostile weather conditions (wind/rain), poor accessibility, logistical organization if reachability is complicated, or inappropriate funding structures. Therefore, “remote sensing is often used as a practical alternative to field studies” as explained in Bhardwaj et al. (2016, p. 197). One major advantage of satellite imagery is the global coverage and its high temporal resolution. This combination influences the fieldwork considerably. It reduces the logistical effort and expenses for site visits significantly since certain regions in the mountains are almost unreachable (Rossini et al., 2018).

Based on this elaboration it is obvious that a new technology also allows new options to track the glaciological changes. However, there are several advantages and disadvantages of the use of UAVs in glaciological studies.

The main advantage of UAVs is that the hardware is less expensive compared to satellite imagery. Furthermore, it can provide high precision data on small scales while maintaining viewing angles and images overlaps (Bhardwaj et al., 2016). Bhardwaj et al. (2016) mentioned another enormous advantage of UAVs. First, the use of UAVs reduces risk of fatal crashes involving human lives. Compared to the data acquisition by plane during poor weather conditions. Another advantage is the ability to fully pre-program flight missions using specific applications, as UAVs are fully automated, and the integrated autopilot follows the programmed flight paths. It controls the onboard sensors for the imaging sequence, which is coupled with a simultaneous Global Navigation Satellite System (GNSS) to acquire the exact coordinates of the images (Bhardwaj et al., 2016).

However, there are also disadvantages of UAV's application in mountain regions. A large issue, for example, is harsh weather conditions of glacial regions. Additionally, mountains can interfere with the GPS satellite signals. Another problem is the relatively short flight duration of UAV. (Bhardwaj et al., 2016). For example, the DJI Phantom 4 RTK has a listed flight time of approximately 30 minutes at optimal conditions (DJI, 2024). Wind and old battery gear can reduce the flight time additionally. Therefore, glaciers investigated in alpine field studies often need to be separated into different survey blocks and be examined in separate flight missions. However, fixed-wing UAVs are more suitable for studies in alpine environments, as they benefit from the aerodynamics (gliding) influencing the flight duration positively (Bhardwaj et al., 2016). Therefore, the eBee-X can fly around 90 minutes (AgEagle Aerial Systems Inc, 2024). On the other side, as Bhardwaj et al. (2016) point out that fixed-wing UAVs need a proper take-off and landing location, which is difficult to find in the mountains. Nevertheless, the authors emphasize the implementation of UAV data collection in mountainous areas since this new method shows great potential and strongly supports the "field-based and remote-sensing based glaciological observations" (Bhardwaj et al., 2016, p. 202).

2.10. Tracers in Hydrology

Artificial tracers are commonly used in hydrology for waterway retracing to investigate flow, flow paths and processes of transport (Benischke, 2021). Tracers can broadly be defined as a chemical substance which is added to a water body, so its concentration can be measured further downstream. The use of conservative tracers is a common application in research of water-body connections since they are known to mimic the water's movements and dynamics as stated by Goldscheider et al. (2008). When

the water is colourized or the signal is recorded by a fluorometer, the researchers know that this water body is connected to the point of injection and are therefore able to backtrack its source. Due to its easy application, this method is prominent in recent research.

Table 2: Summary of the used artificial tracers, taken from Goldscheider et al. (2008).

TYPE:	TRACER NAME (CAS RN):	DETECTION LIMIT:	GENERAL PROBLEMS:	COLOUR:	SPECIFIC PROBLEMS
FLOURESCENT DYES	Uranine (518-47-8)	10^{-3} µg/L	Sensitive to light and strong oxidants	Yellow/Green	
	Rhodamine WT (37299-86-8)	10^{-2} µg/L	Analytical interferences between fluorescent dyes of similar optical properties.	Red	Genotoxic

There are various colour tracers available for hydrological pathway finding, Uranine and Rhodamine WT are the most widely used colour tracers. Uranine is of special interest in research due to its photosensitivity. It decays when exposed to sunlight for too long, while other chemicals may persist. Therefore, the environment does not get tainted by visibly coloured bodies of water as it would with sunlight resistant water tracers. Hence, it is of good use in cave system reconstruction and near civilisation, as people are less likely to be impacted. Additionally, Uranine is well detectable by fluorometers even if diluted to the smallest share (10^{-3} micrograms per litre) and not visible anymore to the naked eye.

3. Study area

3.1. Geographical settings

The area of interest is situated in the valley of Urnerboden, just south of the Klausenpass in the canton of Uri (Figure 4). The glacier, commonly known as Griess Glacier or Clariden Nordfirn, is embedded in a glacier cirque and is protected from sunlight by the enormous Clariden North wall, which towers almost a thousand meters above the ice. Glacier or Clariden Nordfirn is embedded in a glacier cirque and is protected from sunlight by the enormous Clariden North wall, which towers almost a thousand meters above the ice. The proglacial Griesseeli is situated right in front of the glacier, with the ice still being connected to the water. Therefore, icebergs are not an uncommon sight on the lake. The lake lies at an altitude of 2100 meters above sea level, while the glacier reaches up to about 2500 meters above sea level. The glacier lake was formed over the past 40 years. It has been growing constantly, considering the retreat of the glacier terminus due to climate change. Most interestingly, the lake outflow is dry for some parts of the year. Meanwhile, the lake continues to decrease in water level, suggesting that there must be another waterway for the lake water to drain into.

The lake-glacier system is situated right on top of a geological nappe containing limestone, which favours the formation of karst caves and subterranean waterways. The proneness to the development of a karst network is validated in the existence of multiple resurgences around Klausenpass and Urnerboden, where water emerges from the underground through springs. While the springs are mostly charted, it has thus far not been explored, where the water is originally coming from. Several cave systems in the region are under thorough investigation by the OGH – Ostschweizerische Gesellschaft für Höhlenforschung (Society for Cave Research of Eastern Switzerland) – which has dedicated their research camp to the exploration and mapping of the caves in and around the Klausenpass. The members of the OGH are contributing to this study through helping with a tracer injection at Griessloch, a cave high up in the Clariden north wall. A place which only a few people could reach.

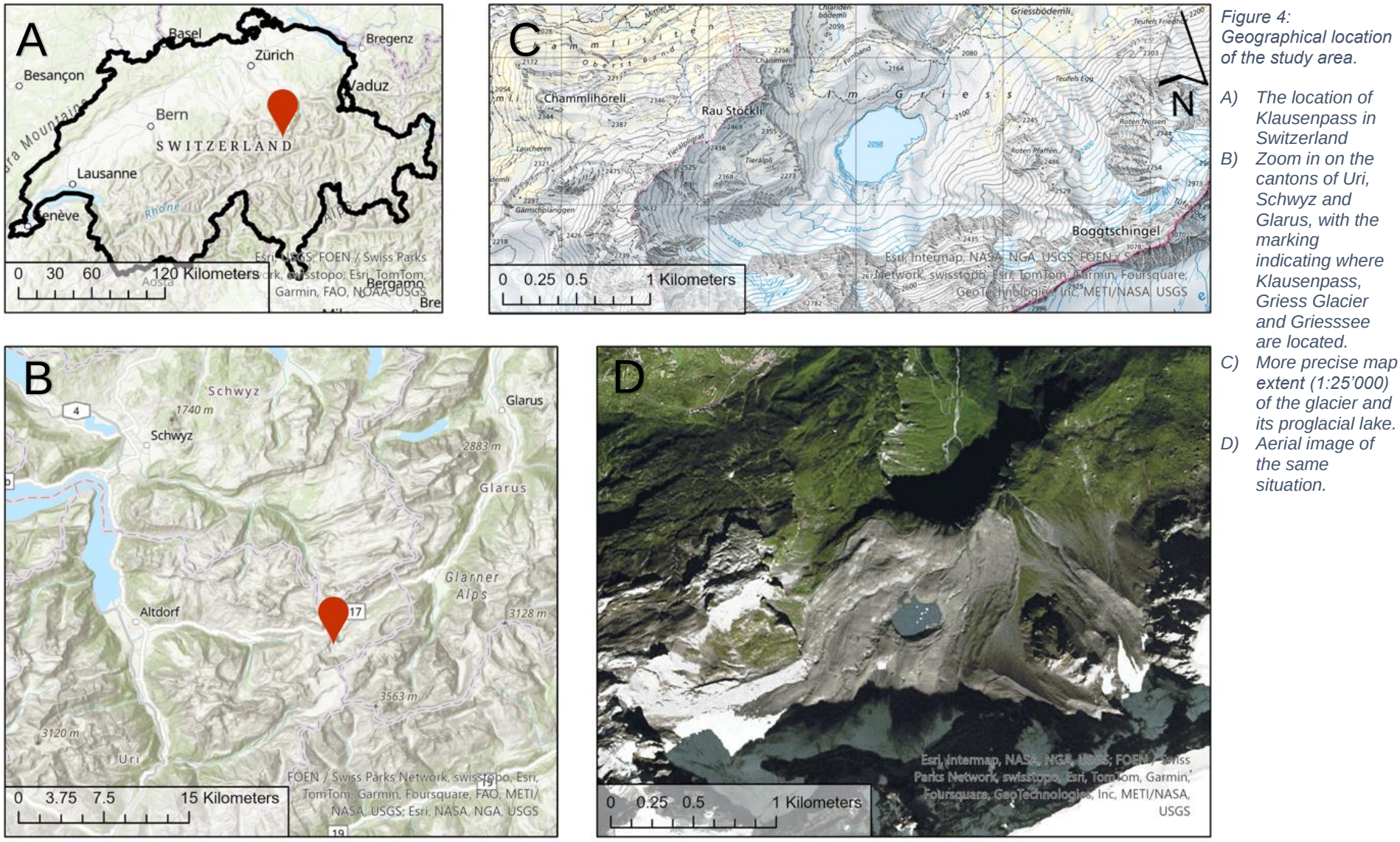

Figure 4: Geographical location of the study area.

A) The location of Klausenpass in Switzerland
B) Zoom in on the cantons of Uri, Schwyz and Glarus, with the marking indicating where Klausenpass, Griess Glacier and Griesssee are located.
C) More precise map extent (1:25'000) of the glacier and its proglacial lake.
D) Aerial image of the same situation.

3.2. Geological characteristics

The area around Urnerboden and the Klausenpass is in the region of the main thrust fault of the Helvetic Nappes. Tectonically, the area is structured as follows. At the very bottom the crystalline basement rock of the Aar Massif consisting of granites and gneisses is situated. It was overthrusted by the Helvetic Nappes during the Alpine orogeny. Moreover, the autochthone Sediments of the Aar Massif and the younger North Helvetic Flysch deposits are situated between the crystalline basement rock and the higher Helvetic Nappes (Ibele, n.d.; Wyss & Hermann, 2021).

The thick Flysch-sequences possess a high clay content and thus have strong water-blocking properties. On top of the North Helvetic Flysch and below the actual Helvetic nappes, two local nappes of smaller size and reduced stratigraphy are situated, called the Griessstock and the Chammlistock nappes (Figure 5). The south- and eastward plunging Griessstock nappe reaches from the Griessstock, west of the Klausenpass, to Linthal and consists to a major part of karstified

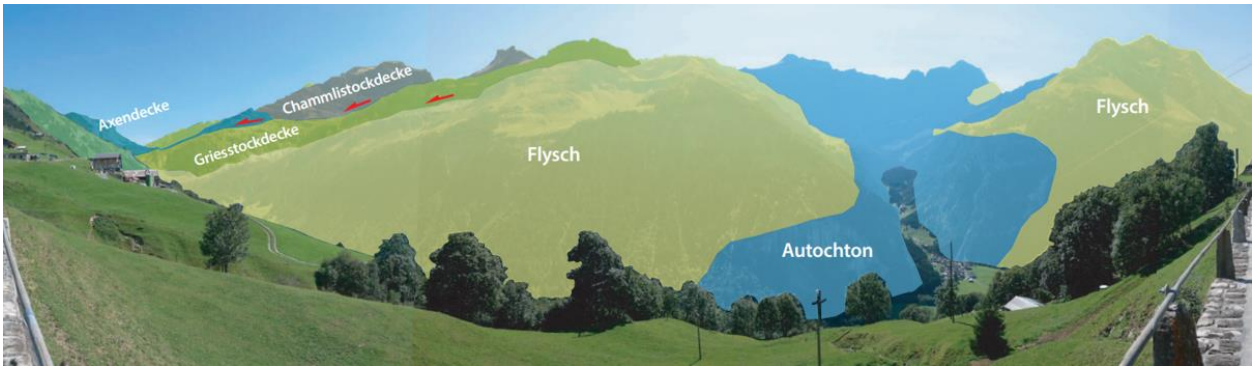

Figure 5: Image showing the Griesstock nappe amongst others, on the western side of Klausenpass. The pass height is located in the saddle on the left-hand side, underneath 'Axendecke' (Wyss & Hermann, 2021)

Quinten Limestone from the upper Jurassic age (Ibele, n.d.; Wyss & Hermann, 2021).

Specifically, the thrust of Griessstock-nappe on to the North Helvetic Flysch in the Chlus demonstrates the water impermeability of the Flysch since several springs emerge along the sharp line of the thrust (Ibele, n.d.; Wyss & Hermann, 2021). These springs emerge from the Griessstock Nappe's large networks of karst caves in the Quinten Limestone (Ibele, n.d.).

The Griessstock nappe was overthrusted by the higher Axen-nappe during the Alpine formation. The Axen-nappe consists of sediments of Triassic to Cretaceous age (Heim, 1871). Triassic rocks dating back 230 million years are found on top of Klausenpass, forming remarkably red claystone on the northern side of the road and brecciated dolomite of light yellowish colour on the southern side. Jurassic rocks, dating back 170-220 million years, form the dark coloured rock walls north of Vorfrutt and Urnerboden (Ibele, n.d.; Wyss & Hermann, 2021).

The thrust fault of the Axen-Nappe over the Griessstock-nappe is assumed to run along the northern slope of the valley, buried by quaternary scree deposits. However, the thrust fault of the Griessstock-nappe and the North Helvetic Flysch is well observable, especially in the Chlus cliff

Figure 7: The Chlus rock face from the Bus stop 'Chlus'. Marked in red is the thrust-fault of the Griessstock nappe onto the North Helvetic Flysch, circled in blue are two springs, the 'Chlus' spring on the left and on the right 'Chlus West' (Wyss & Hermann, 2021).

(Figure 6 or see Appendix 4) and at the Berglistüber waterfall (Figure 7 and Figure 8) above Linthal. These two outcrops have a height difference of 1000 meters over 10 kilometres of distance, emphasizing the inclination of the nappe (Ibele, n.d.; Wyss & Hermann, 2021).

Figure 6: Thrust fault in close-up. On top the Griessstock nappe in light brown and in the middle, the deformed zone which has been squelched. Underneath the loose pebbles, the North Helvetic Flysch is located.

The Griessstock- and the Axen-nappe belong to the complex of the Helvetic nappes, which are deformed internally by faults and folds. Corresponding faults can be observed in the Chlus cliff, while folds are to be seen in the cliffs north of the pass road formed through plastic deformation within the Axen-nappe (Ibele, n.d.; Wyss & Hermann, 2021).

These folds exhibit an axis in eastern-western direction, meaning that the Axen-nappe was thrusted in north-south direction. This corresponds to the overall tectonic regime of the Alpine geology (Ibele, n.d.; Wyss & Hermann, 2021).

Figure 8: The same thrust-fault as at Chlus, but at Berglistüber waterfall close to Linthal GL. On top the Griessstock nappe and below the North Helvetic Flysch (Image taken by Andrin Hauser (2023)).

3.3.Meteorological characteristics

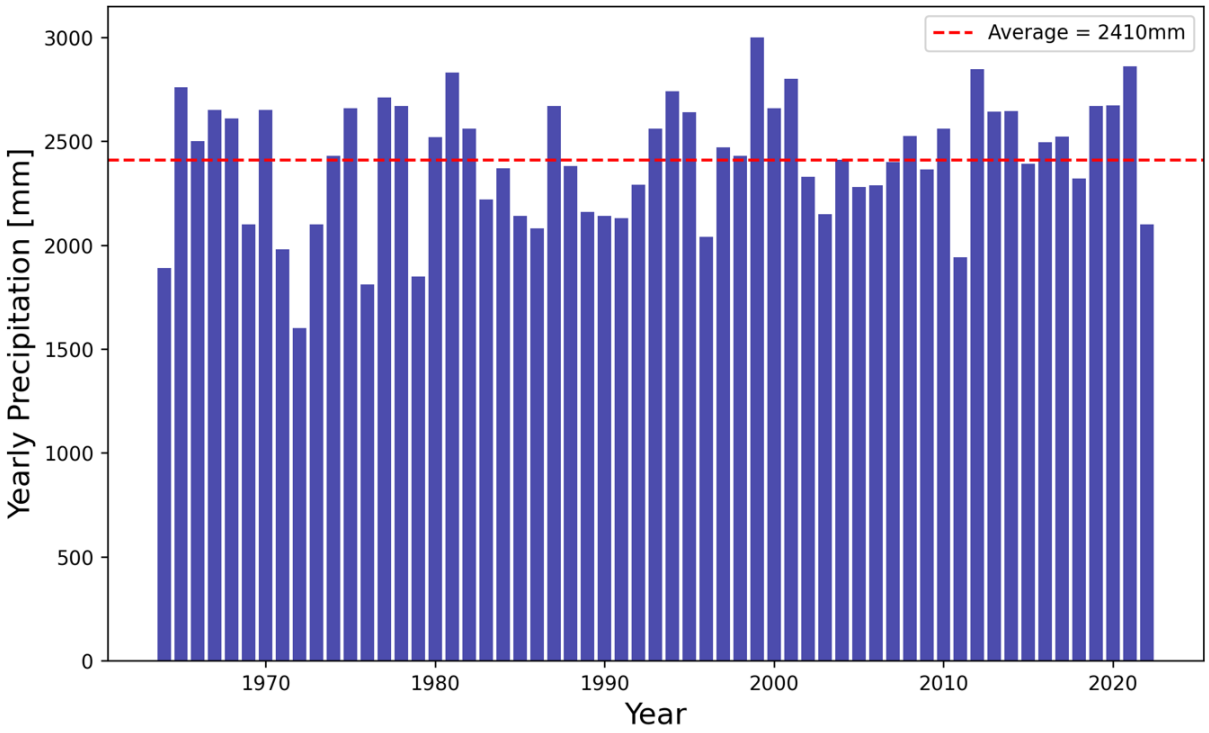

Figure 9: Presentation of the yearly average precipitation of the pluviometer on Tierälpli. This sensor is located on the plateau south of Raustöckli.

This meteogram (Figure 9) displays representative yearly precipitation values for the last 59 years. The pluviometer is located on a small ridge close to the glacier, situated in the same geomorphological hollow as Griess Glacier. It is therefore similarly surrounded by the Clariden Massif as the glacier. The only difference is its elevation above the ice, being located at 2352 meter above sea level. The pluviometer data is only available in yearly total precipitation and therefore only guides as a reference. The yearly average since 1964 to 2022 is 2410mm of precipitation. While in recent years, the yearly precipitation was slightly above the yearly mean, 2022 recorded less than the average. Currently, the precipitation of 2023 can only be determined for the period when the KLAU-meteostation was active, from May till the end of September.

3.4.Hydrological characteristics:

The hydrological aspect of the Klausenpass area and the Urnerboden is mainly characterized by the Griess Glacier in the direct catchment area, located underneath the Clariden north wall. In addition, the glacier lake, which was naturally formed approximately fifty years ago also works as a natural water storage for the valley of Urnerboden. The lake is naturally dammed by the moraine bastion deposited 170 years ago by the glacier (Linsbauer et al., 2021). The lake water is discharged via one above terrain stream.

Additionally, on top of the Chlus cliff, there is a floodplain called Melchbödmeli. A small creek which crosses the plain, ends in a pond of varying size, depending on the water discharge volume of the stream. The pond is located on top of a small system of ponors draining the water into a

subterranean stream system potentially leading to the Chlus cliff or even further down to a spring on Urnerboden.

500m after leaving the lake, Fätschbach reaches the water retention station by KLL (Baggio, 2023). Here, Fätschbach water gets diverted into an artificial shaft, direction water 4.6km through the mountain to Obersand, where it gets further directed to Limmernsee (Appenzeller Kalender, 1967). Continuing the water flow further downstream from the Chlus cliff, the Fätschbach eventually reaches Urnerboden. Along its way, it is occasionally fed by other streams coming down the slopes of the valley, but also by streams emerging from the ground through springs. This water originates from cave systems deep within the mountain, but the origin point of that water is mostly unknown. While there is a big spring in the Chlus (Figure 10), releasing between 1000-10'000 Liters per minute according to Yvo Weidmann (unpublished). Curiously, it is not identified as a spring on the Geoserver of Canton Uri (Lisag AG, 2023). Further downstream, the Fätschbach is joined by cave water, resurging from the two Waldhüttli springs, which can double the discharged water volume of Fätschbach, depending on the season. The Waldhüttli consists of two different springs. The first one is releasing water on ground level (KL-WHB). The water is coming directly out of the wall below a few rocks. The second spring is located about 15 meters above the stream level, flowing out of a cave entrance and feeding a small waterfall (KL-WHF). This part of the Waldhüttli spring-system (Figure 11) was dry in March 2023. It is currently not known whether the same cave system feeds these two springs or if they are independent of each other. However, whether the water is glacial meltwater, water from snow melt, groundwater or even lake water discharging through this cave system underground is not known.

Figure 10: On the left, the Chlus spring in winter (23.03.2023) and on the right in autumn (05.09.2023). These images were taken by Andrin Hauser (2023).

Following the Fätschbach past the Urnerboden village at the marsh of Riedrütenen, the primary stream course is again joined by a second stream. This side stream is fed by another spring at the feet of the Jegerstöck range, releasing more than 10’000 Liters per minute. This spring is located on the northern side of the valley.

The Fätschbach then continues to Glätti, where it is retained and partially discharged through a tunnel system for energy production in Linthal. The rest of the stream follows its natural way to Linthal over the Berglistüber waterfall, where it is joined once again by a side stream originating from a karst cave system. As Leupold (1948) presents, there must be infiltration of river water into the karst underground. As he conducted two tracer experiments in 1948, the Fruttmatt-spring, about 2.8km ENE of the river blockade at the end of Urnerboden, displayed signs of tracer colour. In a follow-up study he injected a tracer further upstream only to have the Fruttmatt-spring reacting again. He deduced that there must be a loss of 6 litres per second of river water, which infiltrates into the ground and joins other subterranean waterways assumed to be coming from Wängiswald-Fisetengrat on the south face of Urnerboden (Leupold, 1948; cited by Müller-Lemans et al., 1997).

Accordingly, assumptive knowledge about the springs in the lower regions of Urnerboden exists, while the resurgences upstream are mostly of unknown origin.

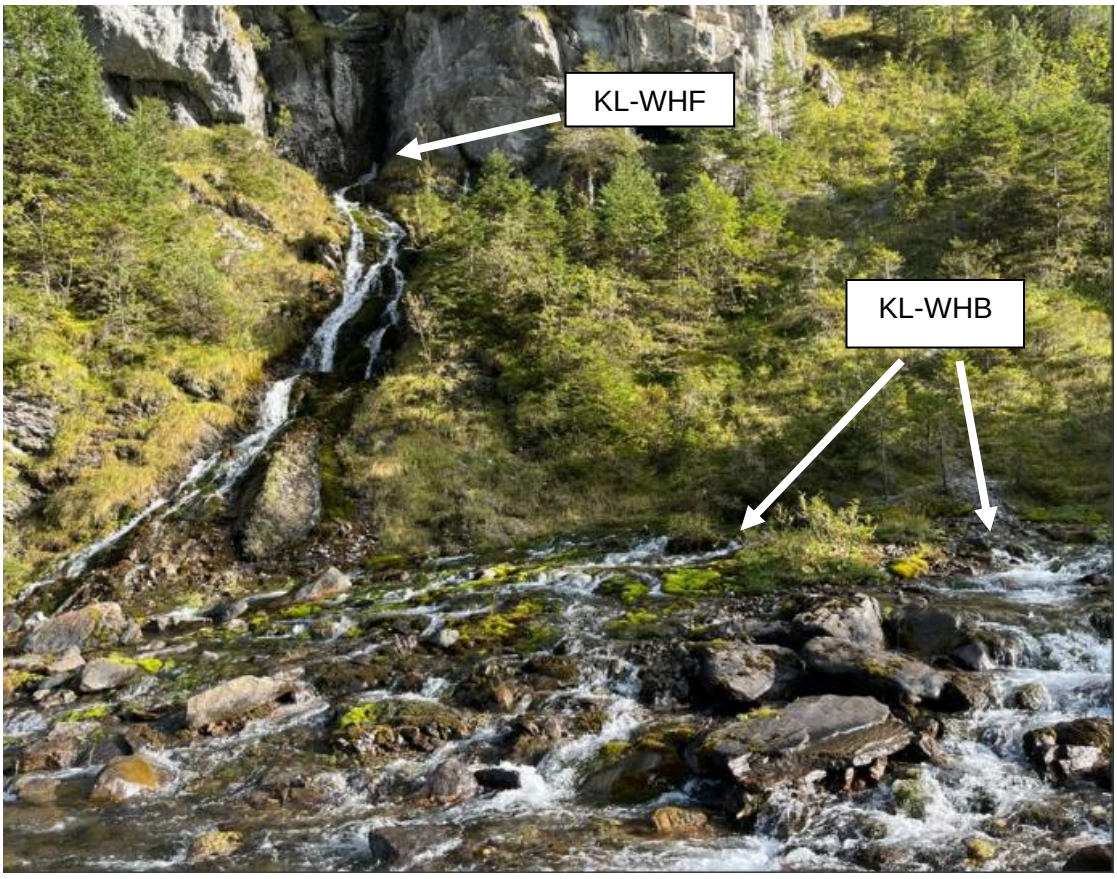

Figure 11: Emergences of KL-WHB and KL-WHF into the Fätschbach, which is not visible here. The water on this photograph is completely discharging from the two springs.

3.5. Glacier and lake development

The region has changed strongly over the last years. Following the retreat of the glacier terminus due to global warming, the lake area continuously increased. The first puddle developed in the early eighties. In the nineties a second lake formed, only to merge with the initial lake a few years later. From then on, the lake grew constantly in size (Figure 12 and Figure 14)., forcing the glacier to retreat every year as reported by Buri et al. (n.d.). The glacier lake and -front have also been part of a travel report blog by Daniel Pfau (2023), who documented the glacier terminus and the lake several times a year since July 2018 (Figure 13). Through his pictures, he also documented rises and drops of the lake water level throughout the year. Derived from the DEMs of 2015 and 2022, the ice thickness loss for the glacier was produced. In total it lost about -12.8m of ice, on average -1.8 per year. For further illustrations of the glacier retreat and the ice loss between 2015 and 2022, see Appendix 18 respectively Appendix 14.

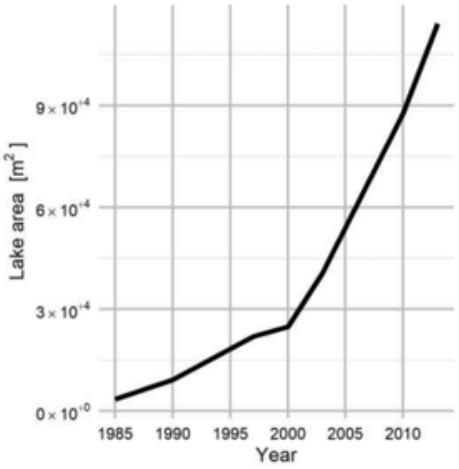

Figure 12: Evolution of the lake area based on Swisstopos aerial images by Buri et al. (unpublished, n.d.).

Figure 13: Drone shot of the Griess Glacier, the Griesssee and the Clariden which is the highest peak on the photograph. This image was taken at the end of June 2021 by Daniel Pfau (2017).

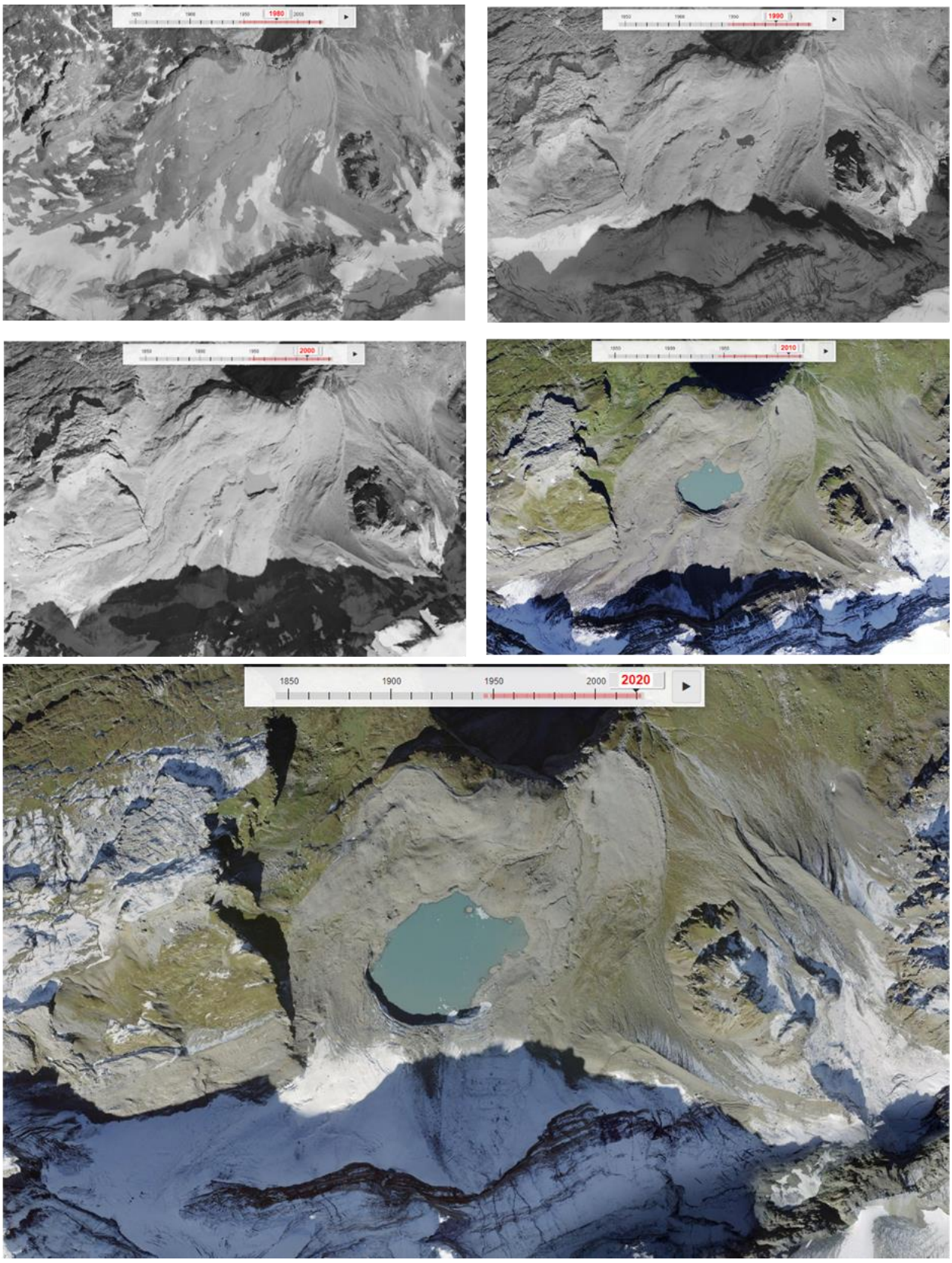

*Figure 14: Image series of the development of Griessseeli and the evolution of Griess Glacier. All images are North oriented. Top left: Year **1980**, no lake visible yet. Top right: Year **1985**, one lake formed in the northeastern part of the Griess basin. Middle left: Year **2000**. Meanwhile a second lake has formed, and they merged to one big lake. Middle right: Year **2010**. Griesssee now fills the basin width, framed by the 1850 moraine bastion. The glacier retreated more than ever before. Low middle: Aerial image from **2020**. This is the closest to the situation of 2023. But the glacier terminus has already retreated further south, and the glaciated area has shrunken. All images are property of SwissTopo* (Federal Office of Topography Swisstopo, 2023).

4. Material and methods

4.1. Drone surveys

For the three-dimensional analysis of the glacier, aerial drone imagery is used. The drone surveys are conducted using a DJI Phantom 4 Pro V2 with an external RTK structure built on top. Since the area of the glacier is larger than 200'000 square meters and the drone's flight time is limited to the battery lifetime, the survey area had to be minimised, as earlier described and similarly done by Bhardwaj et al., (2016). The Phantom 4 Pro V2 was of high standard when it was re-released in 2020. It combines 30 minutes of flight time with 5 direction obstacle sensing, a mechanical shuttle and a 1-inch sensor. But now four years later in 2024, there are much more compact and smaller drones, which perform better in every aspect, albeit in battery life, mid-air stability and flight performance, obstacle sensors, software and even camera equipment.

The area around the tongue and the long glacier arm reaching west is the main part of interest, so the survey area is placed accordingly. It is therefore split into two perimeters (Figure 15), the first one covering the lower part around the lake and the glacier front, while the second one is covering the upper part including the longer west branch of the glacier. Each perimeter is covered by two missions, one where the drone flies the grid in horizontal direction and the other one where the grid is flown in vertical direction. Both missions are conducted on different heights and different camera angles, to have a different perspective on the resulting images. This difference can later in postprocessing be used to find a version which fits the real circumstances the best.

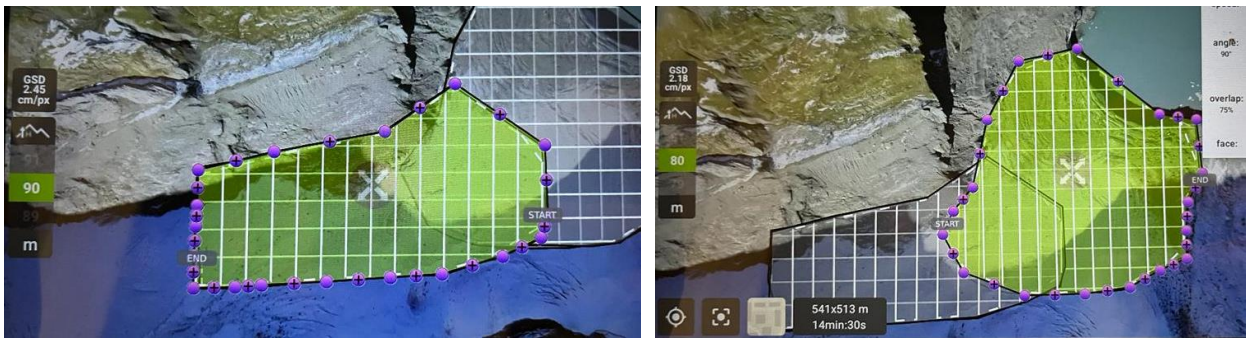

Figure 15: Both drone survey perimeters on the glacier. On the left-hand side the upper glacier perimeter and on the right-hand side, the lower perimeter which is closer to the glacier lake and includes parts of the terminus. These images are photos from the user interface of the application Pix4D.

The drone produced data is also used to gather information on potential ice flow on the glacier. For that purpose, 5 ground targets (GTs) are installed on the glacier. They are bolted onto large boulders which are transported on the glacier's surface and will follow the ice flow, given the glacier still shows ice flow. After the production of the ortho photos and their geo-referencing, the location of the GTs will be marked overlaying on every ortho photo. The resulting point dataset displays the different locations of the GTs over the summer. If the glacier still shows signs of flow movements, the GTs will show a general direction of shift, which can be indicated as the direction

of ice flow. Depending on the distance the GTs shift, the flow distance and potentially the flow pace can be derived. For photographs of the GTs, please see Appendix 11 and for the map of the GT dispersal see Appendix 16.

4.2. Georeferencing and positioning

The drone missions are programmed using the application Pix4D. Pix4D is a Swiss software used for photogrammetry and mapping. Using this tool, the flight grid for the drone can be prepared and all the necessary settings set, so the missions can be uploaded to the drone for them to be flown autonomously. To connect the drone to the Pix4D application, another app called DJI+Control is necessary to establish a stable connection to the drone control.

Different settings are selected for each mission per perimeter. In Table 3, a brief example is listed. The flights were normally flown at a height of 80 and 90 meters above the starting point for the lower perimeter. For the upper perimeter, the elevation settings were 90 and 100 meters above the starting point, since here the glacier gained in elevation and it had to be ensured, that the distance to the ice is always large enough. Otherwise, the resolution would differ too strongly within the images.

Table 3:Examplatory settings for the two different missions in the same survey perimeter.

MISSIONS	FLIGHT DIRECTION	HEIGHT [METERS]	CAMERA ANGLE	FLIGHT SPEED
MISSION 1	Vertical	80	90°	Full speed
MISSION 2	Horizontal	90	80°	Full speed

Later in the process of aerial imagery production, the mission programming platform had to be switched to DJI Pilot, since the DJI+Control app did not work anymore on the software of the newly updated tablet. The new program works slightly different, and the camera angles cannot be edited. The used mapping tool generally uses 90° vertical downwards angles of the camera.

Figure 16: Left: The Emlid basestation set up on the moraine bastion north of the Griessseeli. Right: The DJI Phantom 4 Pro V2 in mid-flight. The black cylinder on top is its build-on PPK antenna.

But otherwise, the mapping generally works the same, the missions just had to be programmed from anew.

The postprocessing part started using the tool EMLID Studio. EMLID Studio processes the data gathered by the drone's PPK Antenna and a base station, to reconstruct the exact coordinates where the drone images were taken. This results in an image of the flight grid with spots marking all photos taken. The base station Reach RS2+ was also a product of EMLID LTD (2024) which continuously recorded data, once activated. The black antenna on the DJI drone worked similarly, it recorded data as long as the drone was activated.

How does PPK work:	PPK means post-processed kinematic and is used in terrestrial surveying for a long time. Its function is to improve the accuracy of GNSS data. The PPK Antenna (Figure 16 left) gathers data from satellites and logs it for after the flight. Due to tropospheric delays, satellite data by itself is prone to errors and may only provide an accuracy of about 1 meter. The base station does the same as the PPK antenna on top of the drone. Combining both makes it possible to correct the satellite data error and brings it down to the centimetre scale. A huge advantage of PPK is that the drone-base station communication data is not needed. Only the telemetry between the drone and base station is required (Wingtra AG, 2020).

The program then produces a grid of all coordinates where the photos were taken. Sometimes it may occur, that the coordinates are not within a certain precision limit, which the program then will mark as float instead of fix. More than 90% of the image locations being tagged as fixed means the accuracy is still within an acceptable range. To this grid the taken images are then added. The number of images added has to match the number of points for taken images on the grid, even if the images are not suited for further use, in this step they have to be included.

The images are then geotagged, which means that the exact coordinates of the images are added to the images' properties. Thus, the postprocessing tool used for DEM and ortho photo production can locate the position of the image with high precision.

The post processing to establish a three-dimensional model of the perimeter surface is done using the software Agisoft Metashape Professional. In a first step the images are aligned, and a point cloud of the perimeter is generated. In a next, very time-consuming step this point cloud is further processed to a dense cloud. Out of that product, the digital elevation model as well as the ortho photo are generated. This is all carried out on the coordinate system of WGS 84 and will be projected later onto CH1903+ / LV95.

Agisoft Metashape Professional working steps:

- Align images, working in WGS 84 → creating a point cloud.
- Create dense cloud out of point cloud.
- Create DEM
- Create ortho photo

After generating all the necessary images, a geoprocessing step had to be taken. The images had to be aligned to each other, so that they are perfectly on top of each other. Initially, this was done using spline interpolation of ArcGIS Pro, but this technique tore apart the images leading to strong distortions on the glacier. It was repeated using the similarity polynomial georeferencing tool, which worked better for it. Then the DEMs and the ortho photos were clipped to an extent in which for all images data is present. In this state, the data was ready to be further analysed and used.

4.3. Geodetic method

The geodetic method is used to derive the mass balance of a glacier, using aerial images in the form of digital elevation models (DEMs). Hereby the surface changes of the glacier as well as the extent is investigated, from that the ablation is retrieved.

Using the corrected DEMs, the total ice loss over the perimeter can now be calculated applying the DEM differentiation technique. The latter DEM will be used as base, while the precedent DEM is subtracted from it. The resulting raster file displays, where and how much ice loss occurred on the glacier during the selected period.

One step further to calculate a numerical value for the ice loss, a perimeter must be chosen, which is fully located on the glacier for the latest DEM and not on border zones to the side or on the terminus. Otherwise, terrain changes not directly influenced by the ice loss are recorded and included into the balance calculation. With that an uncorrected geodetic mass balance can be derived.

Next an assessment of the related error has to be done. There can always be mistakes in the DEMs due to reflections or shadows on the surfaces when taking the images. For the retrieval of said errors, a polygon off the glacier has to be defined, according to Zemp et al. (2013), who stated that the integrative errors of elevation differences are assessed over stable terrain surrounding the glacier. Most conveniently a perimeter has to be defined, where bedrock is appearing underneath the debris, to guarantee no movement in the surface due to physical processes. Using zonal statistics on the polygon where “supposedly no height change” should happen, the average height change can be derived. This value can be assumed as the systematic error of the Drone data. As Zemp et al. state, “the related total random error cumulates the individual sources and years according to the law of error propagation assuming they are not correlated” (Zemp et al., 2013, p. 1233). Since this study is only comparing data from within one year, this random error will not be assessed.

4.4. Glaciological method

In the physical work part of this thesis, 8 ablation stakes were installed on Griess Glacier. All ablation stakes were PVC stakes of 2 metres length with a piece of wire at the lower end to wedge it tight into the ice. A hole of 5cm diameter was drilled into the ice using an ice drill produced by Kovacs Enterprise (Kovacs Enterprise, 2023). The stakes were put into the drillhole, wires at the lowest point. Only one stake per drillhole was inserted since the observation is only for one summer period. As the stakes were in place, their height above the ice was measured (Figure 17). The ablation stakes were measured always on the same day as the drone missions were flown. For measurement, the debris around the stake was removed. To reduce measurement errors, the ablation stakes were always measured from the orographic left side. Later the hole in the debris cover was closed again, aiming to be as similar as possible in thickness as it was before.

Figure 17: Measurement of an ablation stake on Griess Glacier using a twin meter.

The stakes were distributed on the western arm of the glacier as the rest of the ice was not safely accessible. There was always the risk of avalanches or rockfall, therefore these areas were avoided (see ablation stakes map in Appendix 15).

As the stake has melted partially out of the ice, the height above ice-level was larger than the previous measurement. This difference indicated how much ice height has been cumulatively lost at that specific location in the ice. It must be considered that these stakes mark a relative location where the ice is melting and not specific coordinates, since the glacier might still flow downstream. However, ice flow is not expected on Griess Glacier.

The measured ablation data of the stakes was then used to further assess and extrapolate the total ice loss over the whole glacier and was further used for the PDDF calculation.

Often, the glaciological method and the geodetic method are combined later in the process. They are homogenised, corrected for artefacts and biases. It is aimed for the detection and reduction of inhomogeneities, to make observation series internally consistent (Cogley et al., 2010). Furthermore, an uncertainty assessment would be performed, before validating and calibrating the mass balance, resulting in the specific mass balance for a glacier (Zemp et al., 2019).

Commonly seen error sources for stake measurements are mainly caused by human error when measuring. Also tilted and floating stakes as well as insufficient representativeness of the stake's location can have negative influence on the precision of the glaciological method ((Romshoo et al., 2023; Thibert et al., 2008)

4.5. Positive degree day method

Another Method which is often applied in glaciology, is the usage of the positive degree days factor. The PDDF was estimated separately for each stake on the glacier. As explained earlier, positive degree day modelling, can be used in ablation estimation for a glacier and therefore it helps to approximate the melt water lost by the glacier.

In positive degree day modelling, the daily average temperature above the melting temperature gets summed up over a predefined interval. The melting temperature of ice can vary due to local conditions but is set at 0°C as it has been suggested by Juen et al. (2012). The PDDs were acquired through the data recorded by the KLAU meteostation.

As stated in an earlier chapter, the PDDF can be calculated by various means. As part of this thesis, the PDD is calculated based on the temperature at the site of the ablation stakes. Therefore, the temperature curve from the KLAU-Meteostation had to be adjusted to the elevation above sea level, where the stake was placed in the ice. Per 100 meters of rise in elevation, $-0.65°C$ were deducted from the temperature curve. This value is based on the information provided by the Federal Office of Switzerland of Meteorology and Climatology MeteoSwiss (Federal Office of Meteorology and Climatology MeteoSwiss, 2023). Meanwhile in literature different lapse rates for temperature interpolation are used, as for example $-0.008° \frac{C}{km}$ by Juen et al. (2014), as determined for the ablation season by Han et al. (2008). This lapse rate is specifically designed for the Koxhar glacier in the Tien Shan at an elevation of 3000 meters above sea level. It is not clear whether it would be suitable as a guideline for the Griess Glacier in this thesis. That is why the Swiss guidelines of the Federal Office of Meteorology and Climatology MeteoSwiss (2023) were used.

The PDDF was calculated by the help of the stake measurement, combining the measured ablation with the measurement interval length (days) and the elevation adjusted PDDs.

Using the PDDF per ablation stake, the variation in melt can be visualised across the glacier. The PDDF can be used to correct the local ablation per stake to compensate for missing data points in the stake measurement. This would be useful in case some stakes melt out of the ice before the end of the measurement period. The corrected stake ablation and the local debris thickness can then be used to visualize the impact of the glacial debris cover on the ablation. This potential relation can then be approximated using a formula which is given by the trendline of PDDF and debris thickness. It has to be kept in mind that this is not a definitive relation and that there are deviations, since this might not be a perfect relationship. Juen et al. (2014) suggest that the relationship between PDDF and debris cover thickness follows an exponential curve, underlining that fact with a correlation factor of $R^2 = 0.92$. In contrast to this study on Griessgletscher where 8 stakes locations are sampled, Juen et al. (2014) evaluated the PDDF at over 20 locations.

Using the debris thickness data collected, an estimation of the debris cover distribution over the whole glacier can be done. Further combining the debris cover distribution and the relation formula of the PDDF and the debris cover thickness, an estimation of the ablation per degree and day is derived (Eq 1.: in m w.e.; Eq. 2; in m ice loss). Factor Equation 1 with the glacier area, the total melt over the whole glacier is estimated in m^3 water.

Equation 1: The calculation of the ablation per m^2 in m w.e. [Ab = Ablation]

$$Ab = \frac{(\frac{PDDF * PDD * 0.9}{Area})}{1000}$$

Equation 2: The calculation of the ice height loss per m^2

$$Ab = \frac{(\frac{PDDF * PDD}{Area})}{1000}$$

This could then be compared to the lake water level data. Therefore, it might be possible to see, whether the glacier discharges into the lake or whether a large part of the occurring melt is released into the underground before impacting the lake level.

Within this study, the time frame of research starts on the 27.06.2023 and ends on the 01.10.2023. This frame is defined by the installation and the last sampling and retrieval of the ablation stakes on Griess Glacier, and the drone survey performed on these days.

4.6. Wide angle camera Tikee3

The wide-angle camera Tikee3 has been installed to gain a visual insight into the changes of the glacier lake und the glacier front over course of the ablation season. Tikee3 is produced by the

Figure 18: Tikee3 camera placed on the ridge of Raustöckli on May 25th (black-and-white box in bottom-right corner). The lake was still ice covered and barely visible in the middle of the picture. The Griess Glacier extends to the right-hand side and in the top right corner hidden by the clouds is the Clariden.

company Enlaps. The Tikee3 is a two-lens camera covering an angle of 220° and an included solar panel to keep battery levels up for as long as possible. The camera was installed on the 25th of May, on the ridge of Raustöckli (figure 18), where it was presented with a perfect overview for the photographical survey of the glacier and the lake. It was set to an interval of 1 hour, starting at 3 am and ending at 11 pm, resulting in 21 images per day. These timestamps were set to additionally capture the sunrise and sunset as well. But towards fall, more images were in complete darkness, since the sun rose later and set earlier.

Using the acquired images, a visual comparison was conducted to see, whether the pressure sensor in the lake registers water level changes and if they are visually comprehensible. Additionally, the images are used for event detection. They were screened for calving events or ice avalanche to determine whether the pressure sensor also recorded anomalies in the same timeframe. Maybe even the impact of the event on the pressure logger in the lake could be revealed.

4.7. Meteostation

A compact meteostation (Figure 19). was installed on Melchbödmeli (2050m a.s.l.) below the large moraine bastion It was a self-built model by Felix Ziegler. The meteostation measured temperature, air pressure, relative humidity and the cumulative amount of incoming rainwater in 30 minutes interval and uploaded the data into a server cloud, to always be accessible. In this study the meteostation will be referred to as 'KLAU', in reference to Klausenpass. As already implied, the data recorded by KLAU will later be used to extrapolate temperature data for the positive degree day method, and the rain data is used to be compared with the data of the water discharge from the resurgences on Urnerboden, to see how big the delay of rain and routing is.

Figure 19: Meteo station 'KLAU' on Melchbödmeli.

4.8. Snow melt analysis using logger data

To see trends in the snow melt and corresponding water discharges, dataloggers installed at the springs and the lake had to be analysed. These sensors measured pressure in a thirty second interval to find out about water level and water temperature fluctuations. These fluctuations can then be used to identify daily and seasonal changes in the discharged water similarly to what has been done by Brown et al. (2006). For the lake sensor it is hoped that as well larger calving events can be observed.

Griesssee pressure logger:

A big rock on the shore was used to bind the logger encased in a metal tube to. The logger was then hooked on a leash and put as far out in the water as the leash length would allow it. When placed in May, the rock was accessible over a heap of snow and the water surrounding the stone was about 30 to 50 centimetres deep and frozen over. Therefore, a hole had to be poked into the ice to let the sensor descend into the water. The lake sensor was in place from 13.06. until 02.09., which is a total length of 82 days.

Chlus and Waldhüttli pressure loggers:

A second datalogger, measuring pressure and additionally temperature, was placed in the cave entrance of the Chlus cave at the end of march. Using the acquired data on this logger, it can be derived whether that cave system is snow melt driven or relies on different water inputs from somewhere else. If the melt water signal continues until August or never ends, it would indicate that somewhere in the catchment of this spring a glacier is releasing melt water into the karst network.

The sensor was also encased in a metal tube for protection. A whole was drilled in the cave floor at an appropriate height (see Appendix 6), so that the end of the metal tube was totally submerged and would not lose contact to the water, even when water levels are very low. The cave entrance is at the foot of the Chlus cliff (see Appendix 2).

On the same day as the Chlus-logger was installed, another logger was set into place. The third logger was placed at the "Waldhüttli" spring on Urnerboden (see Appendix 3). This spring is very large, discharging over 10'000 litres per minute according to GeoUri (Lisag AG, 2023). This sensor was also measuring temperature and pressure, in an interval of every 30 seconds.

Both sensors were installed on the 24th of March and taken out on the 3rd of September. They were in place recording data for a total of 164 days straight. At Waldhüttli a new sensor was installed to measure the spring's discharge throughout the winter season of 2023/24.

4.9. Tracer experiments

To trace back the connection of the waterways, tracer experiments were conducted using the fluorescent and environment friendly tracer dyes Uranine and Rhodamine WT. If introduced into a stream, the dye is distributed in the water, and imitates the water flow. Therefore, flowtimes, and water flow connections can be retraced.

The tracer dyes are introduced into the waterways at specific locations, for example shortly before the water is disappearing into a creek swallet, into a subterranean or subglacial stream. In this experiment, conservative tracers are used, since they are known for good water dynamics imitations and therefore of good use for research on water flow connections and flowtimes through cave systems (Goldscheider et al., 2008)**.** Tracers as Uranine are of advantage, due to them being traceable to around 10^{-3} micrograms per litre (Table 4).

So even if it was highly diluted, the fluorometers would still pick up a signal. These fluorometers are placed at different water resurgences on Klausenpass and Urnerboden, to detect any remainder of tracer which could be leaving the underground water ways through that spring.

Table 4: Fluorometers produced by two different companies were used (Albillia Fluorometers, 2023; Turner Designs, 2023).

FLUOROMETER	MANUFACTURER	ORIGIN	MINIMUM DETECTION LIMIT
CYCLOPS-7	Turner Designs, Inc., produced by PME, Inc.	UZH	0.01 ppb
TURNER-C3	Turner Designs, Inc.	UZH	0.01 ppb
ALBILLIA GGUN-FL30	Albillia Sàrl	WSL	$2*10^{-11}$g/ml typical (Uranine)

The surveyed springs were selected according to their importance, which is derived from their water output per second. This value is derived from the data acquired by the Canton of Uri (Lisag AG, 2023), who provides information on every spring in the area with a discharge larger than 100L/min. Prioritized were springs with a discharge larger than 10’000L/min, follow by those discharging between 1000L/min and 10’000L/min. Springs with discharge information below 1000L/min were deemed insignificant for the purpose of this project. Also, the location of the springs had to be in an area where it is probable for water to flow to through the underground from potential injection sites. Therefore, the spring at Riedrütenen was not considered, which lies on the northern slopes of the Urnerboden Valley. Its water potentially originates from outside the zone of interest to this study and is therefore neglected in the conducted experiments. The most important springs are the Chlus spring (KL-CHH, Figure 20, number 1) and both Waldhüttli springs. There is one entering the Fätschbach on ground level, flowing directly out of the wall (KL-WHB) and a second one about 15 meters up the wall. The latter will be referred to as ‘Waldhüttli Waterfall’ (KL-WHF, Figure 20, number 2) and the other one as ‘Waldhüttli Bach’ (Figure 20, number 3).

Table 5: Information on the name giving of tracer injection sites and springs all around Klausenpass and Urnerboden. The names consist of the region 'KL' = Klausenpass, and two letters of their name 'GF' = Griessfirn. The third letter is to simplify and distinguish two points at the same location.

Injection sites		**Springs and fluorometer locations**	
Short	**Location**	**Short**	**Location**
KL-GFB	Chammli-Griessfirn Gletscherbach	KL-WHF	Waldhüttli Wasserfall
KL-GLH	Griessloch Höhlenbach	KL-WHB	Waldhüttli Bach
KL-GPB	Gämschplanggen Chammlibach	KL-CHH	Chlus Höhle
KL-GRS	Griess-See Gletschersee	KL-CHQ	Chlus Quelle (Höhle)
KL-GTB	Gletschertunnel Bach	KL-CHF	Chlus Wasserfall
KL-CBP	Chlaridenbödmeli-Ponor	KL-GGB	Griess Gletscher Bach
KL-MBB	Mälchbödmeli-Bach	KL-RSB	Ribi Schächen
		KL-FBS	Fätschbach See

For all tracer studies to be conducted, multiple injection sites have been determined (Table 5). One of them was Griessloch, a cave in the Clariden North wall, located about 100 meters above the ice of the Griess Glacier. Another location is the small stream which leaves the ice cave, south

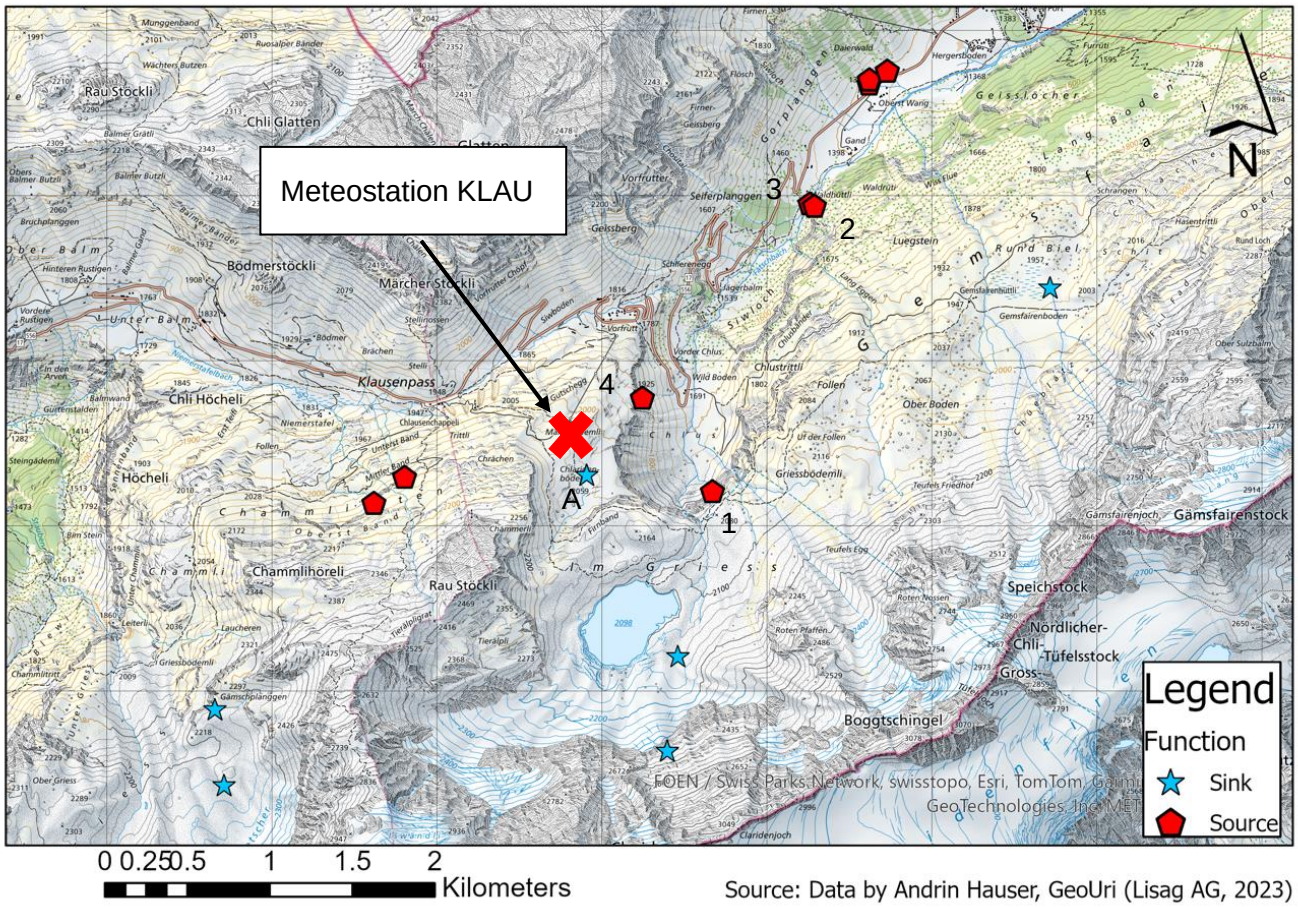

Figure 20: Map of Klausenpass, Griess glacier and parts of Urnerboden, locating sources and sinks in the area of interest. Most but not all the illustrated datapoints will be inspected and included in the study of hydrological network. (1): KL-CHH; (2): KL-WHF; (3): KL-WHB; (4): KLCHQ.

of the lake. This small stream crosses an ice-free area and then resubmerges beneath the glacier ice again, to not resurface again in a similar size. Also, according to personal recommendations by the geologist Tobias Ibele (unpublished, n.d.), the area on the western side of the Klausenpass, north of Chammliberg and Schärhorn also provide some dolines. There is a chance that this water could flow past the Klausenpass in the underground and resurface somewhere at Urnerboden. He based this thought on the geological structure in the underground, where the Griessstock-nappe inclines towards east to Urnerboden. This nappe is potentially a water confining layer and therefore directs the water eastwards where it could resurface (Ibele, n.d.).

The map in Figure 20 shows all important and sampled springs and injection sites (sinks) in the Klausenpass area.

The first tracer experiment was also to test the fluorometers. There is a small creek swallet, located in midst of the Chlaridenbödmeli (KL-CBP). The Chlaridenbödmeli is a flat plain located below the moraine bastion approximately 750 metres north of Griesssee (Figure 20, A; Figure 21). The creek flows across the plain and ends in a pond of about 4 square meters in size, where the water infiltrates into the ground through small ponors. The maps of SwissTopo (2023) further show the presence of two additional dolines on this plain, while the surveyed sinkhole possibly is the remainder of a third one.

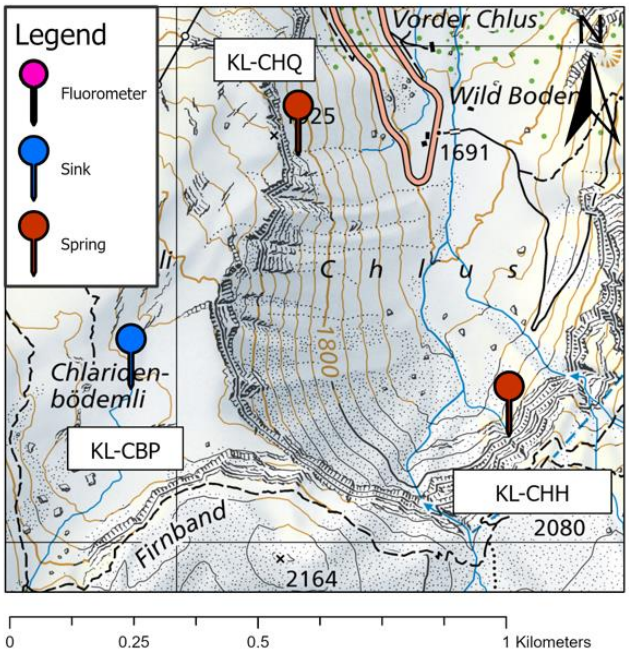

Figure 21: Map of KL-23-01-CBP-UR, injection site in blue and the springs in red

The aim was to find out about the underground connections and where the water draining into that ponor is directed to. To measure the Uranine concentration at possible springs, two fluorometers were installed at separate locations. Since the Claridenbödmeli is located right above the Chlus cliffs, it was suspected that the geographically and topographically closest springs in the cliffs are potential outlets of the underground waterways. 2 different kinds of fluorometers were used for this first tracer study, but both possess similar kinds of sensors and are capable of similar performances according to the producers (see Appendix 5; Turner Designs (2023)). Some further specifications on the fluorometers are listed in Table 4. The cyclops-7 datalogger was placed in the creek resurfacing in the Chlus spring. Meanwhile the Turner C3 logger was installed in the creek below the Chlus West Spring (Figure 20, number 4; Figure 21). This small water resurgence was the suspected spring for the tracer-containing water.

On the 13.06 at 10:28 UTC, 20.05g of Uranine was injected into the pond with the swallet (see Appendix 7).

The tracer injection of *KL-23-02-GLH-Ur* took place at the cave stream of Griessloch, performed by three members of the OGH; Res Link, Yannick Baebler and Fabrice Franz. The Griessloch cave is situated in steep terrain, approximately 100m above the glacier in the Clariden North Face. About one hours of way into the cave, a small stream flows through the cave. The water emerges from within the mountain only to vanish shortly after in another sinkhole. This was an optimal location for a tracer injection, since it is neither known where this stream of water is coming from, nor where it resurfaces. Accordingly, Uranine was injected in said stream in the Griessloch cave,

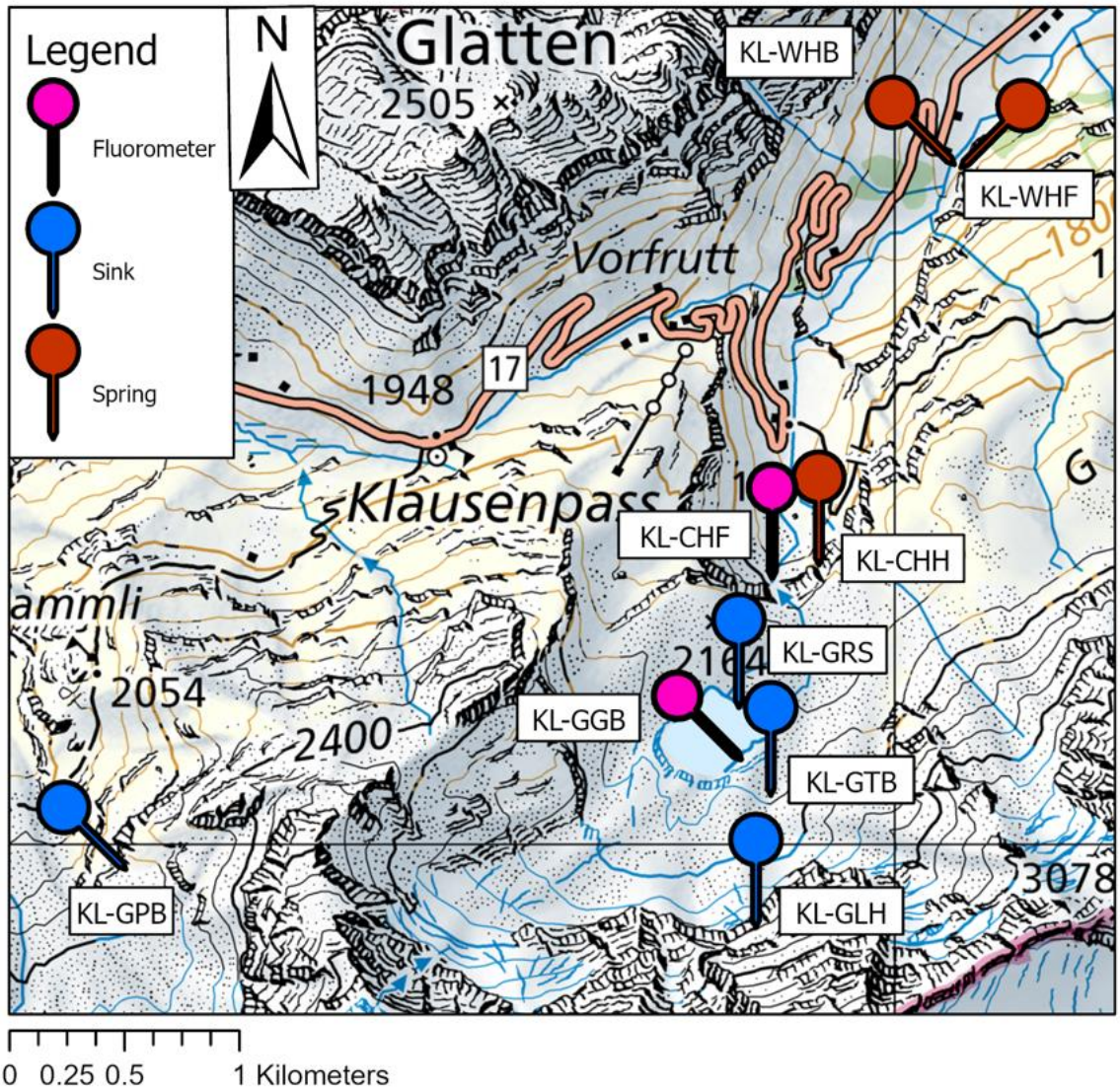

Figure 22: Map of all important locations which were a part of KI-23-02, KI-23-03, KI-23-04, KI-23-05. Beside the sinks, also springs and placed fluorometers are signalled.

in hopes that it reemerges at one of the sampled springs. If the Uranine was detected by one of the sensors, it would provide further insight into the hydrological system of Klausenpass and the

surrounding area. 51.32g of Uranine water tracer was injected at 11.00 (09:00 UTC) on Monday 04.09.2023 (Figure 22, Appendix 8).

On the same day 50ml of Rhodamine WT (KL-23-03-GTB-Rh) was injected at the Glacier Tunnel (KL-GTB, Figure 22, Appendix 9). At this location water is leaving a large ice tunnel and submerges 100 meters further downstream again underneath the ice. The goal is to find out which where this water stream is flowing to. There are several possible outcomes. Either the water flows along the glacier side on to the plain within the eastern moraine walls, joins the Fätschbach and flows down the waterfall. Another possible outcome is, that the stream somewhere submerges into a ponor into the ground. It could then end up at multiple different locations, but the two Waldhüttli springs are a valid option due to their high stream flow. A third possible flow path is, that the glacier is building an impermeable blockade to the front, and that it would therefore travel northbound into the lake, where indeed a set of small streams of water is emerging through gravel, supposedly from below the ice wall.

Also, for KL-23-06-GRS-Rh Rhodamine WT was introduced at the lakefront on the east shore later on the same day (see Appendix 10). It was poured in at several different locations, some of which seemed to show some flow direction towards the lake shore and some of which were close to the lake outflow. Aiming to find red coloured water infiltrating the moraine debris, that could give away another outlet of the lake. If there was another outflow, it would explain the decline of the lake water level even if the lake outflow was dry.

Figure 23: Fluorometer placed in the Waldhüttli Bach spring, where the water emerged through a pile of rocks.

The next study was conducted on the following day at a different location. The experiment was expanded to the other side of the Klausenpass in the Schächen Valley right below the Chammliberg. Uranine was introduced into a creek which ends into a sinkhole, covered by gravel behind the side moraine of the other glacier called Griessfirn. The introduction point was at Gämschplanggen at the coordinates 2'706'794.8, 1'189'905.6. This location was suggested by Tobias Ibele, aiming to find out, whether the subterranean waterways direct the water underneath the Klausenpass, to the Chlus spring or another resurgence on Urnerboden.

Accordingly, on Tuesday the 05.09.2023, at 13:27 MET (11:27 UTC), 100.00g of Uranine were injected into the creek. It took the Uranine almost an hour to completely infiltrate into the underground.

The results acquired through the latest experiments were not totally definitive and did leave open questions which were only to be answered through follow-up studies. Therefore, the introduction sites on the western side of the Klausenpass were tested again 4 weeks later. Yet not only was Rhodamine WT introduced into the sink at Gämschplanggen (KL-GPB), but also Uranine into the ponor beside the glacier (KL-GFB, 2'706'739.5, 1'189'411.9). Now, a clear differentiation between the two tracer colours should be visible on the sensors, placed once again in the KL-CHH, both KL-WHB and KL-WHF (Figure 23), and additionally this time into the Vorder Schächen close to Ribi (KL-RBS), where the mountain stream is flowing down to Altdorf UR.

The injection sites and the sampled springs of the experiments of the 27.09 are presented on the map in Figure 24.

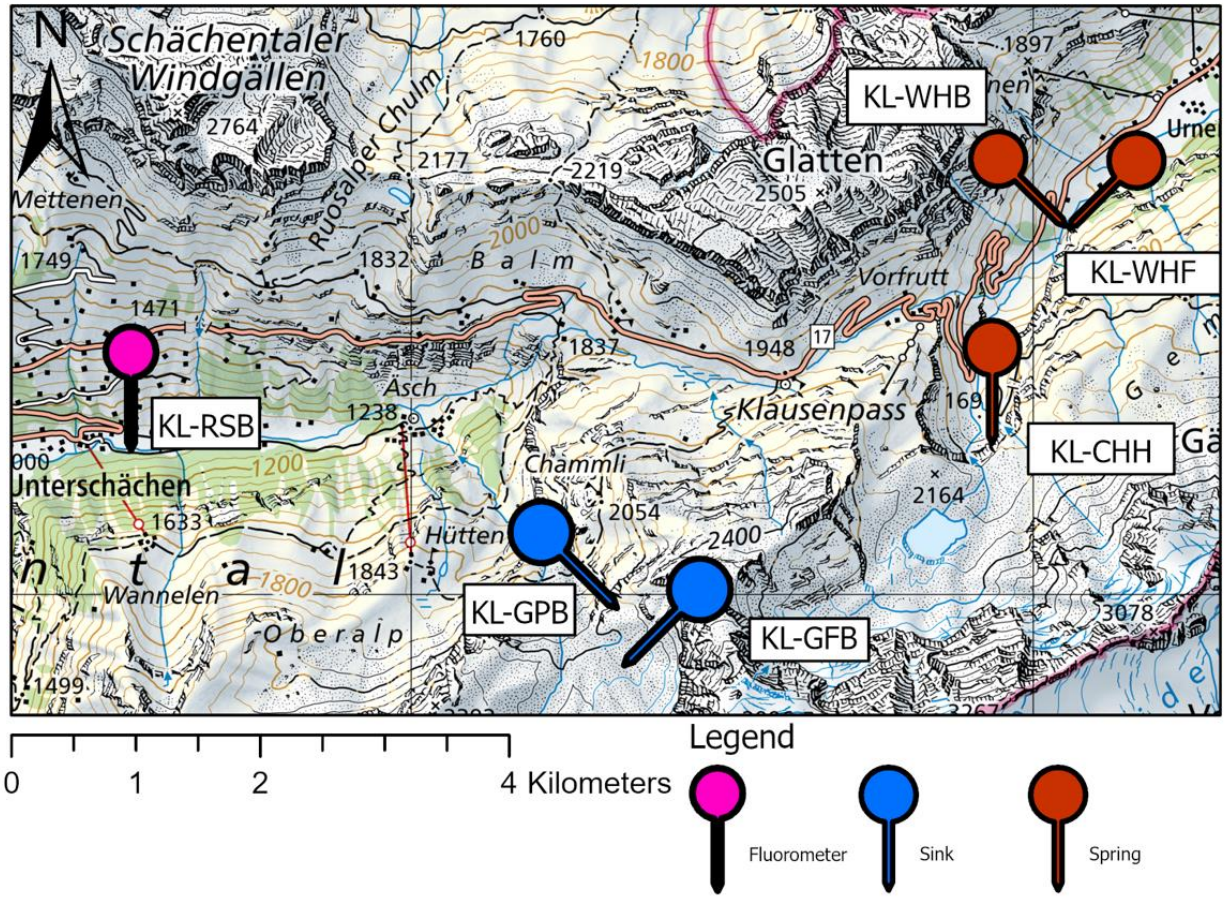

Figure 24: Map of the experiments conducted on 27.09, all sampled locations are marked. The fluorometer at Ribi is not bound to a spring, it is placed in the river. The other fluorometers were placed right at the emergence and therefore labelled with 'Spring'.

5. Results

5.1. Meteorological survey of the area

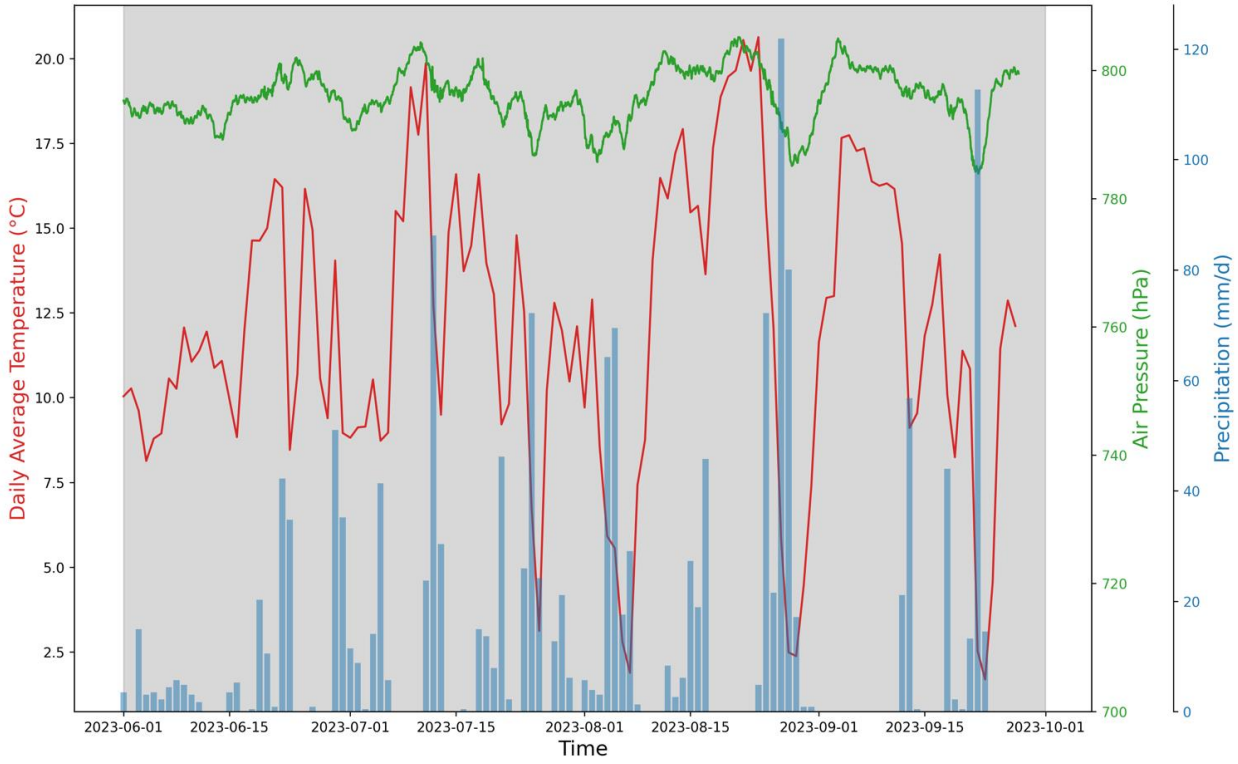

Figure 25: Meteogram of the weather conditions during the summer months.

Acquired from the meteostation KLAU set up on Melchbödmeli, the data is summarized in Figure 25 into a meteogram. The average daily mean temperature recorded over the summer is 11.9°C. During the course of the summer, there are four major temperature drops, on 26.07, 07.08, 29.08. and on 23.09. As displayed by the air pressure curve, these temperature drops also come with major drops in air pressure, especially on 28.08. and 23.09. All the major temperature and air pressure drops are also accompanied by three of the larger precipitation events. During the most recent events, the pluviometer recorded about 120 mm of precipitation per day. Contrastingly, between the 1st of September and the 11th of September there was a dry phase with no precipitation at all.

5.2. Hydrological analysis

As introduced earlier, a first tracer study (*KL-23-01-CBP-Ur)* was conducted to gather first insights into the hydrological system. After the Chlaridenbödmeli injection, several more tracer studies were conducted (Table 6). They were necessary due to potential mixing of the signals in the result data of the studies *KL-23-02-GLH-Ur, KL-23-03-GTB-Rh, KL-23-04-GPB-Ur, KL-23-05-MFB-Rh* and *KL-23-06-GRS-Rh.* Therefore, the Gämschplanggen injection of KL-23-04-GPB-Ur had to be repeated to avoid data confusion.

Table 6: Overview on all tracer studies performed on Klausenpass in 2023.

Name	Location	X	Y	Time UTC	Tracer	Amount
KL-23-01-CBP-Ur	Chlaridenbödmeli-Ponor	2708940	1191370	13.06.2023 10:28	Uranine	20.05g
KL-23-02-GLH-Ur	Griessloch Höhlenbach	2709280	1189580	04.09.2023 09:41	Uranine	51.32g
KL-23-03-GTB-Rh	Gletschertunnel Bach	2709400	1189900	04.09.2023 12:01	Rhodamine-WT	50ml
KL-23-04-GPB-Ur	Gämschplanggen Chammlibach	2706740	1189910	05.09.2023 11:30	Uranine	100.0g
KL-23-05-MBB-Rh	Mälchbödmeli-Bach	2708940	1191480	05.09.2023 15:30	Rhodamine-WT	20ml
KL-23-06-GRS-Rh	Griess-See Gletschersee	2709270	1190640	04.09.2023 16:00	Rhodamine-WT	30ml
KL-23-07-GFB-Ur	Chammli-Griessfirn Gletscherbach	2706590	1189300	27.09.2023 12:44	Uranine	199.44g
KL-23-08-GPB-Rh	Gämschplanggen Chammlibach	2706750	1189910	27.09.2023 13:30	Rhodamine-WT	100ml

In KL-23-01-CBP-Ur, Uranine was introduced into the water sink at Chlaridenbödmeli. 20.05g of Uranine tracer were used. 3 hours later, the sensor at Chlus spring (KL-CCH) recorded an Uranine signal. Also, the visual feedback of Fätschbach was positive (Figure 26). The stream turned greenish for more than one hour. This tracer test was the only one with a bell-shaped unimodal breakthrough curve (see Appendix 13). About 87.5% of the tracer were recovered.

The linear distance between sink and source is about 800 metres, but the water had at least a distance of 1.2 kilometres to cover, since it had to stay within the wall of the Chlus.

For the second set of tracer field studies, six fluorometers were installed at different locations throughout the Klausenpass and the Urnerboden area. In addition to the Chlus spring, also the Fätschbach waterfall in the Chlus, the Waldhüttli Bach spring and Waldhüttli Waterfall spring, as well as the Fätschbach lake on the eastern end of Urnerboden were sampled. The sixth sensor was initially placed on the gravel bank between the glacier and the lake shore, south of Griesssee. It was later moved to the Chlus West for the rest of the day, to see whether this spring is also connected to the sampled system.

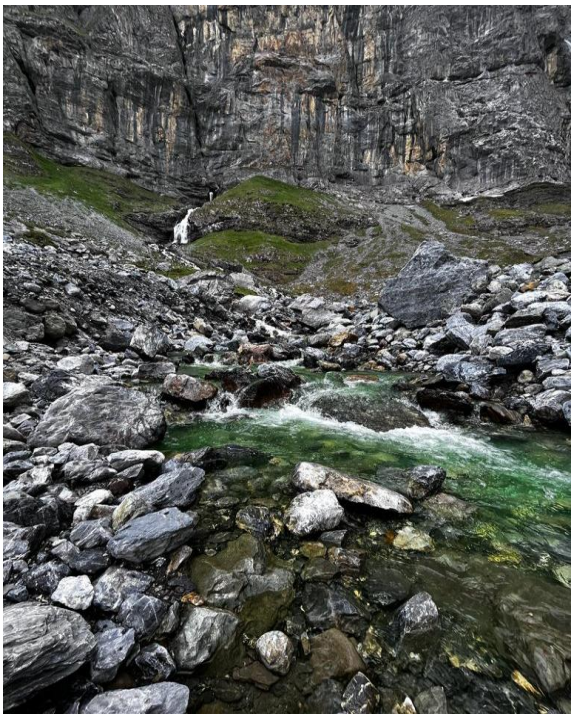

Figure 26: The greenish Fätschbach at KL-CHH, after the tracer injection on Chlaridenbödmeli (KL-23-01-CBP-Ur). The Chlus spring is visible in the background, above the small waterfall.

For KL-23-02-GLH-Ur, 51.32g of Uranine were injected into the cave stream at Griessloch in the Clariden north face. As a result, an Uranine signal was detected fitfully at the Waldhüttli Waterfall

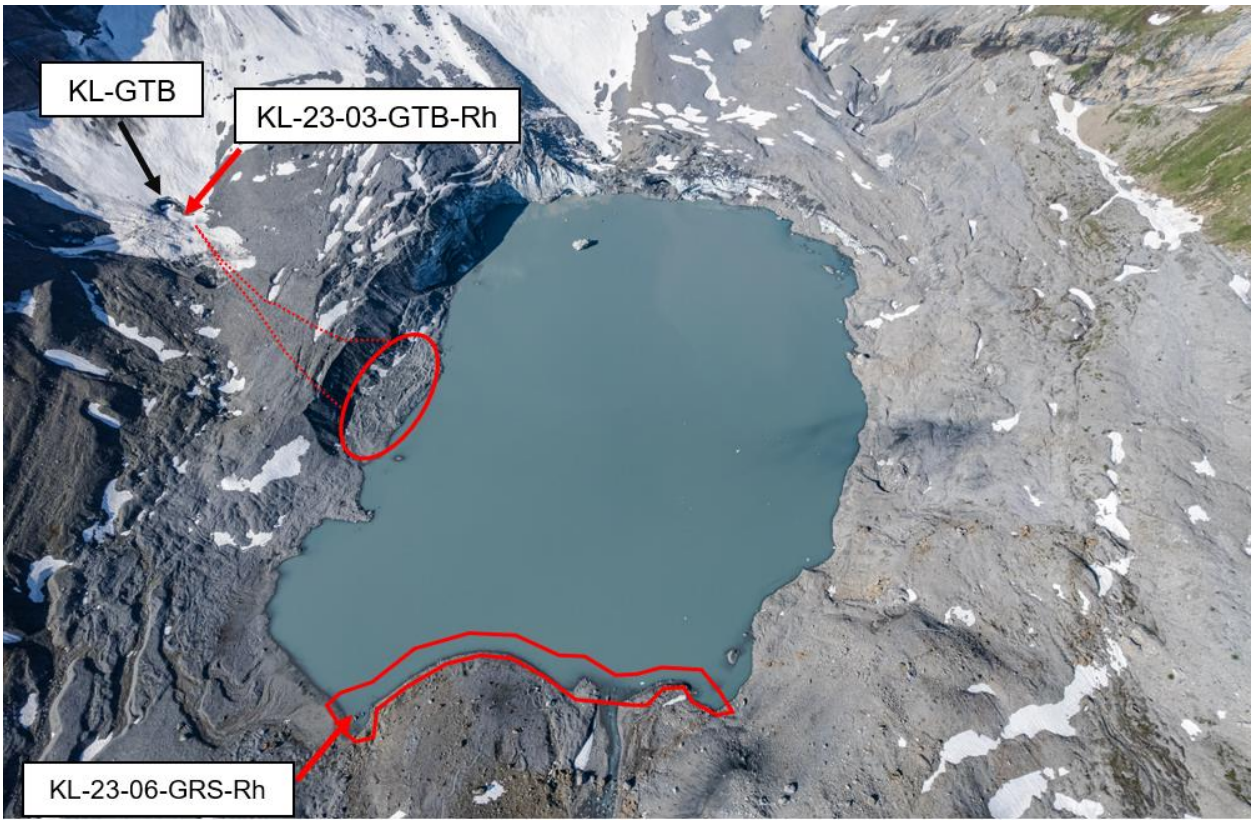

Figure 27: Aerial view of the Griesssee with the Griess Glacier in the upper half of the image. Injection sites are marked with a red arrow and red locations mark where Rhodamine WT introduced. Image by Pfau (2023).

spring as seen in Figure 28. Commonly in a tracer experiment, the tracer breakthrough curve follows the distinct pattern of a bell-shaped curve with one or two peaks (unimodal or multimodal) and a long fade out tail (Benischke, 2021; Leibundgut & Seibert, 2011). But this is not the case for the Uranine signal at Waldhüttli Waterfall. About 10 hours after the injection, the sensor at the Waldhüttli Waterfall detected a signal of Uranine. It appeared with a continuous but strong increase in concentration, then vanished abruptly. The following 12 hours the signal was weak or non-existent. Then it suddenly reappeared again, resulting in a new and second peak, only to vanish again. This pattern continued in that manner in a frequent time interval.

At 12:01:30 UTC 50ml of Rhodamine WT was introduced at the Gletschertunnel Bach (KL-GTB). 20 minutes later the water emerging from the debris below the ice wall into small water streams started to colourize reddishly (KL-GGB, Figure 27). The amount of water flowing from the ice wall to the lake was not comparable to the streamflow where the Rhodamine WT was introduced. The ice tunnel stream carried more water, but it is difficult to determine the ratio, since the water leaving the ice wall was spread over various runnels emerging at different locations. The first coloration was for example discovered in a puddle which appeared to not contain any water flow but only residual water.

The results for this part of the experiments are not very distinct, since they seem to blend in and mix with the tracers introduced the day before. No clear results were produced from that, but nonetheless, the recorded data indicates the potential arrival of Uranine from Gämschplanggen on the 6th of September at Waldhüttli Bach, as seen in Figure 28. To produce additional data to support what has been indicated in KI-23-04, additional tracer studies from ‘Chammli-Griessfirn Gletscherbach’ were initiated.

The navy-blue coloured line in Figure 28, the behaviour of Waldhüttli Waterfall spring is displayed. Abrupt and simultaneous drops of Uranine-, Rhodamine WT- and Turbidity-levels are seen within the first 24 hours. After the 3rd peak, the Uranine curve seems to decouple from the other two, only leaving Turbidity and Rhodamine WT behaving similarly. However, the Waldhüttli Bach (Figure 28, orange curve) shows a different behaviour. Having a very low Uranine level in the beginning, to then becoming highly variable in the afternoon of the 06.09. On the other hand, the Rhodamine WT level is very unstable before the Uranine peak, yet on a low level. Once the Rhodamine WT curve calms, the Uranine starts to increase.

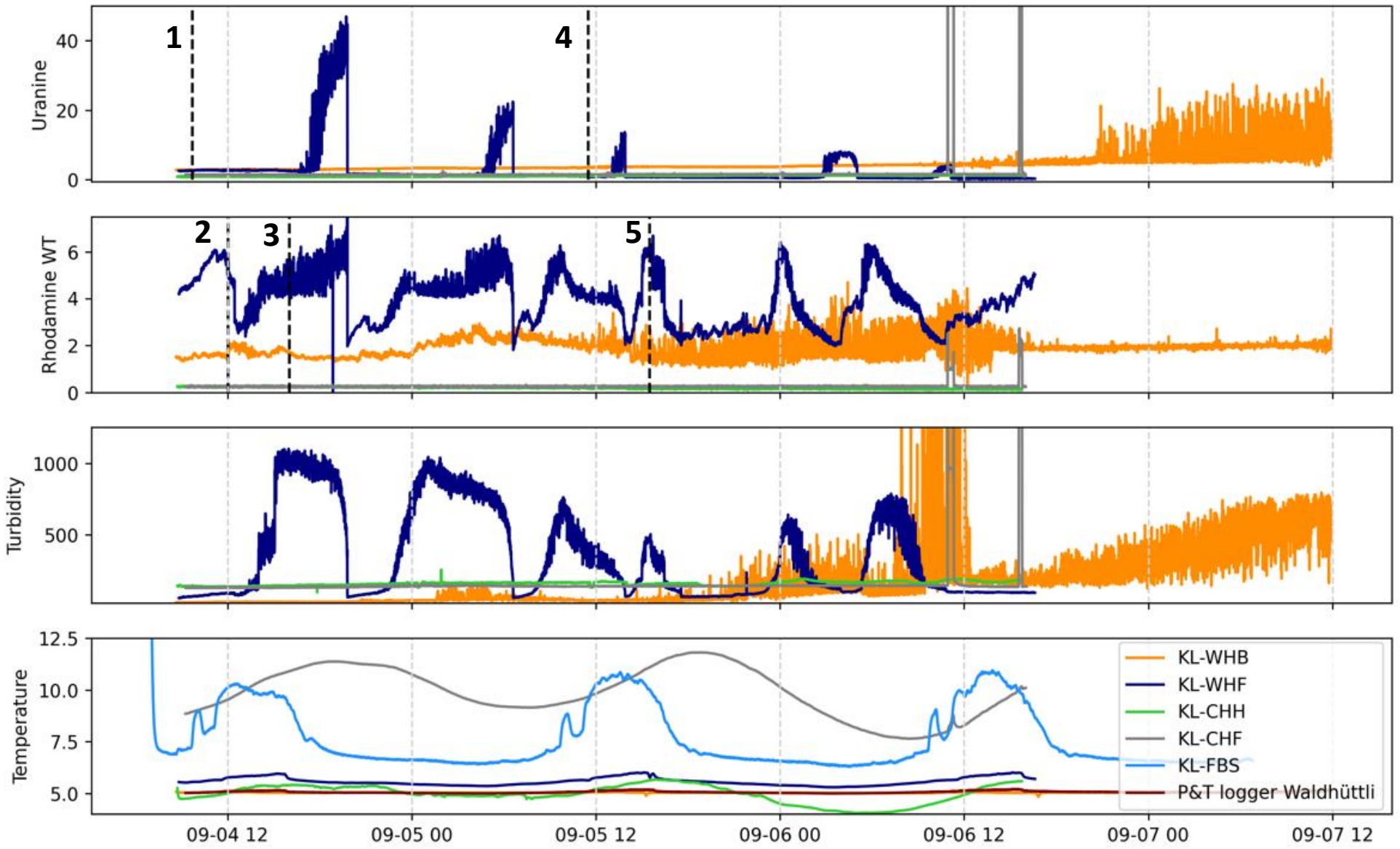

*Figure 28: Recorded data from tracer experiments on 04.09 and 05.09, split into the 4 sensory channels. Each colour representing a spring in the area. Very diverse behaviours of the springs are coming forth. The line marks stand for the tracer injections (**1**) KL-23-02-GLH-Ur, (**2**) KL-23-03-GTB-Rh, (**3**) KL-23-06-GRS-Rh, (**4**) KL-23-04-GPB-Ur and (**5**) KL-23-05-MFB-Rh.*

Interesting to see is the behaviour of the two sensors at the Chlus (KL-CHH, KL-CHF). Both are not reacting at all to either of the two tracer signals, Chlus Spring being completely low level on all curves constantly. Chlus Waterfall only shows two spikes, but simultaneously on all 4 sensor bands. On the 6. September, 10.55 UTC (double peak, second spike at 11:20) and at 15:34 UTC, Uranine, Rhodamine WT and Turbidity bands show strong increases in concentration levels, only to drop quickly again within 30 minutes. Additionally, the temperature curve shows a slight change of behaviour in those time frame, having recorded a slight abrupt temperature difference. Additionally, the lowest subplot of temperature also shows the data recorded by the Cyclops fluorometer. It was placed in the lake at the end of Urnerboden (KL-FSB). It recorded temperature changes of almost 2°C within 24 hours, displaying a frequent and steady curve route. Except that the temperature curve displays a sudden temperature drop only to be followed by a sudden increase again at 10:40 UTC in the morning, which is briefly before 13.00 local time. Simultaneously, the temperature curve of KL-WHF shows a daily variable behaviour, showing the highest temperature peaks in the afternoon at 3.10pm UTC and lowest temperatures 12 hours shifted at around 3.30 UTC in the morning as presented in figure 29. Interestingly, the temperature sensor of KL-WHB recorded a drop of 0.2°C for a period of 20 minutes in the afternoon at 15:15 UTC on the 5th of September and on 16:50 UTC one day later. As visible in Figure 29 the three temperature curves are very different for the fact, that they are all located in a radius of 10 meters. Even the pressure sensor of Waldhüttli (KL-WH) which supposedly sampled the same spring as the fluorometer, just at another exit, has a totally different temperature course. It is closer to the course of KL-WHF, however it is less pronounced.

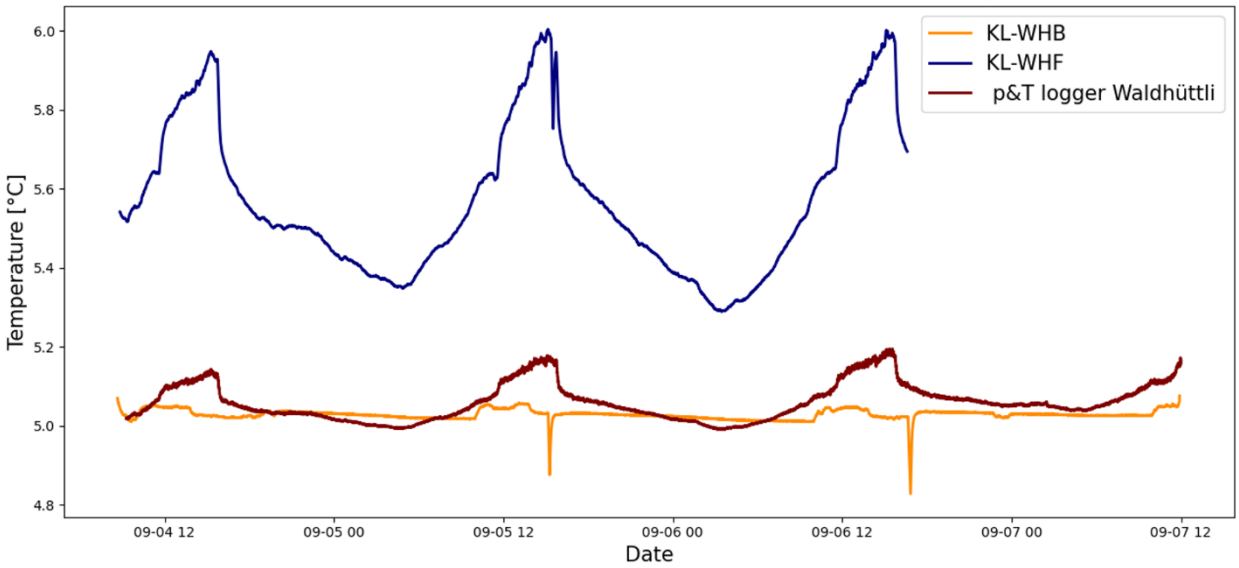

Figure 29: Comparison of the three temperature sensors during the second set of tracer studies. Waldhüttli Bach (KL-WHB) and Waterfall (KL-WHF) are fluorometers and p&T logger Waldhüttli was the pressure sensor located at a different outlet of the Waldhüttli Bach spring. KL-WHB and KL-WHF were assumed to be same spring or cave network, but they show different patterns in temperature behaviour. All three spring outlets display drastic temperature drops in the afternoon, while KL-WHB displays such behaviour only on the 05.09. and on the 06.09. but not on 04.09.

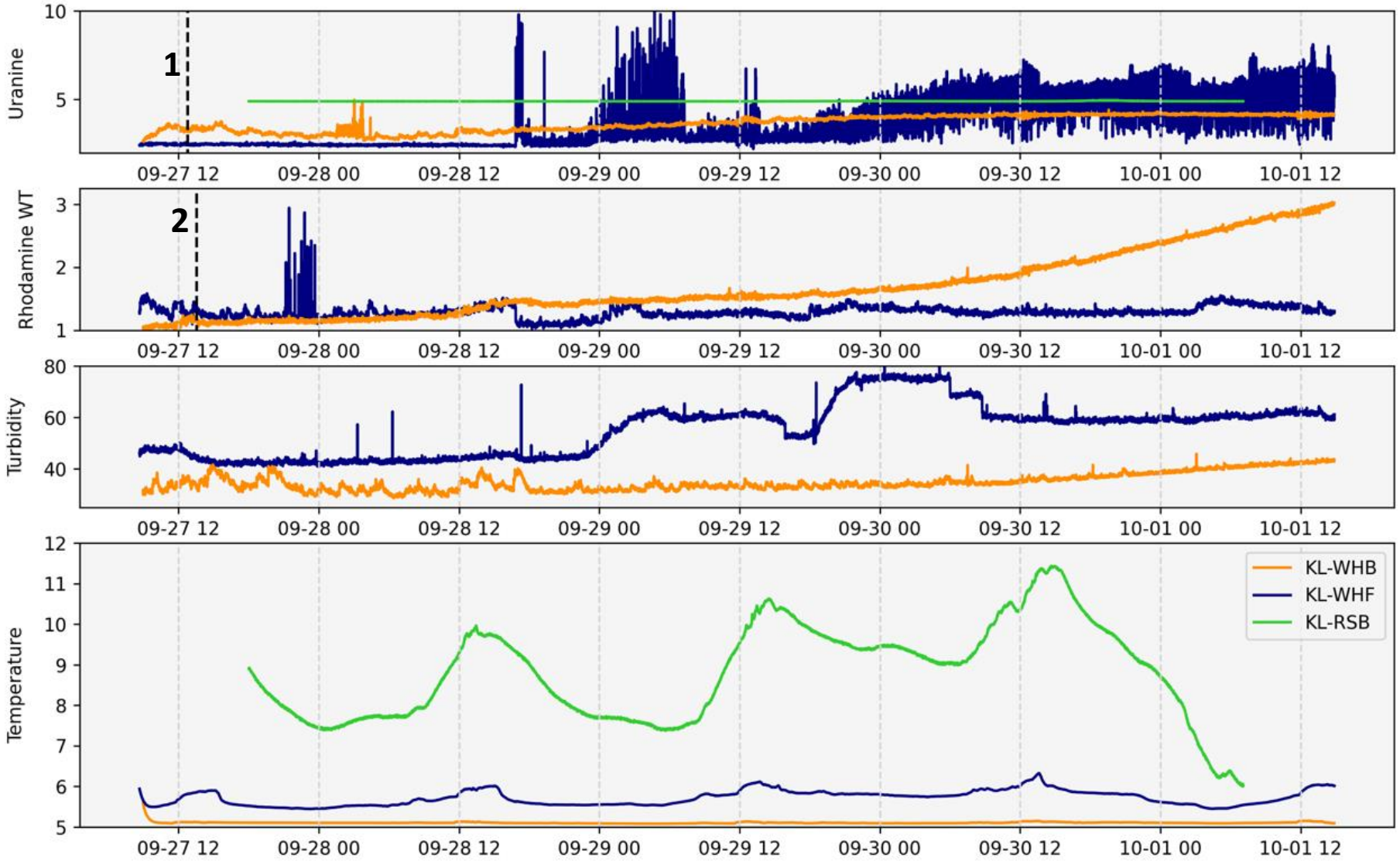

*Figure 30: The results of tracer experiment KL-23-07-GFB-Ur (**1**) and KL-23-08-GPB-Rh (**2**) which have been conducted on the western side of Klausenpass. After the tracer injections the sensors placed in different locations recorded the illustrated signals. Even though a sensor was placed in the Fätschbach at Chlus spring, it did not register a signal and is therefore left out of this plot. The Uranine curve of Ribi has been elevated by 5. It looks like no signal was recorded, but a weak almost undiscernible signal peak exists.*

The last set of tracer tests (KL-23-07-GFB-Ur and KL-23-08-GPB-Rh) was performed on 27.09. The sensor at Chlus did not show any signal at all, while the fluorometers at Waldhüttli again indicated a connection between Urnerboden and Gämschplanggen.

Uranine levels at Waldhüttli Bach (KL-WHB) were stable, however Rhodamine WT levels seem to increase over the course of the experiment. The experiment seems to have come to a halt in the middle of the constant rise of Rhodamine WT levels. Meanwhile the spring Waldhüttli Wasserfall (KL-WHF) shows a contrasting behaviour, having recorded a high variability in Uranine from 16.50 UTC of the 28th of September on. But not expressing clear peaks only increasingly high variability, combined with a slight rise of the curve. Included in the Uranine graph (Figure 30) is also the measurement of Ribi (KL-RSB), where only the Uranine concentrations have been measured. The curve of KL-RSB has been elevated by 5, since the cyclops sensor data was not calibrated and therefore showed negative results. Nonetheless, the sensor displayed relative changes and recorded a signal about 48 hours after the introduction. The peak is apparent, when displayed on its own (Figure 31). However, the signal's amplitude is only about 0.07 which indicates only very little change in comparison to the measured signal of before, but still some sort of signal was picked up by the Cyclops-7 which means that at least parts of the Uranine came through here.

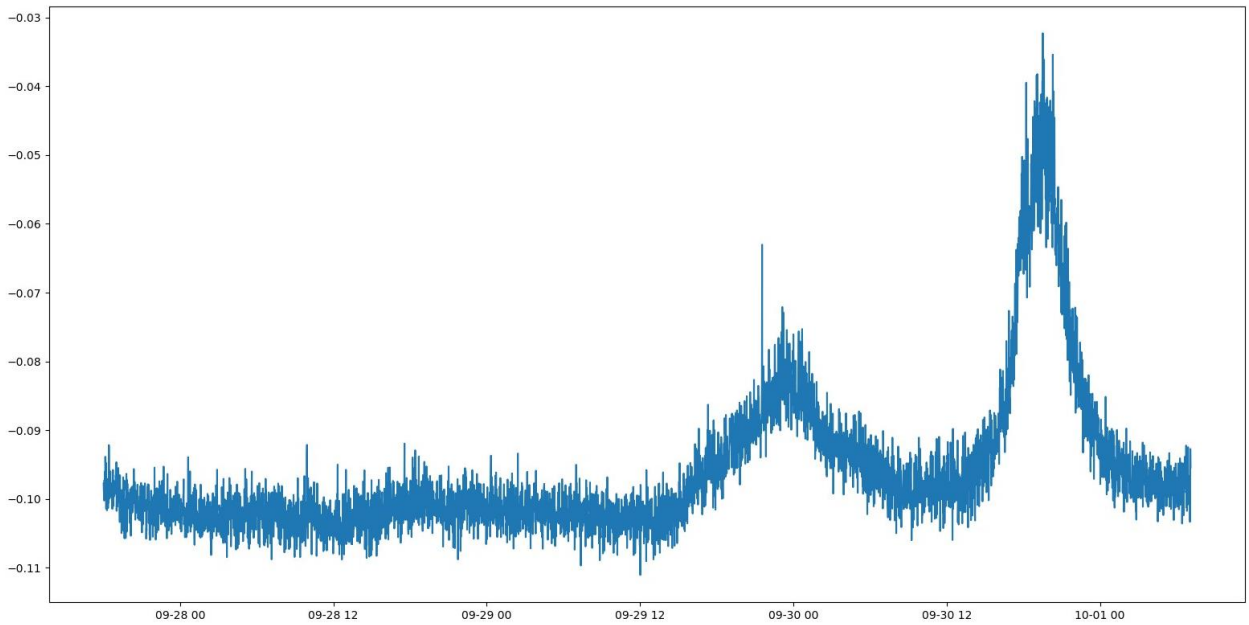

Figure 31: Relative signal of the Uranine Sensor in the Vorder Schächen at Ribi. A first lower peak is visible at around 23:00 UTC on the 29.09.23 and a second and higher peak can be observed at around 19:30 UTC of the 30th of September. After that the signal drops and returns to the level measured before the first peak.

Due to inconsistent tracer curves, possibly interfering tracer combinations and unknown discharge, recovery curves of the tracer could not be modelled. Therefore, the tracer experiments are mainly used for the investigation of connections between sinks and sources.

The results from the tracer studies Kl-23 provide in-depth visualisations on connections between different sinks and sources in the area of Klausenpass and Urnerboden.

Table 7: Replenished Table 6, with the potential connection indicated, acquired through the tracer studies at Klausenpass.

Name	Location	X	Y	Time UTC	Tracer	Amount	Resurgence
KL-23-01-CBP-Ur	Chlaridenbödmeli-Ponor	2708940	1191370	[2023-06-13 10:28:00]	Uranine	20.05 g	Chlus (KL-CCH)
KL-23-02-GLH-Ur	Griessloch Höhlenbach	2709280	1189580	2023-09-04 09:41:00	Uranine	51.32 g	KL-WHF
KL-23-03-GTB-Rh	Gletschertunnel	2709400	1189900	2023-09-04 12:01:30	Rhodamine-WT	50ml	Griesssee¨ (KL-GRS)
KL-23-04-GPB-Ur	Gämschplanggen Chammlibach	2706740	1189910	2023-09-05 11:30:00	Uranine	100.0 g	KL-WHB
KL-23-05-MFB-Rh	Mälchbödmeli-Fäbebach	2708940	1191480	2023-09-05 15:30:00	Rhodamine-WT	20ml	-
KL-23-06-GRS-Rh	Griess-See Gletschersee	2709270	1190640	2023-09-04 16:00:00	Rhodamine-WT	30ml	-
KL-23-07-GFB-Ur	Griessfirn-Chammli	2706590	1189300	2023-09-27 12:44:00	Uranine	199.44g	KL-WHF, KL-RSB
KL-23-08-GPB-Rh	Gämschplanggen Chammlibach	2706750	1189910	2023-09-27 13:30:00	Rhodamine-WT	100ml	KL-WHB

5.2.1. Temperature and pressure sensors:

The analysis of the pressure sensors reveals some interesting facts as illustrated in Figure 32. Striking are the episodic peaks of warm water at both springs. In the beginning of May, the temperatures start to rise and fall more distinctively, especially the Waldhüttli sensor recorded very strong variations. Meanwhile, the period of very strong variations in the Chlus is mainly observable between the end of May and the end of June. Afterwards the variations frequency is reduced, while the amplitude level increases, and the total curve rises as well. It has to be stated,

that the temperature is always around 4°C to 5°C for the Waldhüttli spring, while the Chlus released water between 3°C and 3.5°C in the first 3 months of the observation period and then increases above 4°C.

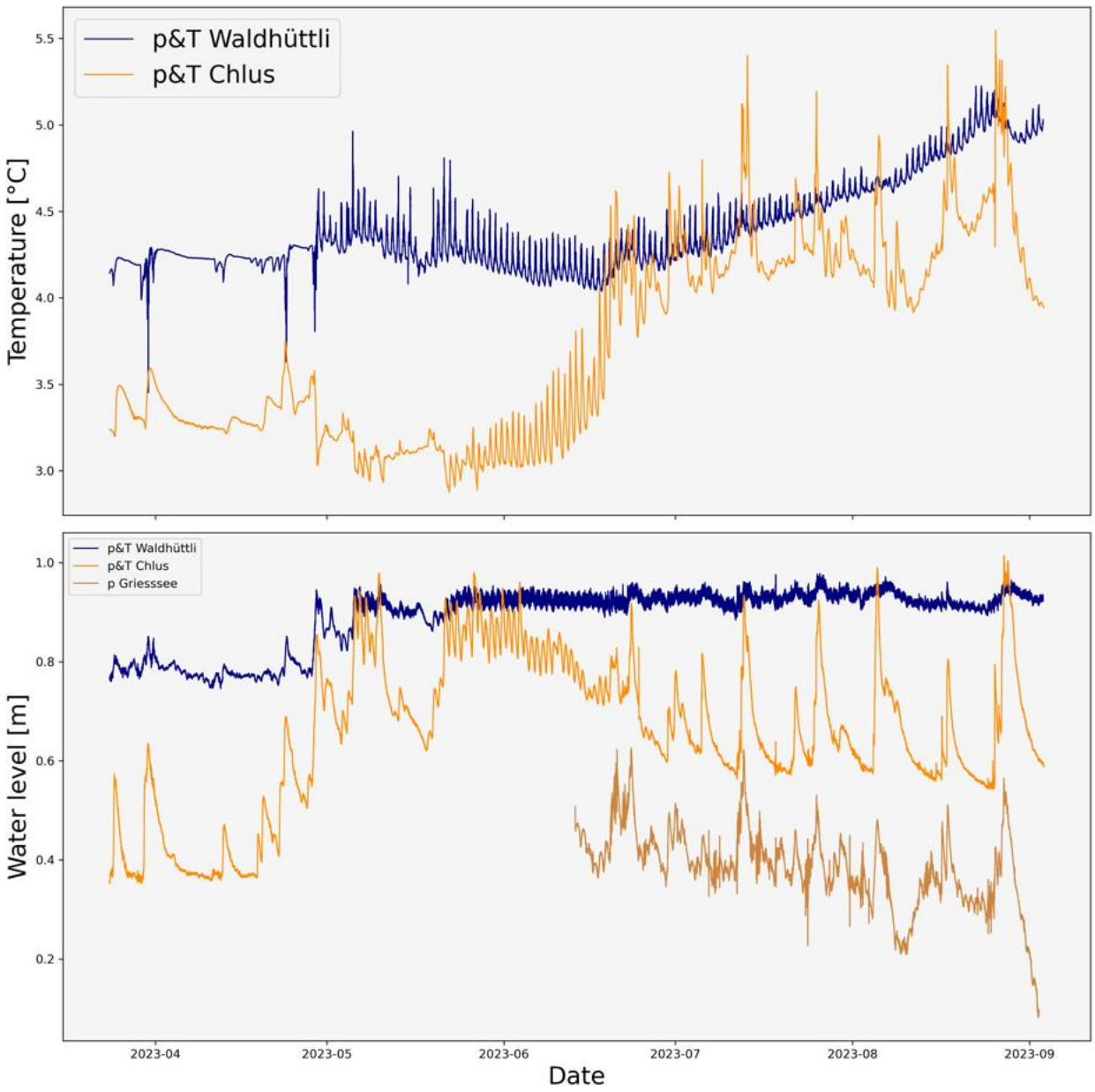

Figure 32: Comparison of the data recorded by the 3 pressure and temperature sensors installed in the area. The pressure logger in the lake was installed later than the other two p&T loggers and recorded the pressure.

In the lower plot of Figure 32 the water levels of the springs and of the lake are further assessed. The p&T logger at Griesssee has supposedly been taken out of the water several times. These errors in the data have been corrected, by clipping the wrongful data and replacing it through values more in line with the temporally surrounding data. Nonetheless, strong similarities are visible between the Griesssee sensor and the Chlus sensor. They seem to react in the same way, whereas the Waldhüttli sensor recorded very different pressure behaviour. While Waldhüttli only shows a slight increase in water discharge with the beginning of May, the Chlus spring clearly

increases its water level. In general, the Chlus spring shows the highest variability in discharge levels.

Also apparent is the drop of the lake sensor in September. The lake level sank greatly and even after the sensor was removed, the lake level lowered considerably. When the last field data was collected on the 1st of October, the lake level was approximately 1.5 meters below the location, where the sensor was previously fully submerged.

Figure 33 shows the behaviour of the water pressure variability of the lake on, and display certain changes which are not well visible in Figure 32 (diese vorher). The signals of interest are those where the line thickens on the plot. This indicates a brief increase in lake level variability, which can be used as proxy for an event, which had an influence on the water level. This could for example be a calving event, a storm or heavy winds, or an avalanche which increased wave activity in the lake, leading to different and highly variable measurements. Also interesting are locations where the signal only spikes for a brief moment to both sides, only to display normal behaviour afterwards again.

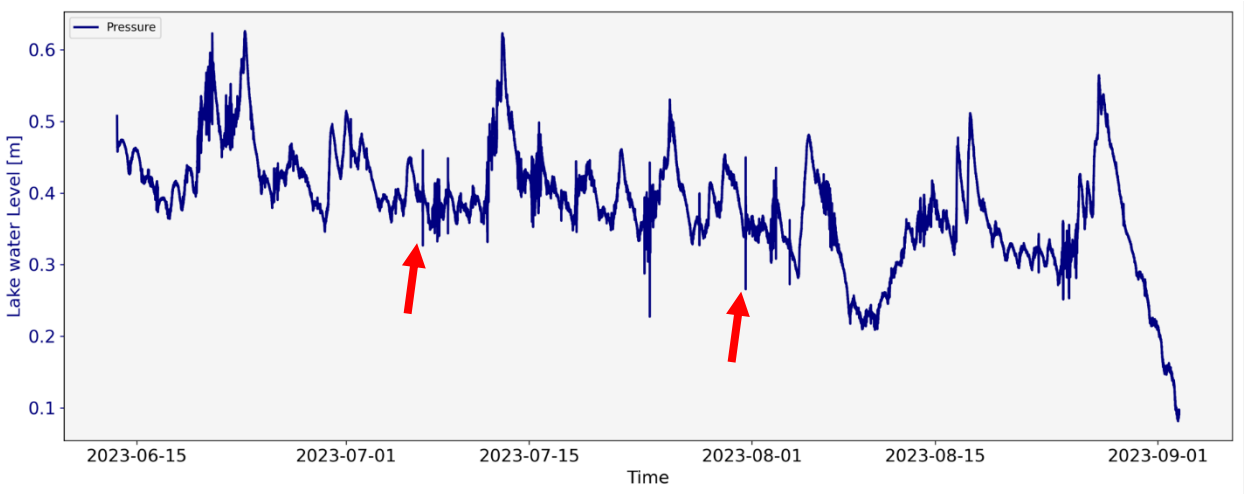

Figure 33: Zoom-in on the lake water pressure variability and zones of interest, two of which are indicated with a red arrow. About 9 locations on the timeseries indicate some kind of event, influencing the water level variability.

5.2.2. Potential melt events

In Figure 34, the course of the lake level and the mean daily air temperature are used to uncover a potential relationship. At first sight, the two curves do not really coincide with each other, but if looked at them closely, one can see that before the larger raises of lake level, the temperature curve peaks as well. A clear connection is only visible twice in the second half of June and in the middle of August, as indicated by the black circle. Marked by the black arrows are some examples where a peak of lake level coincides with a temperature low. There are other times, where a rise of water level is preceded by a rise in temperature, but the temperature levels already dipped, when the lake level started to react. Interestingly, in the second half of August, the mean temperatures rose to the peak of this summer, but simultaneously the water levels dropped during

the warm period. They only rose again, when the temperatures dropped in late August as indicated in Figure 34 by the arrow most right.

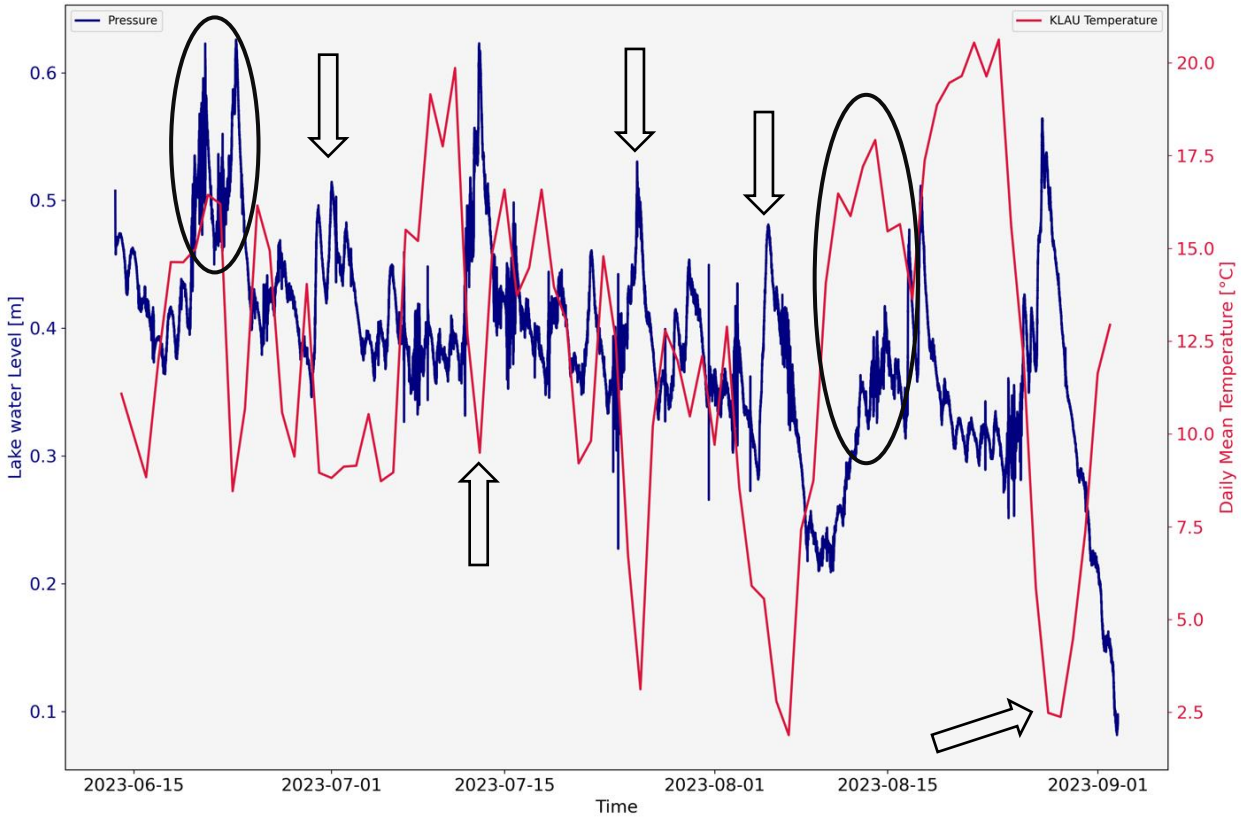

Figure 34: Here, the mean daily temperature measured by the KLAU meteostation with the measured pressure conditions in the lake which represent the variety of the lake level.

5.3. Glaciological analysis

5.3.1. Drone survey analysis

The images taken by the drone were put together to a point cloud using Emlid Studio and Agisoft Metashape and from there, warped into DEMs and ortho photos. In total 18 DEMs and 18 ortho photos were produced, always two of both perimeters on each mission day. On day 2, only perimeter 1, the one closer to the lake, was surveyed, since technical issues arose and made it impossible to start the second pair of missions. In Table 8, the most important data of the missions is presented. The average DEM resolution is 4.96 centimetres per pixel with a standard deviation of 0.34 centimetres per pixel and the average total error of the ortho photos is 13.12 centimetres with a standard deviation of 5.47 centimetres. Highlighted in Table 8 are the highest 4 error values, all above 15cm of deviation.

Table 8: Information of DEM resolution and total error of the ortho photos.

MISSION	DEM RESOLUTION [CM/PIX]	TOTAL ERROR ORTHO PHOTO [CM]
MD1_F1	4.5	8.2
MD1_F2	5.1	14.6
MD1_F3	4.9	9.1
MD1_F4	4.5	15.9
MD2_F1	4.7	9.4
MD2_F2	5.4	13.1
MD3_F1	4.7	13.9
MD3_F2	5.3	15.2
MD3_F3	4.9	12.1
MD3_F4	4.5	30.9
MD4_F1 (!)	5.2	7.7
MD4_F2 (!)	4.8	12.7
MD4_F3 (!)	5.5	14.9
MD4_F4 (!)	5.4	20.3
MD5_F1	5.2	11.8
MD5_F2	5.3	6.6
MD5_F3	4.4	8.8
MD5_F4	4.9	11.2
MEAN:	4.96	13.1
SDA	0.34	5.5

There are several outliers, one of them exceeding the box plot as seen in Figure 35.

These images were then geo-processed manually, so that they are exactly at the same location and on the same height, in order to correctly perform the DEM-differentiation. Examples for the produced DEMs, hill shades and ortho photos can be found in the Appendix 19-24.

5.3.1.1. *Glacier movement on the basis of the ground targets*

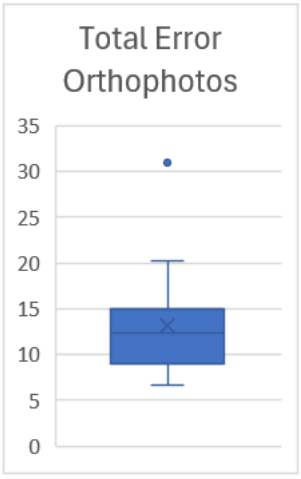

Figure 35: Box plot of all total errors of the ortho photos, presenting the total scattering of the errors.

Ground target 5 was «lost» during the summer, apparently the rock tipped over and the GT fell off and got transported away by the wind. Most other GTs were stable throughout the campaign timeframe. GT1 was once found to be located on the right rock, but in the wrong place. It has been moved and rocks were put on it again for weight by some strangers. Unfortunately, the new location was about one meter off the original place. This was only found out after the drone survey on mission day 2. It was then relocated again to the location it was supposed to be.

Additionally, on the same day after the drone flights, it was discovered, that GT3 has been moved, most certainly by the wind, because it was lying on the debris three meters beside the boulder where it should have been. Therefore, on mission day 2 GT 1 and 3 are out of place and from then on, GT5 has been lost, only to be rediscovered on the last flight day.

The GT location from every flight was mapped to have a conclusive overview, whether the glacier displays a clear direction of flow. The pattern was about the same for every GT location. It did not

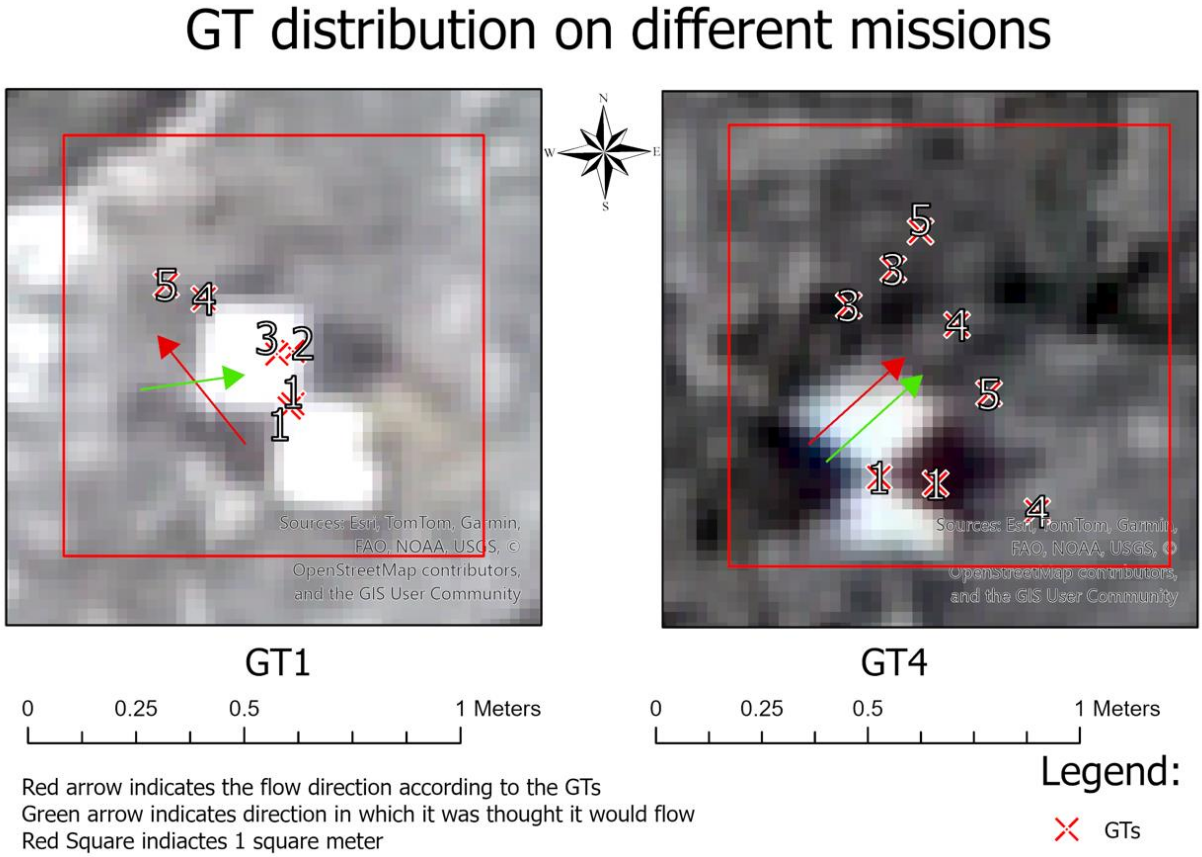

Figure 36: These two images display the offset of the GT measurements. The red square marks one square meter and therefore indicates the shifts of the ortho photos. Note that the flow direction of the glacier should be E/ENE for GT1 and NE for GT4. In that direction lies the closest point of the terminus and the proglacial lake. Mission day 2 on GT1 is an approximation, since it had been moved on that day.

show a clear flow line, but rather a square meter wherein the GTs moved around, sometimes indicating a weak flow direction (Figure 36). GT4 implies a slight movement trend, where a broad direction of flow could be determined, indicated by a small red arrow. The green arrow indicates the flow direction, which was assumed for this location, due to the topology of the glacier. With the use of the GTs potential movement zones are detected on the glacier.

5.3.1.2. DEM Quality Check

As mentioned earlier, the quality of the different digital elevation models and ortho photos was very diverse. The DEMs were aligned vertically to each other, since they had a height difference of more than 5 meters at some points. All DEMs were aligned to point A on the bedrock, which is the same altitude for all DEMs. Additionally, the DEMs were also checked for general errors within them. To have a comparison for that, a second point (B) off the glacier was selected. Both locations were situated on bedrock and would therefore not move neither in XY-direction, nor in Z direction. The elevation of these points on each DEM was recorded and subtracted from each other using the following procedure:

Table 9: Fix point comparison of elevations of point A and point B on each DEM. One can see, that point B spreads about 50 centimetres where it is actually supposed to always be the same. Not every mission covered the two points, therefore not every flight is listed here.

Flight ID	Elevation Point A (above Sealevel)	Elevation Point B (above Sealevel)
MD1F3	2258.374512	2239.228516
MD1F4	2258.374512	2239.415527
MD3F3	2258.374512	2238.952637
MD3F4	2258.374512	2239.233154
MD4F1	2258.374512	2239.489014
MD4F2	2258.374512	2239.164307
MD5F3	2258.382812	2239.009033
MD5F4	2258.385254	2239.107666

$$Diff_{DEM_n} = PointA_{DEM_n} - PointB_{DEM_n}$$

Table 10: Differences of a fix point comparison of all drone flight in the upper glacier perimeter.

Highest Difference	Smallest difference	Median	Standard Deviation
0.938m	0.692m	0.84m	0.06602 m

If the images were of highest precision, then this height difference between the two points should be the same for every DEM. This is a suitable technique to find out whether there are alterations between the two points on the various DEMs. This is where the apparent issue comes in. They are spreading on about 50cm differences, where there is supposed to be a difference of zero, since this point is not moving horizontally nor vertically.

As shown in Table 9, all DEMs were corrected to Point A at 2258.374 meters above sea level. MD5F3 and MD5F4 still possess slight shift of the elevation, but it is only around 1 centimetre off. Meanwhile point B, which was located on bedrock as well, displays a range of elevation from 2238.95m a.s.l. to 2239.49m a.s.l. This gap of 53.6 centimetres, the variability and the lack of precision within the captured and processed drone data is a big source of uncertainty for further analysis. It is deduced, that for the work with DEMs, only the images with less deviation in comparison to the first mission will be taken into account, as they are more precise.

The highest height difference between the points A and B was 0.938 m for MD1 flight 1 and the lowest difference between the two points was recorded at MD2 flight 1 with 0.692 m (Table 10). Based on the standard deviation the general error of 6cm can be deduced.

Further analysis of the image errors has been performed for the final volume difference calculation. For this procedure, two polygons have been constructed on the bedrock and the DEM differentiation has only been conducted for these two polygons (Figure 37). The resulting raster file indicates variability and distortions of the DEMs. In this analysis the generated values spanned from -0.84m to 0.61m with a standard deviation of 0.07m and a mean error of -0.03m as illustrated by the histogram in Figure 38.

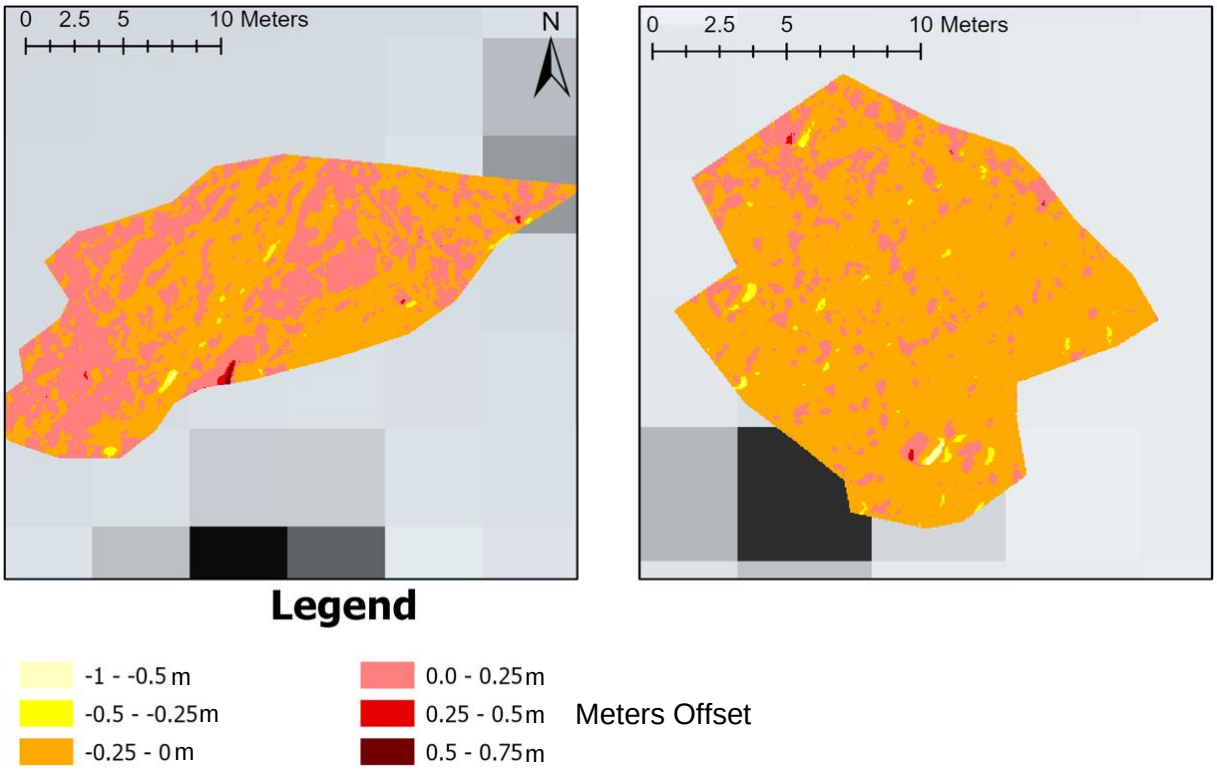

Figure 37: Error polygons on bedrock areas north of the glacier. Both show a different general trend. While the left polygon tends towards 0 to 0.25m difference, the right image displays mainly negative offsets between 0 and -0.25m

Two kinds of error were established before. The first error type described the potential errors of the DEMs themselves, how they can vary within. The second error type determines how the stable surface differs between the DEMs.

With both error types showing a standard deviation of 0.06m and 0.07m, this can be accepted as uncertainty in the drone images.

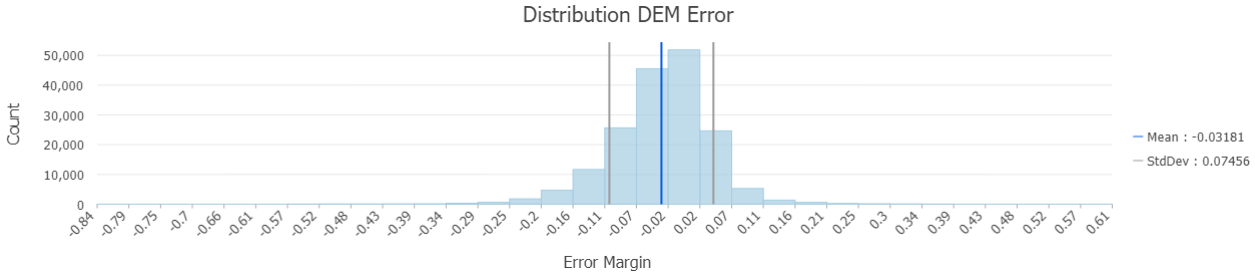

Figure 38: Pixel distribution of the error polygons between mission day 1 and mission day 5. Mean offset is -0.03m with a standard deviation of 0.07m.

5.3.1.3. Volume differences calculation

In order to calculate the local differences developed over the course of the ablation season, the generated elevation models were differentiated. Using this method, the spatial distribution of ablation can be recovered based on aerial surveys retrieved from drone flights. As described before, the gathered information is not as precise as intended, but it can still be used as reference and a comparable mean for the stake measurements.

Table 11: Presentation of the resulting ablation for the two different survey perimeters.

	Lower Survey area	**Upper Survey area**	**Terminus Zone**	**Total Zone (Figure 11)**
Area [m²]	114’054	101’438	24’344	172’124
Mean ice height loss [m]:	-2.99	-2.21	-6.18	-2.79
Meter water equivalent:	-2.7	-2.0	-5.6	-2.5
Volume lost in m3 ice:	-342’000	-224’500	-150’500	-481’000
Volume lost in m3 water:	-308’000	-202’000	-135’500	-433’000

The two survey areas show different loss of ice over the summer ablation season 2023, as determined in Table 11. A partial zone of the lower perimeter has been isolated for an additional targeted analysis (Appendix 26). This subzone indicates the melt at the front cliff of the glacier terminus. The terminus zone was defined by the lower end of the ice cliff on the first ortho photo

and by the upper end of the cliff on the last ortho photo. Therefore, the DEM-difference between the first DEM and the last DEM, indicates the volumetric ice loss at the very front. The strongest height loss occurred here, on average 6.18m of ice melted away, which results in 150500 m^3 of ice on an area or 24343.83m^2.

Great loss of ice occurred especially in the easternmost parts of the surveyed area, where the glacier is located right on the lake shore. The parts with the most melt are the ones right south of the lake, where the ablation map indicates between 2 and 5 meters of ice loss, right beside larger zones where the melt is even between 5 and 35 meters as seen in Figure 39. This is the main zone of the terminus where also a collapse of the ice could be observed, as indicated by the 5+ meter ice reduction areas in Figure 39.

In the upper part of the survey, an increase of melt with elevation is present. The flatter areas in the north-eastern part of the glacier survey (Figure 39) showing less melt, only having between one and two meters of ablation.

The drone surveys were done in two separate but intersecting perimeters. The calculations were first done for each zone separately, then united into one complete raster, representing the ablation of summer 2023, as depicted in figure 39. In the total surveyed zone, the ablation is on average 2.79 meters of ice, resulting in -481248m^3 of ice loss over the total area.

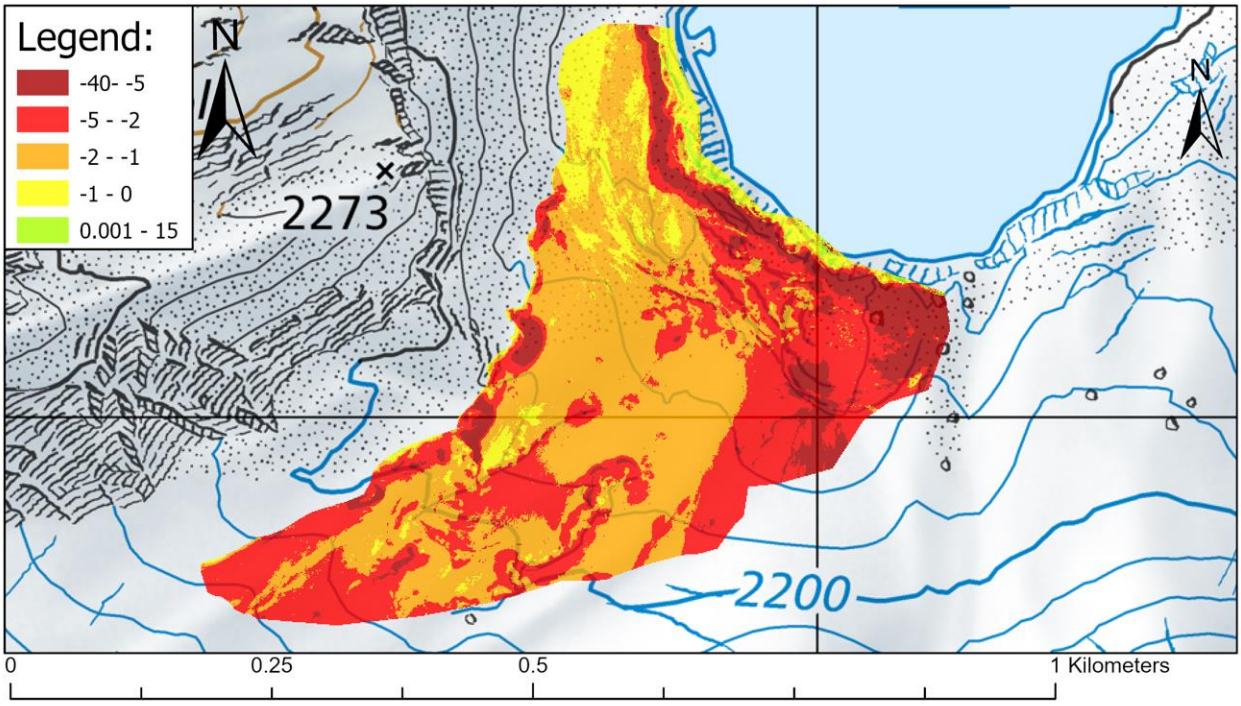

Figure 39: This image represents the drone measured ablation on the Griess Glacier from between June 27 and October 1, 2023. This data has been acquired through the drone-based aerial surveys. The scarce green zones on the glacier front indicate a rise of ground elevation. All other reddish or yellowish colours represent reduction of ice in meters of ice. Strictly, if there was flow present on the glacier, this would only represent height loss, but as with the GT discovered almost no ice flow is present, this can be viewed as similar.

5.3.1.4. *Observed Ice cliff back wasting:*

In addition to volume loss, also horizontal ice retreat can be observed. Especially sound depictions of glacier retreats are visible at ice cliffs which displays exemplary 'ice cliff back wasting'. This can not only be observed at the terminus, but also at supraglacial channels and at marginal locations on the northern side of the glacier, close to Tierälpli south of the peak of Raustöckli. The latter ones are the ice cliffs showing the strongest retreat.

Different back wasting intensities are observed (Figure 41 / boxplot), but in some parts the cliffs have retreated more than 6 meters in just under 100 days. Opposed to the locations where the glacier is not forming clear cliffs, here the ice retreat is increased in the horizontal axis. For the terminus, 20 samples of cliff retreat have been measured. On average, the cliff retreated 9.43 cm/d for the summer of 2023. This measurement is dependent on the drone missions. Not all of the melt has been recorded. The melt which happened before May 27th and after October 1st is not considered.

On the northwestern side of the glacier, there are 2 major ice cliffs which have been observed over the summer of 2023. The retreat here is not as pronounced as on the terminus, but nonetheless, some areas show high ice retreat signs (Figure 40.3).

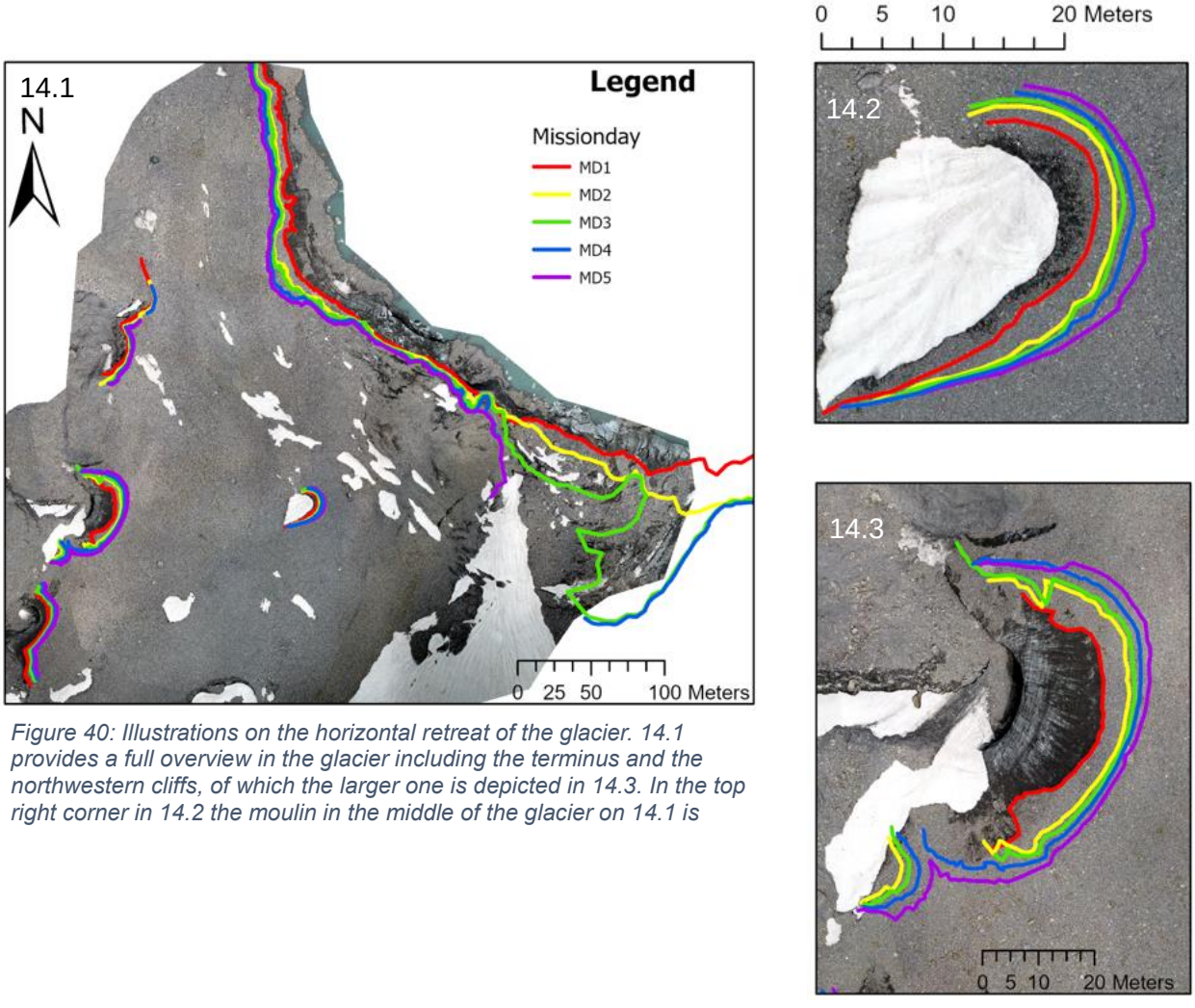

Figure 40: Illustrations on the horizontal retreat of the glacier. 14.1 provides a full overview in the glacier including the terminus and the northwestern cliffs, of which the larger one is depicted in 14.3. In the top right corner in 14.2 the moulin in the middle of the glacier on 14.1 is

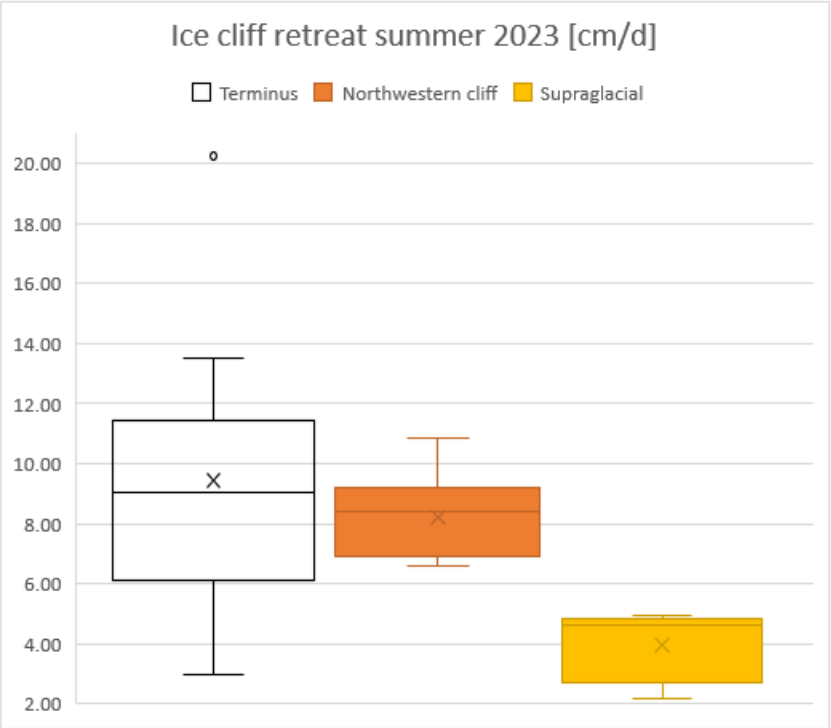

Figure 41: The different ice cliffs observed on the drone images had different melt rates along the cliffs. This box plot provides an overview over the melt rates at the different ice cliffs of Griess Glacier.

5.3.2. Stakes analysis

The results derived from measuring the ablation stakes and the local ice loss are only accurate to a certain degree. The measured data represents the minimal ice loss, which has appeared at the stake sites. This is due to the problem, that most stakes melted out of the ice quicker than expected and were only reintroduced into the ice at the beginning of September 2023. Only stake number 3 represents the whole measurement period. These curves therefore show only the minimal ice loss which the corresponding ice stake site has experienced. Stake 3 has also experienced the most ablation over the course of this summer. Stake site 3 recorded 218.3cm of ice thickness. Meanwhile stake site 4 recorded 184.4 cm and the smallest ablation has been recorded at stake 1. It has only registered 81.4 cm of ice loss, due to melting out. It is very unfortunate that all but one stakes have melted out of the ice at some point and did therefore not record a complete time series (For a summarized version of the ablation stake protocol, see Appendix 25).

To have a complete time series, the values of the incomplete time series were proportionally extrapolated to the measured values of stake site 3 (Figure 42). In the first measured time frame, all stakes have experienced ablation and recorded ice melt. The proportionality factor of each stake to stake 3 from the first measurement period can be taken and the ice loss at each stake can be extrapolated. One must be aware that these results are based on one single measurement period and only serve as an approximation of the rate of ablation at the stakes.

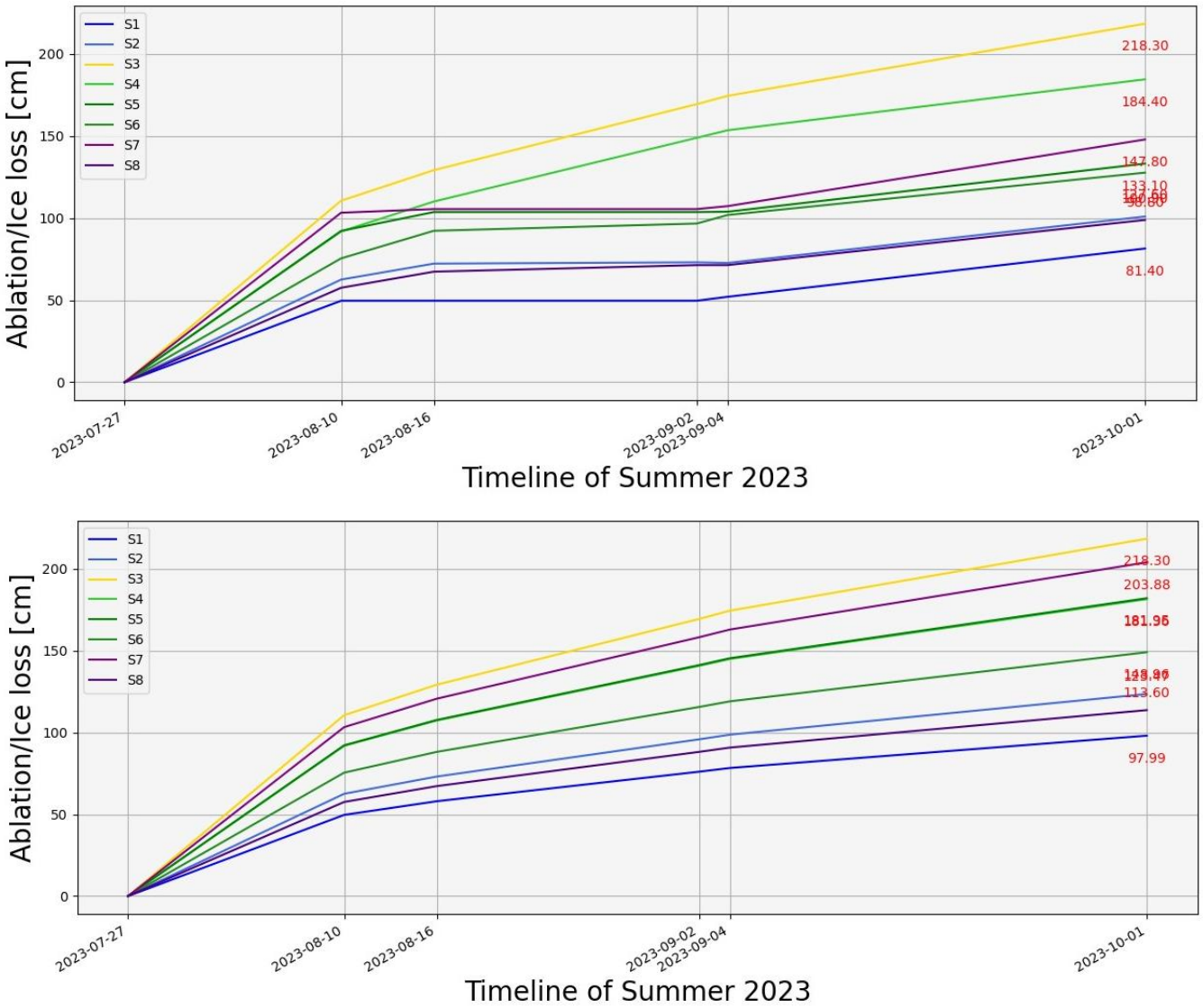

Figure 42: Plot representing the ablation recorded at the ablation stakes. The upper plot (1) shows the ablation which has been measured in the field, including measurement gaps. The lower plot (2) displays the same ablation stakes with extrapolated values, oriented by stake 3, which has never melted out in the whole measurement period.

The ice ablation on the glacier is not proportional. Despite the small distance differences there are already local trends visible. If for example the measuring periods one and five are compared, S1 has a melt rate which is approximately the same in both periods (1.13cm/d in P1 and 1.09 cm/d in P5). Interesting is, that the stake locations are spread across the glacier width, but only very little upslope. So, the stakes variation result represents more the impact of the debris cover on the ablation, than the altitude and temperature, which would be a crucial point when using the contour line method for ablation interpolation. Therefore, the positive degree day method is further useful to gather some additional information on the impact of debris cover thickness and the ablation distribution over the glacier surface.

Normally the uncertainty for the physical measurement of ablation would be defined according to the standard deviation of the stakes' measurements. The standard deviation of the ablation measurements of summer 2023 is 0.41 m. From this an uncertainty in stake ablation of ±0.41m

ice loss or 0.37m w.e. can be derived according to Romshoo et al. (2023). The mass balance averaged over the ablation stakes can therefore be estimated as 1.8±0.4m or 1.62±0.37m w.e.

5.3.3. Positive degree days method

To calculate a representative positive degree day factor (further referred to as PDDF) for the glacier, the method of positive degree days (PDD) was applied. The PDD were calculated for the total time of stake measurement and separately for each timeframe. This timeframe interval is defined by the day when the flight missions with the drone were done, and the stakes were measured. This is not a regular interval, and the stake measurement contains gaps, as already mentioned earlier. In Table 12, the specific PDD values are displayed. Using this data, the PDDF was calculated. The measured ablation for every stake was isolated for each of the 4 measurement days (ZR1-4). From there the mean ablation per day was derived, which was divided by $\frac{PDD_{ZR}}{ZR_{number\ of\ days}}$ to retrieve the PDDF per ZR. Since not every ZR had complete ablation data these gaps were filled with the mean PDDF over all 4 ZR. The mean PDDF illustrates how much melt has occurred at the given stakes per day and °C. For this data to differentiate between the stakes, the PDD has been adjusted to the elevation above sea level on which the stake was located.

Table 12: Contains the PDD values for the total measurement timeframe as well as the PDD specifically for each sub-timeframe, sorted from Stake 1 to Stake 8.

	27.06-10.08	10.08-16.08	16.08-04.09	04.09-01.10
PDD Summe Total ZR	PDDZR1 [°C]	PDDZR2 [°C]	PDDZR3 [°C]	PDDZR4 [°C]
1037	446	91	235	265
1019	438	90	232	260
1002	429	89	228	256
1007	432	89	229	257
1013	435	90	230	259
1031	443	91	234	263
1031	443	91	234	263
1055	455	92	239	269

Multiplying the PDDF per stake with the corresponding PDD results in the specific ablation which could have been measured at each stake according to the PDDF. Using this techniques, data gaps can be closed and the theoretical melt which has not been recorded by the stakes can be extrapolated.

This resulted in a unique pattern, where the stakes differ strongly as one can see in Table 13. It is apparent, that stake 3 is the only measurement series which comes close to the extrapolated ablation. This is because it was drilled in deep enough not to melt out during the measurement period. Stake 3 only differs by about 8 millimeters from the measured ablation.

Using the PDD, an estimation of the melt from the whole glacier can be done first. To be more accurate an estimation of the debris cover thickness has to be done. 15 points spread on the glacier were sampled for debris thickness, the rest has to be approximated using different techniques. First the border where the debris cover stops has to be determined, using different images taken over the course, either by drone or a hand held camera, since the aerial images taken by SwissTopo (2023) or Google Earth (2023) are not utilizable, due to a snow cover in the upper part of the ice. Its not clearly visible where the debris stops covering the ice. According to images taken by the drone, the debris is covering the glacier everywhere in the flat part. The ice gets starting visible, when the slope on the south western arm starts increasing onto the rock face of the Clariden.

Table 13: Presentation of the PDDF, measured ablation, the extrapolated ablation and the local debris thickness per stake.

PDDF per Stake	Measured Ablation [cm]	Ablation with PDDF [cm]	Local debris thickness [cm]
1.11	79	115.28	20.6
1.28	100.5	130.63	21
2.19	218.3	219.07	9
2.06	153.4	206.91	11.2
1.75	121.4	176.68	12.8
1.46	118	150.54	17
2.03	143.8	209.28	5.5
1.16	94.8	122.77	27.5

Additionally, the Positive Degree Day Method has been applied to the northwestern ice cliff and the terminus of Griess Glacier. To be specific, the average retreat of the north-western facing cliffs has been converted to centimeters retreat per degree per day, as it has been done for the ablation stakes. The north-western cliffs retreated on average by 7.9m according to the 10 sample measurements acquried through the ortho photos. Applying the same method as for the ablation stakes it results in a PDDF of $7.8\,\frac{mm}{°C*d}$ for the north west cliff's retreat during the summer. With a mean retreat of 943cm along the surveyed terminus, the PDDF results in $8.9\,\frac{mm}{°C*d}$ (Table 14).

Table 14: Relationship between PDDF and ice cliff back wasting.

	Elevation [m a.s.l.]	*PDD total period*	*Mean retreat of the cliff [cm]*	*Mean retreat of the cliff [mm]*	*Mean retreat of the cliff per day [mm/d]*	*PDDF* $[\frac{mm}{°C*d}]$
Northwestern cliff	2190	1018	790	7900	82	7.8
Terminus	2120	1055	943	9400	98	8.9

5.3.4. Combination of DEM, stake measurements and PDDF extrapolation

A clear difference is visible between the different ablation acquisition methods, but no pattern of error can be detected. The measured stake ablation is incomplete for all stakes, but for stake 3. Accordingly, the data used to produce the PDDF is not faultless, since the PDDF is based on the data available and produced in this study.

Therefore, to compare the ice loss, only PDDF extrapolated melt and DEM acquired melt can be considered. Some of these two measurements are very similar to each other, as for example stake 2 or stake 7, which are separated by a single-digit centimetre gap. Meanwhile others are differentiated by a larger gap, as stake 3 and stake 4, where the difference exceeds 30 centimetres.

Table 15: Comparison of the different melts measured and extrapolated. This is separated for each stake and further illustrated in Figure 43. All the displayed values indicate ice loss in cm ice loss.

Stake number	Ice loss Stakes measured		PDDF extrapolated Ice loss	Ice loss DEMs		Ablation with Corr PDDF [cm]	Ablation Corr PDDF and rain melt added
Stake 1	79	+-41	115.3	134	+-7	103.7	115.3
Stake 2	101	+-41	130.6	134	+-7	119.4	131.0
Stake 3	218	+-41	219.1	190	+-7	207.4	219.1
Stake 4	153	+-41	207.0	177	+-7	193.3	204.9
Stake 5	121	+-41	176.7	167	+-7	165.1	176.7
Stake 6	118	+-41	150.5	152	+-7	139.3	150.9
Stake 7	144	+-41	209.3	199	+-7	197.7	209.3
Stake 8	95	+-41	122.8	106	+-7	111.5	123.1

Interesting to see, is that the measured ice loss, the PDDF extrapolated ice loss and the ice loss recorded by the DEMs embody varyingly strong differences. But no clear trend of systematic error is visible, stake 1 measured less than the DEMs and stake 3 measured 30 centimetres more loss of ice than the DEM recorded.

The ablation data is highly variable due to the unevenly spread debris cover thickness, therefore a further step using the contour line method as planned to retrieve complete ablation is not further pursued. Instead, the positive degree day method to estimate ablation over the summer melting season is further applied.

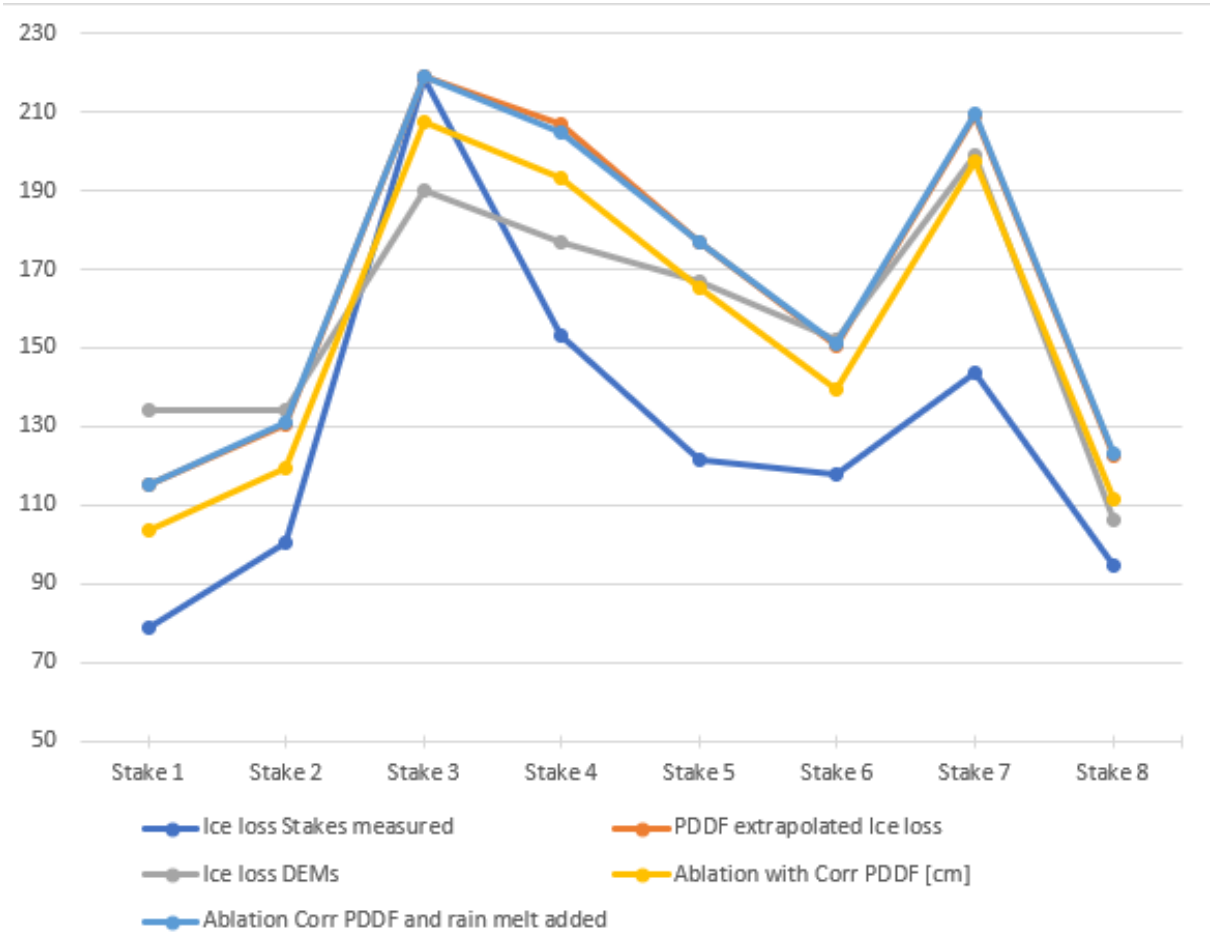

Figure 43: Data presented in Table 7 illustrated as line plot. With this plot the different melt rates are compared visually which reveals more details about the different curves.

5.3.5. Debris thickness interpolation and extrapolation over the whole glacier

For the debris thickness measurements, the debris was scooped aside, until the ice appeared, and then the thickness of debris was measured. It has strong variation also horizontally on the glacier. On the plain close to stake 7, the debris cover was only 5.5 cm thick, meanwhile on the same plain at stake 1, the debris increased to a thickness of 20.6 centimetres, separated by a horizontal distance of 70 metres. The debris thickness does not strictly follow a specific pattern on the glacier, but there is a trend for a decrease with elevation. Outside the measured points, thickness was assumed through visual assessment of images taken by drone or hand-held camera. Closer to the lake shore, the debris layer is tending to increase in thickness, it was assumed to be similar to the other side of the lake, where it was measured. On the main eastern plain its assumed to be around 20 centimetres of debris. The landscape there is not totally unknown, because it has been observed multiple times, when walking around on the glacier.

The cone separating the eastern and the western part of the glacier is only covered by a very thin layer of debris, where the ice is well visible between the gravel. Therefore, it has been determined

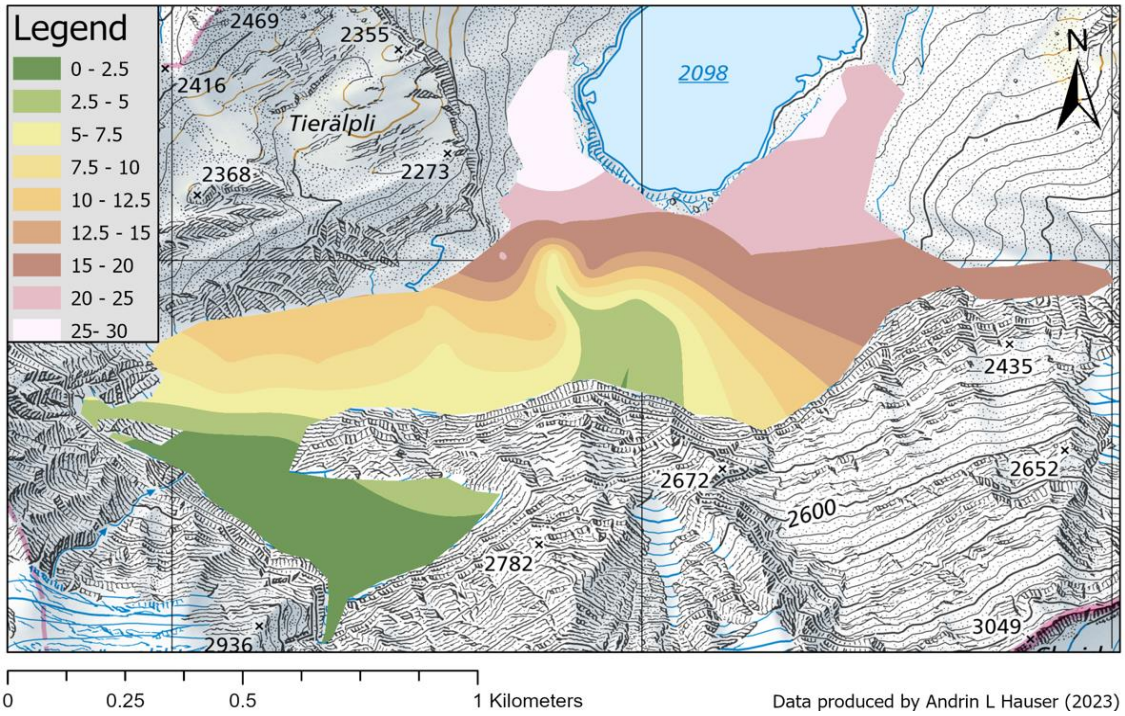

Figure 44: Distribution of the debris cover of Griess Glacier [cm]. It is interpolated as well as extrapolated according to 14 debris cover thickness measurements taken on the glacier in 2023.

to be a layer around 2.5cm in height. The zero centimetres thick debris cover area was determined in the upper most parts of the glacier on the western wing. The flat areas of the eastern and western glacier wing are both completely covered by a thick debris layer more than 20 centimetres high. Using this data and the corresponding assumptions of debris thickness at point locations, an interpolated raster was produced, which assumes the approximate debris thickness of each cell (Figure 44).

Using this interpolated map as a basis, the PDDF per cell can be deduced. This is based on the earlier acquired relation between PDDF and debris thickness. According to the debris layer's mightiness, a new raster layer is produced on which every cell contains its specific PDDF. It must be kept in mind, that this PDDF value is an average value over the whole period of the measuring season, and that it does vary over the different measuring intervals. The glacier measured to be 825'769 square meters in area, averaging at an elevation of 2285.61 meters above sea level. This value has been defined using the DHM25 by Swisstopo ((Federal Office of Topography Swisstopo, 2023)). Deducing from this data, the glacier wide PDDF is averaged at 1.8 mm/°C/d and the mean debris thickness resides at 11.9cm.

Using this PDDF per cell, the ablation per cell can be deduced, multiplying the PDDF per cell and the PDD of the measuring period from 27th of June until 1st of October. This timespan results in a PDD of 986°C*d, then applied to each PDDF-cell. Summing up the ablation of every single cell and dividing it per area, comes to a total ice loss of 1600mm (1.6m) water equivalents of ablation over the whole summer. This is approximately 1'340'000 m^3 of water which was released into the hydrological system only by the glacier, just over the course of summer 2023.

Further the melt can be differentiated into melt by rain and melt by temperature. When the melt through rain has been calculated, it can be subtracted by the total melt to receive the melt only

Equation 3: Formula used for the estimation of melt produced through warm rainwater. It consists of the Precipitation [P] and the measured Temperature [T]. the 1.543 is a correction factor used to correct the temperature measured at the KLAU meteostation for the average height of the glacier, based on the 0.65°C decrease per 100 meters in height increase. Meanwhile c is the specific heat capacity of water [$\frac{J}{kg*K}$], s is specific melt heat [$\frac{J}{kg}$] and ρ = density of ice relative to the density of water [$\frac{kg}{kg}$].

$$RM = P * (T - 1.543) * \frac{c}{(s * \rho)} = P * (T - 1.543) * \frac{4182}{(3.335e5 * 0.9)}$$

caused by temperature. Redoing the PDDF calculation with the new melt data, results in a corrected PDD Factor. In the whole measurement period, a total of 1638.12 millimetre of precipitation has been recorded by the KLAU Meteostation. Combining that with the formula seen in Equation 3, the melt which has occurred due to the rain can be deduced. For the measurement campaign of KLAU meteostation this resulted in 116.2 mm ice melt due to rain for summer 2023 adjusted to the mean elevation of the glacier. Thus, it can be subtracted from the melt at the stakes, but only specifically adjusted for the time periods of measurement. After the reduction, the process of PDDF calculation per stake can be repeated. Combining this with the mean debris cover thickness, the corrected PDDF for the whole glacier is now set at 1.71 mm/d/°C. Combining the corrected PDDF with the PDD and the number of days, the total ablation of 1.7m was calculated, which was based on temperature only. This approximates to a loss of 1'255'000m^3 of water during the ablation period of 2023. The previously presented data is summarized in Table 16 and Figure 46 and Figure 47.

It has been noticed that the ablation calculated for 2023 only reflects the summer, framed by the first and last drone mission days. To extrapolate the ablation further, the PDD measurements of KLAU were used to extrapolate to the whole measuring period of KLAU, which started on 25th of May. The PDD for including the additional month was rounded to 1300 degree days. Deriving from this PDD, the average ice for Griess Glacier can be estimated at 2.38m and 1'760'000 m^3 of water.

Table 16: Summary of the calculated PDDF and the corresponding ablation of summer 2023 differencing between Survey frame by the drones and extrapolated ablation according to the PDD data of KLAU. The extrapolated melt for the corrected PDDF has not been assessed, as the main result for further interpretation is the normal PDDF.

Version	*PDDF* [$\frac{mm}{°C*d}$]	*Ice height loss [m]*	*Ice loss [m w.e.]*	*Estimated water loss [m^3]*	*Total IH loss [m]*	*Total IH loss [m w.e.]*	*Total Water loss*
Corrected PDDF without rain melt	1.712	1.69	1.52	1'255'000	-	-	-
PDDF according to measured ablation data	1.83	1.80	1.62	1'340'000	2.38	2.13	1'760'000

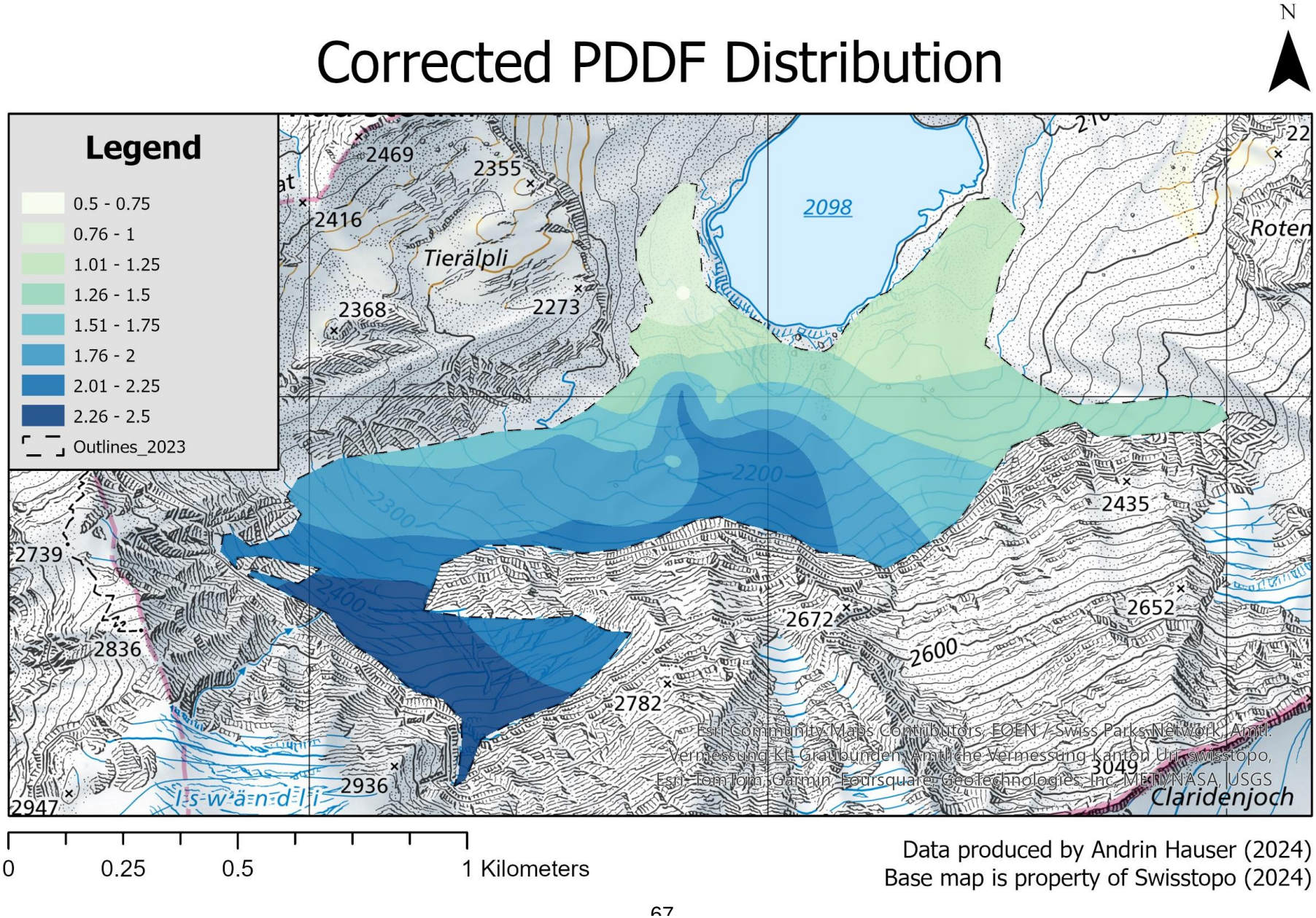

Figure 45: Map displaying the distribution of the corrected PDD Factor over the whole glacier. The darker colours indicate more ablation with higher temperatures. The zones closer to the lake are lower in altitude but are covered by a significantly thicker debris cover.

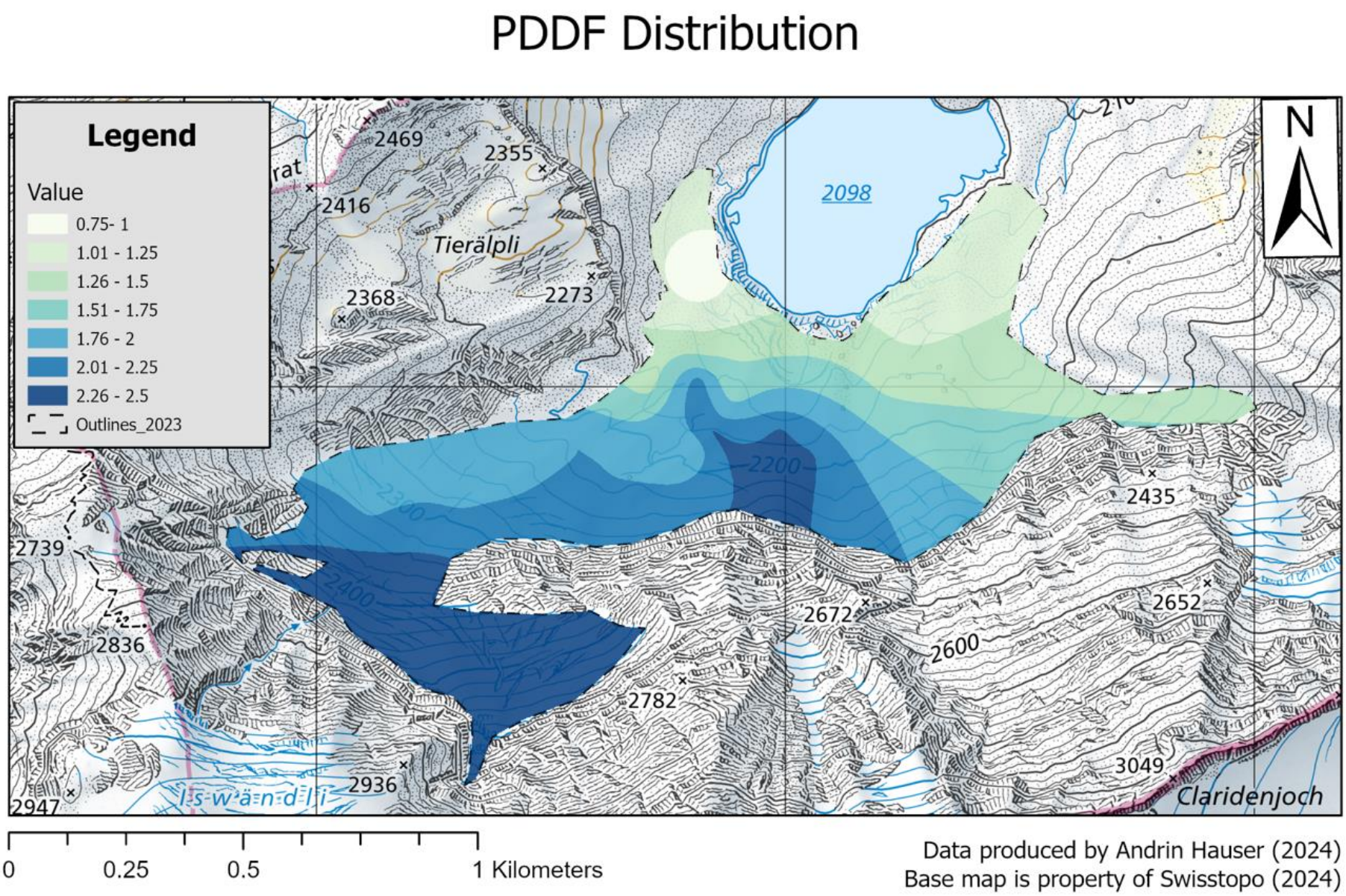

Figure 46: Map of the measured and calculated PDDF over the glacier surface. This map is based on stake ablation measurements, extrapolated debris cover thickness and temperature data provided by KLAU meteo station at Melchbödmeli.

5.4. Wide angle camera

The Tikee 3 camera placed on Raustöckli captured images of the glacier and the lake all summer long, every hour from 4 in the morning till 11 at night. Through the lenses of the camera, the glacier and the weather conditions can be observed well. There were at least three separate incidents of snow fall, of which two could potentially have been over more than one day. The first happened on the 26.07., the second event took place with certainty on the 06.08. and potentially also on the 07.08. and the third was between the 28.08. and the 30.08. Amongst the snowfall events, also other weather patterns could be seen, for example sometimes the fog rising from Linthal can be seen pushing through Urnerboden and towards the Klausenpass.

The camera also captured the thawing process of the frozen lake. When the camera was installed, the lake was frozen over more than 95%, still covered by snow. Over the following days, the lake ice started to melt, building ice floes in the beginning of June. The melt processes increased in the middle of June, being almost completely ice free on the 20th of June 2023. Within 20 to 25 days, the lake went from completely covered by snow and ice, to complete “ice freeness”. For further analysis of the glacier the terminus area has been separated into different zones, to keep track where calving events occur (Figure 48) and the events are summarized and explained in Table 17.

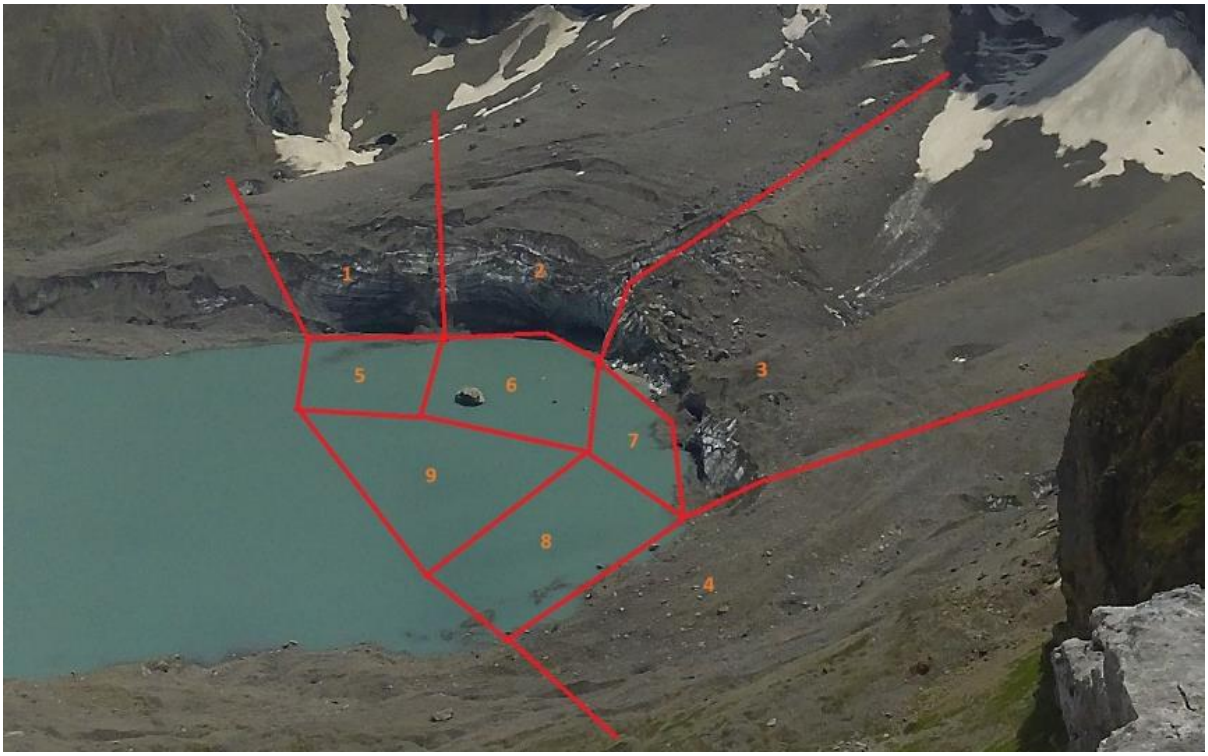

Figure 47: Griess Glacier and lake terminus split into 9 pieces to better retrace the descriptions of observed events. Parts 1-4 are to describe where on the glacier terminus the events occur, 5-9 to describe the behaviour of the ice masses floating in the water, whether they stay at the terminus, drift along the shore or if they are forced to the lake middle.

Table 17: Major events which occurred in summer 2023 on the front of Griess Glacier.

Event	Date	Time of first observation UTC (Timestamp Tikee)	Event
1	01.07.2023	09.59	Layer of ice on the water surface right in front of the terminus in zone 2. Potential calving event.
2	07.07.2023	03.59	Calving Event in zone 2. A layer of ice on the water. Additionally, a stream of ice floes stretches across the lake, indicating a larger incident between the two images taken. Parts of it torn away by wind or other forces impacting the lake's surface in zone 9.
3	08.07.2023	06.59	Calving event, not very strong, but leaving its traces on the lake surface close to the ice (zone 3).
4	12.07.2023	08.59	Potential roof collapse of the ice cave developed in zone 2. Another layer of ice covers the water close to the terminus.
5	17.07.2023	11.00	Potential roof collapse of the ice cave developed in zone 2. Another layer of ice covers the water close to the terminus. Ice drifting into the lake
7	24.07.2023	04.59	Large Calving event, tearing down large parts of the terminus in zone 2. Major event, leaving behind sheer masses of ice on the lake surface.
8	28.07.2023	03.59	Small calving event between zone 2 and zone 3.
9	31.07.2023	12.59	Calving event in zone 2 parts of the glacier terminus broke off and fell into the lake, resulting in a light grey sediment lobe in the lake.
10	27.08.2023	10.59	Heavy rain event, many waterfalls on the Clariden North Face
11	07.2023	09.59	General drop of water level visible over the whole summer. There are gravel banks breaking through the surface along the shoreline, which were submerged during large parts of the study.

This event analysis only displays the larger events clearly seen on the camera. All of them happened over the course of the thawing and melting period of 2023. The camera on Raustöckli did not cover the whole glacier. Therefore, mainly events impacting the ice cliffs on the lakeshore were detected.

Also, on-ice events could only be observed to a certain extent, ice on water is much better visible and therefore easier to spot by the person analysing the images. Figure 49 presents the recorded event number 8. This event was one of the largest recorded in summer 2023. As seen in Table 17, other events occurred as for instance event number 10, which is displayed as before

Figure 48: Major calving event happening on the southern side of the lake, recorded in 3 images by the Tikee 3 camera on Raustöckli. Image 1 was taken on 23.07. at 18:59 UTC. Image 2 was taken on 24.07. at 03:59 UTC and image 3 on the 24.07. at 04:59. Unfortunately on image 3, condensed water droplets have formed on the lens, therefore the image is slightly blurred.

and after series in Figure 49. The result of the mass displacement is a layer of ice floating on the lake surface. The ice masses seemed to have broken off at the ice cliff front. Another example for a similar event (Event 9) is presented in Figure 50.

Figure 49: Small calving event which took place briefly before noon on the 31st of July between 10:59 (left image) and 11:59 (right image). Again, the sediment lobe in the water is clearly visible and a pile of ice debris is deposited in front of the glacier, indicated by the red ellipse in image 2.

5.4.1. Event Nr. 1 – 01.07.2023

The observed event of the 1st of July has been recorded by the pressure sensor. The event was recorded briefly before at 8.49 UTC. According to the Timestamp of the camera, the event has taken place before 10.00. It had not been observed in the image of 9.00, because the view was obstructed by fog in the Griess Basin. Event 2 lead to a water level variation of 6cm.

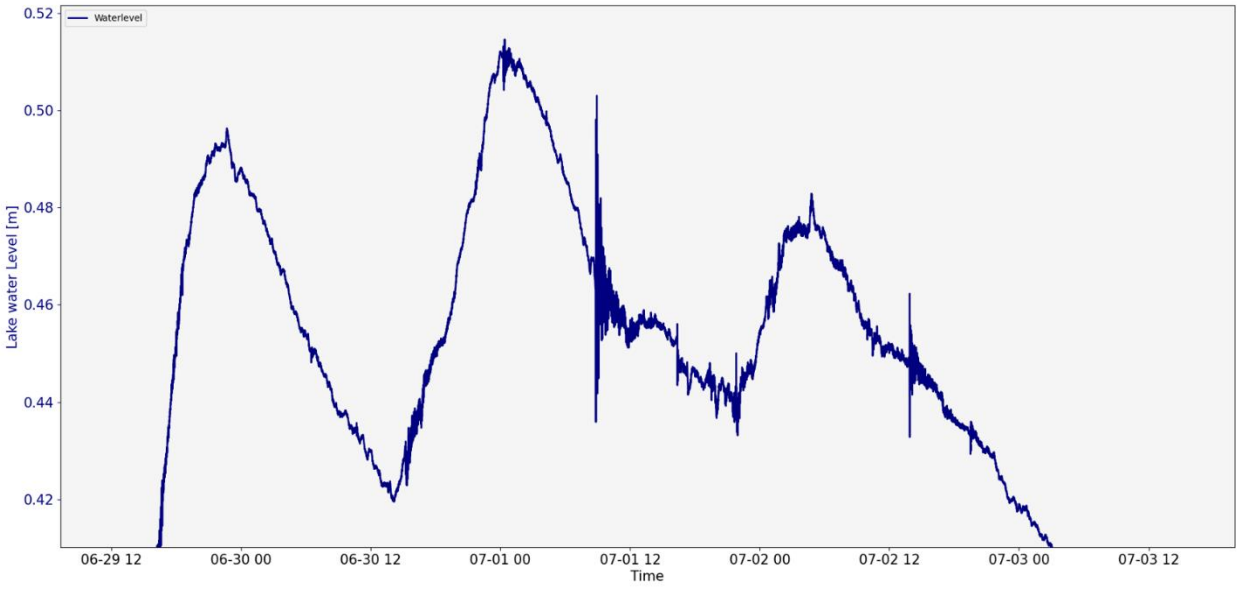

Figure 50: Rise and falls of the water level between the 29.06 and the 03.07. Besides two strong increases and decreases of lake level within 48 hours, there has also been a strong signal which is different than the rest recorded here.

5.4.2. Events Nr. 2,3,4 and 5 – 07.07. / 08.07. / 12.07. / 17.07.2023

This section shows the lake surface variability between the 6th of July and the 20th of July. Several events are visible on this clipping, especially apparent are the increased variability on

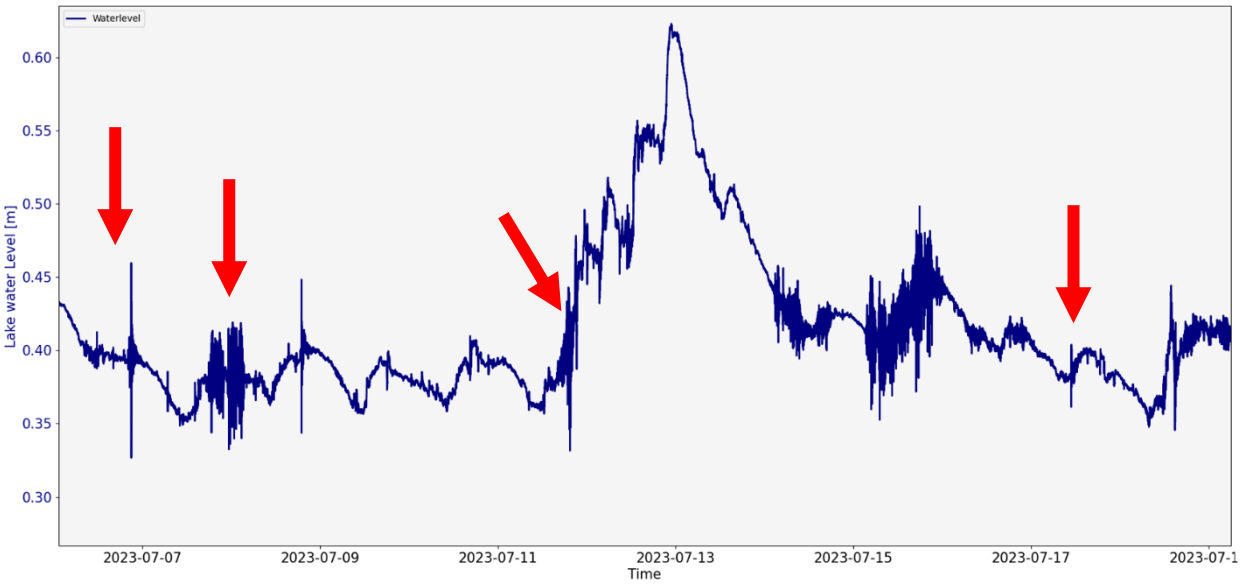

Figure 51: Events 2 to 5 are indicated here. Also visible, a strong increase of lake level of 27 cm within 36 hours.

the 8th of July and on the 15th of July. Also, the strong rise and drop of 27cm within 36 hours is apparent. The level then drops again within 24 hours by 20cm.

While the highly variable zones in Figure 24 indicate an event as calving, the prompt rise rather shows a rain event. This can be confirmed using rain data from the KLAU Meteostation, as on the 12th of July the KLAU Meteostation recorded 14.8mm of precipitation. This peak was also compared to the discharge of KL-CHH. While the spring reached its peak discharge at 00.00, the Griesssee started to drain 1 hour before, at 22.50.

5.4.3. Event 6 – 24.07.2023

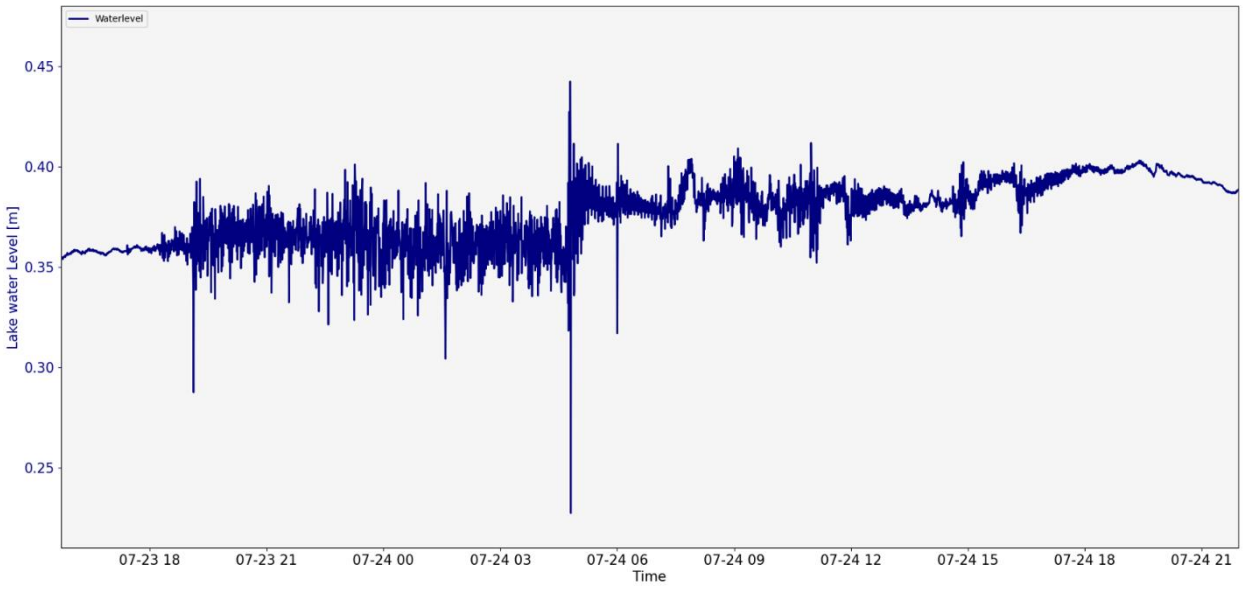

Figure 52: Illustration of high lake surface activity on the evening of 23.07.2023 and the early morning of 24.07.2023.

The event illustrated on Figure 25 must have taken place before 04.59 MET/02.59 UTC according to the images of the Raustöckli camera. Interestingly there is a very strong signal in the pressure measurement at around 5.00 UTC which indicates some kind of event, but too late compared to the camera data. The large amplitudes are strong indicators for such an event as it has been recorded. There is a potential error present in the images.

What is clearly visible here is that the sensor is continuing to measure on an elevated level compared to before the event took place. It also has to be mentioned that the amplitude's difference between peak and bottom is 22cm according to the data logger in the Griesssee. This would be a height difference of 2 meters in water column above the sensor.

5.4.4. Event 7 – 28.07.2023

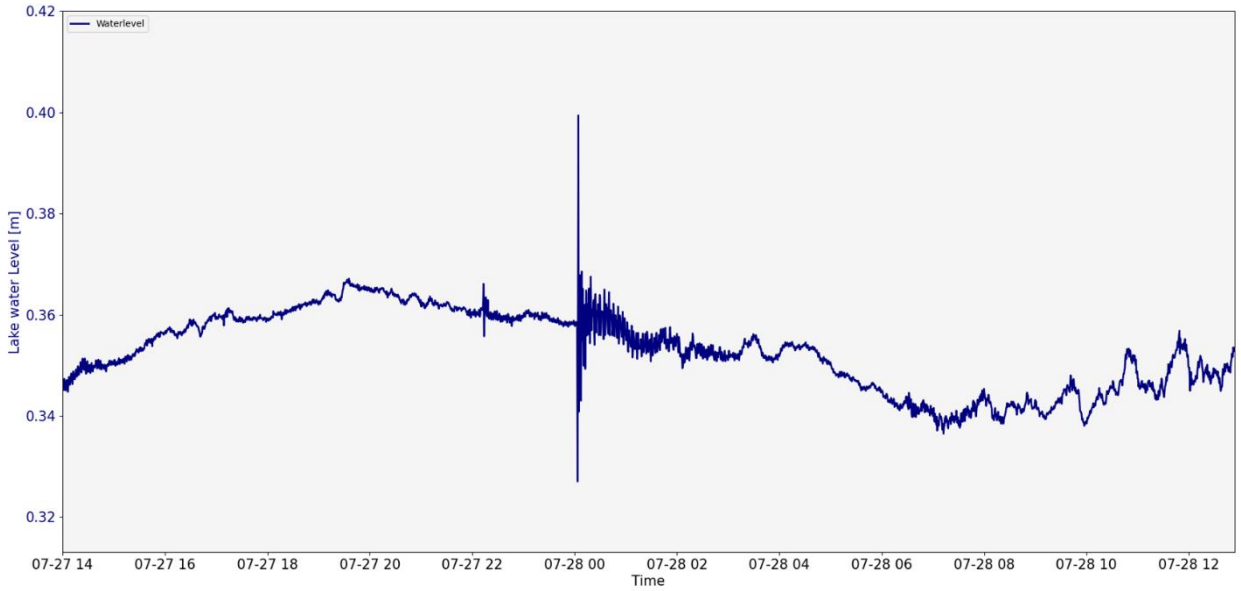

Figure 53: Illustration of the event at midnight of the 28.07. Strong signal of 18cm water level differences has been recorded.

A clear signal is illustrated here on figure 26. The strong amplitude outliers form the start of the signal. It quickly decreases to only small variations again. The outliers on both sides were only measured once, before the lake surface recovered its balance. This signal peak to peak is a difference of 18cm in water level.

5.4.5. Event 8 – 31.07.2023

Again, here a very illustrative depiction of a registered event is visible. The brief and strong rise and falls of the sensor. This event registered a difference of 18cm. Then the signal recovers quickly and the normal lake level and wave amplitude is reached about 2 hours after the incident.

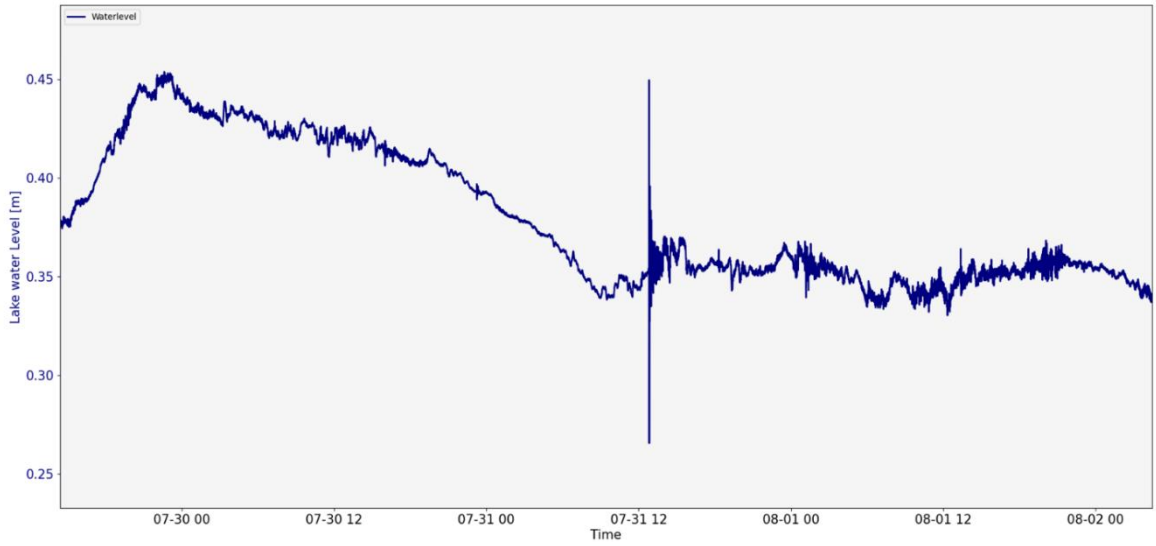

Figure 54: Peak characteristics of event 9 happening at 12.49 on the 31.07.

5.4.6. Event 9 – 27.08.2023

This event recorded by the camera turns out not to be something instantaneous, but rather a continuous process. The lake level is raised 25cm within 12 hours. But then the curve dipped again but did not reach its before levels within the following 7 hours. Also, around the lake level peak, the brief changes of amplitudes increase for 1 hour in strength, before the amplitudes decrease with the reduction of the lake level.

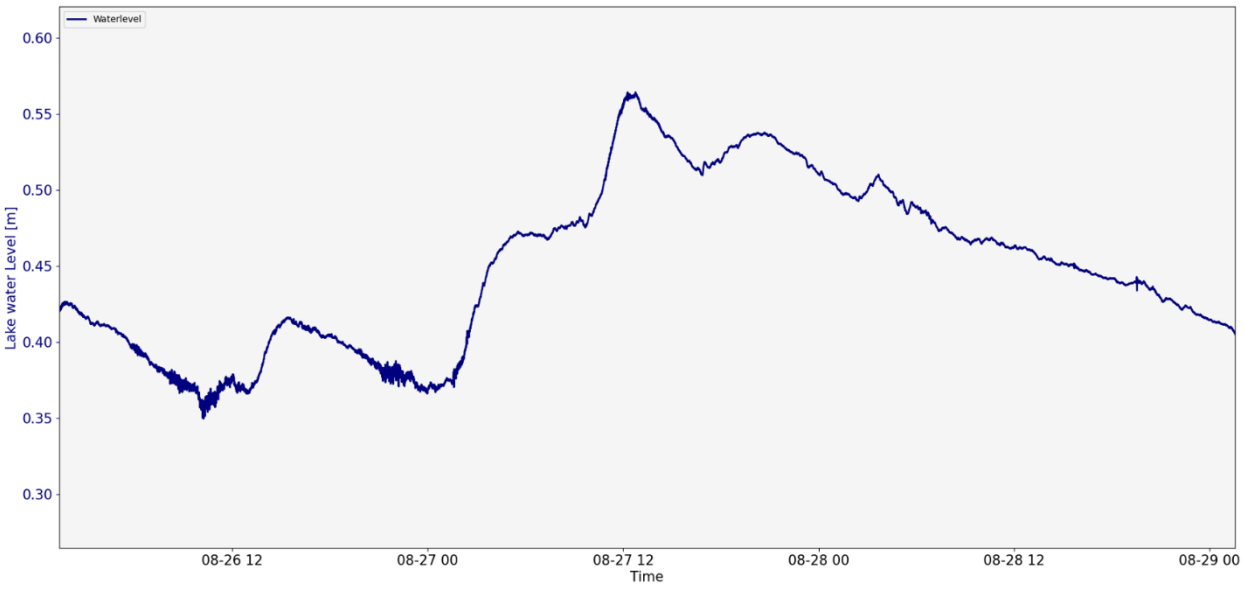

Figure 55: Event 9 displays an increase in lake level but not a typical behaviour with quick increase in amplitude as the other registered events.

6. Discussion

Regarding the meteorological continuity it cannot be stated whether the conditions of this summer are representative for the last few years. However, it is arguable that the weather conditions differ strongly from the last years. According to MeteoSchweiz (2023), the summer of 2023 was the fifth warmest summer since the measurement's beginning in 1864. As they state, the summer temperature was 1.6°C above the norm of the countrywide mean temperature from 1991 till 2020. The summer of 2003 is currently in the leading position for the hottest summer, but in the last five to ten years, the mean summer temperature has approached the temperatures of 2003. For a representative reference temperature curve the summer daily mean temperature of the Klausenpass region or Urnerboden from the last few years would be needed. The closest measuring point available is a meteo station from SLF (Schweizer Institut für Schnee und Lawinenforschung) at Älplersee, which is on the other side of the pass and valley located at a similar altitude. However, comparing the temperature curves of KLAU and Älplersee, it becomes apparent that the signal at Älplersee is less pronounced. Most of the time, the positive peaks of KLAU are around 5°C higher compared to the Älplersee's signal. Additionally, the daily minima are also at least 1°C lower. Therefore, these measurements cannot be used as representative mean curves for the last years. To set the summer mean temperature into perspective, Swiss summer mean temperature was 15.5°C, while KLAU's summer mean temperature was 12°C during 2023. According to the lapse rate used to correct temperatures for elevation in the PDD calculation (-6.5°C/km), KLAU would be located about 540m above the Swiss average elevation (1500m a.s.l.). Following the data provided by the Central Intelligence Agency (2011), Switzerland's mean elevation above sea level is 1350. It can be deduced, that KLAU's mean summer temperature is only 150m off. This discrepancy can have several reasons, for example the chosen lapse rate is only an approximation and can vary as well as there are several different sources for the average elevation of Switzerland, each one with a slightly different mean elevation above sea level. Therefore, it can be said that the mean summer temperature seems acceptable for the location.

Four major temperature drops have been recorded by KLAU. All of them come with high precipitation. Three of these drops coincide with a snowfall event, as the Tikee camera showed. The precipitation sensor is a rain gauge with a tipping scale. It measures precipitation through tipping when enough water has been captured. Therefore, the data might not be as precise because snow does not trigger the tilting sensor as well as water.

The fourth temperature decrease was after the Tikee camera has been dismantled. It is assumed that it also coincided with a snowfall event since a precipitation peak and a major air pressure drop were also observed.

6.1. Tracer studies:

Kl-23-01-CBP-Ur

The tracer studies were fairly revealing in terms of waterway connections, but also lead to further questions. Clear connections could be constructed between the Chlus spring and the Melchbödmeli sink in the experiment Kl-23-01-CBP-Ur. It was first expected that the water of Chlaridenbödmeli (KL-CBP) flows to Chlus West (KL-CHQ) due to the sink's geographically closeness. Therefore, the suddenly greenish coloured Chlus-water caused utter astonishment. Nonetheless, this rather surprising result might be explained by the incline of the geological nappe in the underground. Since the Griessstock nappe plunges southwards towards the Chlus, it allows the water to flow along the stratigraphy of the nappe. Tobias Ibele (n.d.), the local geologist, agrees on the validity of the current result considering the explanation above even though he shared the initial hypothesis that the Melchbödmeli is connected to the Chlus West spring.

Kl-23-02, Kl-23-03, Kl-23-04, Kl-23-05, Kl-23-06

The following five tracer studies showed some definitive results. The glacier tunnel (KL-GTB) on the southern side of Griess Glacier has a creek leaving the ice, going again subglacial shortly after. The injected Rhodamine WT was visually confirmed on the lakeshore between water and ice in the gravel (KL-GGB). At several locations small water runnels were pressing out of the gravel. These started slowly to turn red twenty minutes after the injection. However, based on the visual impression these creeks carried remarkably less water than the stream where it was injected. Additionally, the flow velocity was very low whereas the original stream had a significantly higher water flow activity. The discharge of the Glacier Tunnel creek (KL-GTB) and these various smaller streams (KL-GGB) has not been empirically measured, therefore it cannot be stated with certainty that less water flow is present at KL-GGB.

It is assumed that not all the Rhodamine WT tracer was released from underneath the ice wall on the lake shore. There is the possibility that some of the water infiltrated into the underground and entered a karst network. Furthermore, this creek from KL-GTB might have other flow paths but only one could be detected. If there was a second above-ground discharge channel, it most certainly would have to join Fätschbach before flowing down the Chlus rock face since no other surface stream close by has been discovered. This is strongly supported by the fact that the sensor at Chlus waterfall would have picked up a Rhodamine WT signal if it went over the waterfall. However, this was not the case. Therefore, the tracer has either infiltrated into the underground or the signal on the lake shore was indeed all of it.

The reason for the possibility of infiltration is a minor Rhodamine WT signal on both Waldhüttli springs (KL-WHB, KL-WHF). It is very weak with maximal values of 6 ppm. The interesting thing

is the special behaviour of the signal especially at KL-WHF. It is very similar to the Uranine signal and the turbidity levels in the same spring showing drops at the same time but displaying longer intervals of higher levels. Not only KL-WHF responds in a curious manner, but also KL-WHB starts to show uncommon behaviour on the Rhodamine WT channel from 12.00 UTC on the 05.09.2023. A clear peak is not present but a strong variability in concentration levels and an increase in amplitude. This signal might be either another component in the water, which is wrongfully registered by the Rhodamine WT sensors, or indeed some Rhodamine WT, which passes the sensor.

The Uranine signal registered at KL-WHF (Figure 57) clearly indicates a connection between Waldhüttli and the Griessloch (KL-GLH). However, this signal shows a very unusual pattern containing this massive and instantaneous drops after the peaks. It seems as if the water which carried the Uranine was released fitfully into the stream reemerging through the Waldhüttli Waterfall spring (KL-WHF).

It could be possible that the substance traced by the KL-WHF sensor's Rhodamine WT channel is just a high concentration of Uranine which is wrongfully traced since especially the drops coincide in the beginning. However, if this was the case, there would be no explanation for the increased variability of the Rhodamine WT level. This might happen due to an error in the sensor used at KL-WHF or unexpected interruption of the signal recording since the Rhodamine WT curves shows similar characteristics in drops and peaks as the turbidity curve. However, the latter theory is more plausible. The Rhodamine WT had only been introduced on the 04.09 at 12.00 UTC into the ice cave, but the Rhodamine WT signal already shows one peak at this point of time. It may be that sediments were transported in the water. They have similar light absorbing characteristics as Rhodamine WT and therefore lead to a disruption.

While the temperature curve at KL-WHF is uniform and very similar every day, the Uranine records display different behaviour. If the water flowed steadily from Griessloch (KL-GLH), the Uranine data would not display this imminent concentration drops. This measured signal indicates a water retention phenomenon. One good suggestion is provided by Tam et al. (2004), as they indicate, that a multi-peak tracer breakthrough curve could be an indicator for cave-system with multiple levels. This statement is highly probable for the KL-23-02-GLH-Ur situation as well, as the water covers approximately 1000m of height difference within the mountain.

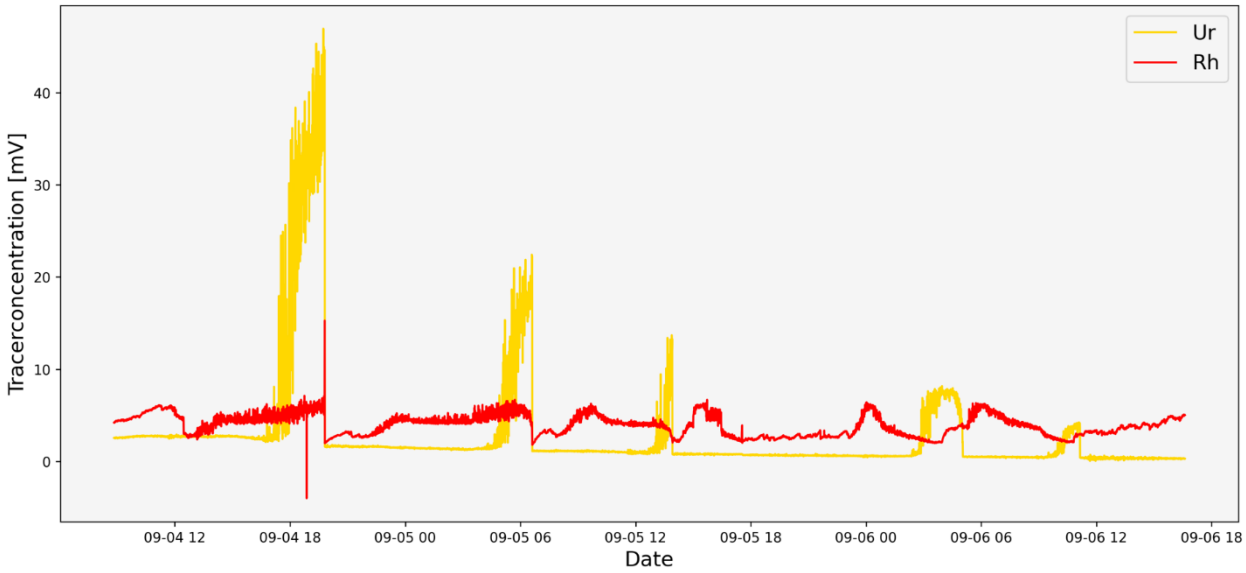

Figure 56: The Rhodamine WT (red) and Uranine data recorded at Waldhüttli Waterfall (KL-WHF) between the 04.09 and 06.09.

To further investigate this occurrence, pressure data of the water discharge variation would be needed. If the water discharge showed a similar inconsistent pattern of swells as the Uranine data (oscillating signal), it would indicate that additional water emerges from Waldhüttli Waterfall (KL-WHF). This would propose that another waterway feeds the KL-WHF outlet having a stronger influence on the discharge than Griessloch (KL-GLH). However, this hypothesis could not be further investigated in this thesis since there was no water discharge data available.

Referring to the Uranine signal in the Waldhüttli Bach spring (KL-WHB), the signal is measured very late right before and during the removal of the sensor. Unfortunately, this experiment stopped when the Uranine flow was present. As it can be observed on the graph, the signal is highly variable and shows strong peaks around 20 ppm. Additionally, the turbidity levels of KL-WHB show major variations. As soon as the Uranine signal is recorded, the turbidity level increases permanently. The experiment was stopped due to battery lifetime, and a second study (KL-23-08-GPB-Rh) was later conducted at Gämschplanggen (KL-GPB) to confirm a potential connection to KL-WHB.

Rather unexpectedly, the current results propose that the Chlus spring (KL-CHH) is not connected to the areas of the tracer experiments conducted on the 04.09 and 05.09. After the positive feedback in Kl-23-01-CBP-Ur, the rest of the water in the Chlus was assumed to be coming from the lake and the surrounding area. Since in KL-23-02-GLB-Ur Uranine was injected at Griessloch and Rhodamine WT the glacier tunnel (KL-GTB), it seemed to be obvious that at least one of the injected tracers spikes a signal at KL-CHH. However, this was not the case. Conclusively, the Chlus system is neither connected to the southern side of Griess Glacier nor to KL-GLH. Furthermore, it also looks like the Chlus system is independent of the Waldhüttli springs. It seems feasible that they are outlets of different systems. As for the Waldhüttli springs,

apparently, they are also independent of each other even though the spring's outlets are only ten to twenty meters apart. This is supported by the tracer as well as the temperature data, which indicate totally detached systems.

The Waldhüttli springs were initially separated into two different outlets (KL-WHB, KL-WHF). However, the temperature data of the data logger (KL-WH) suggested otherwise. There might even be 3 different spring outlets. The pressure and temperature sensor (KL-WH) was placed in the streambed at a big rock, underneath which a stream of water appeared. Supposedly, this outlet was thought to belong to KL-WHB. In contrast, the temperature curve was unlike the KL-WHB's and KL-WHF's measurements. While it displayed a temperature variation like the waterfall, it was constantly about 0.5°C lower, which aligns with on the temperature level of KL-WHB. The other two sensors recorded daily variations with a clear and definitive peak at around 15.00 UTC (17.00 MET). Contradictory, the KL-WHB sensor recorded a slight temperature rise at 10.00 UTC on all days of the field study. There are several different ways to interpret the temperature course. A temperature drop may indicate the addition of melt water to the discharge (Bastiancich et al., 2022), whereas temperature rises may indicate water that had been flowing on the surface and was warmed up. As (Grabovšek & Turk, 2010) highlighted, different temperature behaviour indicates different origins of the water.

This may indicate a connection to an area which is exposed to the sun earlier in the morning since the sunlight would slightly warms up the water compared to the other area. This may also happen to the catchment of the other two outlets. They display warmed water temperatures in the afternoon until 16.00 UTC (18.00 MET). The water temperature then drops rapidly. The sharp decrease may be triggered by the sudden disappearance of sunlight. Furthermore, the KL-WHB shows the highest temperature variations. It also has been shown in KL-23-02-GLH-Ur that it is connected to Griessloch (KL-GLH), and therefore, it is very likely that the water originates from somewhere in the Clariden North wall. The water takes approximately 8 hours to reach Waldhüttli from KL-GLH according to the Uranine tracer experiment data. The temperature rise at KL-WHF starts at 5.00 UTC (7.00 MET). This suggest that this water travelled through KL-GLH at 21.00 UTC (23.00 MET) the day before. Contradictory, the temperature peak is reached at 15.00 UTC (17.00 MET). This proposes that the warm water flows by at Griessloch at approximately 7.00 UTC.

It is difficult to determine whether the temperature peaks are created by water exposed to sunlight or whether the low temperatures are indicating glacier melt water which is then influencing the cave water flow. As this water travels long time within the mountain, it would make sense that the temperature lows indicate the melt increase through the afternoon sun. As the temperature rise starts passing through Griessloch at 21.00, it indicates that then the melt was reduced, therefore this water was melted around 17.00-19.00 somewhere on Clariden or Claridenfirn. To give further insight into the Griessloch water flow, further tracer studies should

be undertaken, including for example a tracer injection on Claridenfirn. With the help of further tracer studies, the origin of Griessloch-water (KL-GLH) might be discovered.

Therefore, to find out more about KL-WHF, further information on the KL-GLH's stream properties is essential. It would be very revealing to place a pressure and temperature sensor in the Griessloch cave. This could help to determine more precisely where the water really originates. Additionally, cross referencing the Griessloch with the Waldhüttli Waterfall data would clarify the proportion ratio of the Griessloch water in the discharge at Waldhüttli.

Another interesting thing of the experiments happened around noon on the 6th of September 2023. All channels of the Chlus Waterfall (KL-CHF) sensor have simultaneous but brief peaks (Figure 58). Uranine as well as Rhodamine WT show a quick concentration increase. Additionally, the turbidity rises twice only to significantly decrease instantly again. Furthermore, a small temperature rise is visible. This is surprising and unusual since the temperature curve's course remains constant in pace meandering between 8°C to 12°C in the afternoon. It is highly unlikely, that the Uranine and Rhodamine WT signal increase for a brief moment at the same time, especially if kept in mind, that neither have they been injected at the same time somewhere, nor does the signal continue in any way. Therefore, this measurement may show

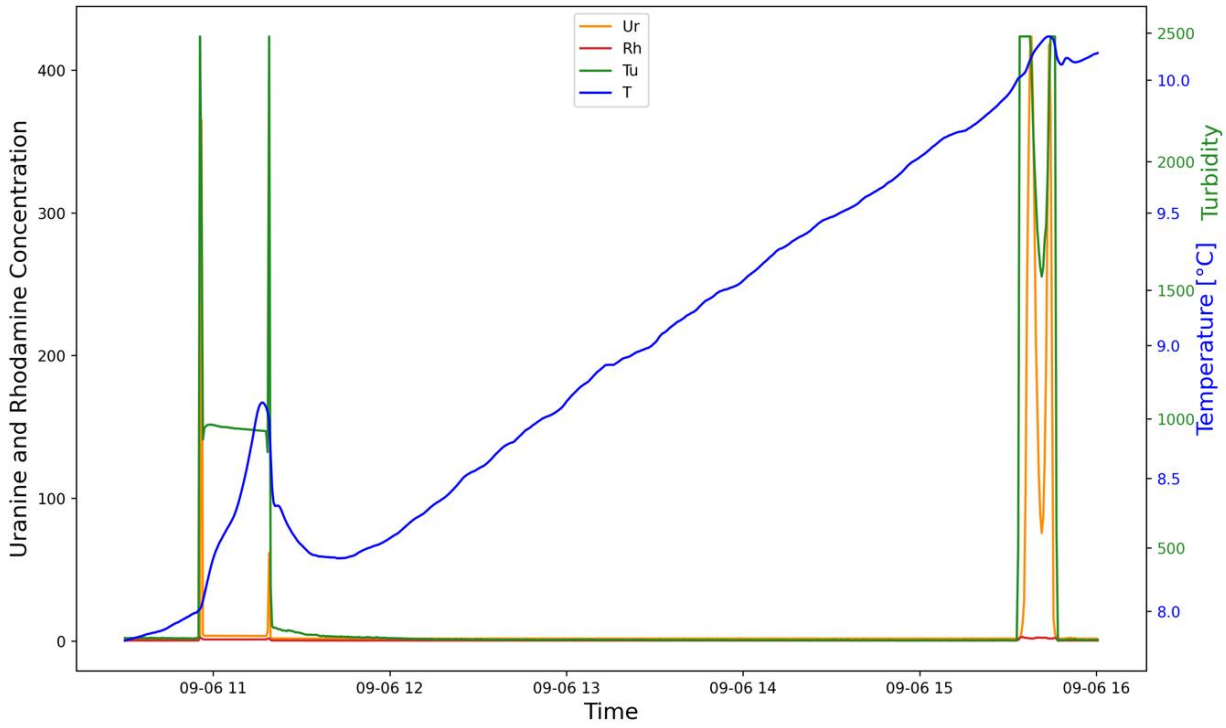

Figure 57: Strange signal behaviour on the recorded data of all fluorometer channels at the waterfall at Chlus (KL-CHF). This partial data is from noontime on the 06.09.

external disturbance. This hypothesis is supported by an additional turbidity sensor spike. It is highly possible that very turbid water with a high suspension load was transported in the water down the Chlus waterfall, which also was registered on the Uranine and Rhodamine WT sensor.

Marco Baggio of Kraftwerke Linth-Limmern (KLL) was asked about this occurrence since the KKL owns the two water captures above the waterfall. The water captures were not flushed on that day. Therefore, they are not responsible for this short but major increase in turbidity. However, they have observed that the second water capture above the Chlus usually carries very turbid water after heavy rain events. Aligning with this observation is that the water of Fätschbach 2 might not come from the lake, but more from the flanks of Boggtschingel and Speichstock. Conclusively, during heavy rain the loose sediments would be transported in the water without being deposited in the lake first. However, as rain was not present during the field study, something else is responsible for the sudden release of the turbid water. Further investigation of the waterfall is needed to clarify whether this situation was a random distortion or a signal of an unknown phenomenon. Discharge data of KL-CHF would perhaps help to clarify whether there also was an increase in water flow. Maybe a sudden release of a water pocket occurred further up in the mountains which brought along these signal distortions. But if that was the case, the signal would probably not rise and fall as it did in this instance. Another possibility would also be that the sensor was briefly hit by sunlight which distorted the water to an extent that it was caught by the sensor. In either case, it remains unclear what happened here exactly, and it would be interesting to see whether this was just a one-time artefact or whether this distortion appears more frequently in the Chlus waterfall.

Kl-23-07-GFB-Ur and Kl-23-08-GPB-Rh

Follow-up studies were conducted to further investigate the connection between the western part of Klausenpass at Gämschplanggen (KL-GPB) and the Waldhüttli springs. On the first site inspection for Kl-23-04-GPB-Ur, a second ponor on the Griessfirn underneath Chammliberg (KL-GFB) was discovered. Taking advantage of a second water inlet in the area both tracers were utilized for Kl-23-07-GFB-Ur and Kl-23-08-GPB-Rh again to differentiate between the injection sites. Consistently, the Chlus sensor (KL-CHH) did not record a signal, which further demonstrates that the water of Chlus originates from the eastern side of Klausenpass. The point of source may be around the Griess Glacier, the Griesssee or it might even be further up Clariden or even from Claridenfirn further south.

The sensor at Ribi (KL-RSB) recorded Uranine indicating that parts of the glacial ponor drain into the Schächen. Since this sensor could only record Uranine, Rhodamine WT could not be measured here. Additionally, there is the possibility that parts of the Gämschplanggen ponor (KL-GPB) is directed to Uri. However, both Waldhüttli sensors (KL-WHB, KL-WHF) registered different signals. The Uranine introduced at the glacial ponor was only discovered on Waldhüttli Waterfall (KL-WHF) and the Rhodamine WT signal was observed at Waldhüttli Bach (KL-WHB). This is interesting since both springs seem to have their origins in the same area, but they stay totally separated from each other and do not mix. In conclusion, the water from Chammli-

Griessfirn flows towards Urnerboden following the way pre-set by geological structures in the underground.

Another occurrence which needs to be discussed in this paper is the temperature difference between the two sensors. While KL-WHB stays monotonous with almost no variation, KL-WHF shows more variability. As already established in KL-23-07-GFB-Ur, a part of KL-WHF's water comes from the Chammli-Griessfirn. This is clearly visible in the temperature curve. The daily temperature drop supports the connection to glacial melt water. But also, the water warming effect is observable, best in Ribi's (KL-RSB) data collection. The water flows above ground for a while and therefore reaches higher temperatures induced by the afternoon sun.

To further investigate the area tracer experiments during snow melt, when more water is flowing, could be conducted. Due to more discharge, additional flow paths might be tapped. New connections could be discovered, or the networks, which are currently established, could deliver more supporting results.

6.1.1. Flow times

The eleventh research question in this study was on general flow times in the Klausenpass' karst networks. The discovery of the signal of KL-23-01-CBP-Ur at KL-CHH was initially unexpected. The tracer emerged at 13.30 UTC from the cave waterfall. It took the water three hours to travel through the Chlus cliff. The flow time of KL-23-03-GTB-Rh was shorter. The tracer appeared twenty minutes after the injection beneath the ice cliff, but also had less distance to cover.

KL-23-02-GLH-Ur was started at 9.41 and the first signal was recorded at KL-WHF at 16.45. This results in a flow time of at least seven hours between Griessloch cave and Waldhüttli Waterfall. However, as the observation revealed uncommon signal spikes every seven to nine hours, it is assumed that there is a syphon drainage occurring or something with a similar effect on discharge. If this was the case, then the flow time would be dependent on the frequency of this draining mechanism and would show significant time variations. Additionally, KL-WHB has recorded a Uranine signal at 20.45 on the 6th of September, two days and eleven hours after the injection of KL-23-02-GLH-Ur and one day and nine hours after the KL-23-04-GPB-Ur introduction. Two and a half days (60 hours) for an approximate distance of four km seems rather long. On the contrary, the distance to KL-GPB is approximately 5 km and is covered in 35 hours. Additionally, this result is supported by KL-23-08-GPB-Rh's findings. 30 hours after the injection there is a slight drop, before the concentration starts to increase constantly to 3 mV, before the sensor was removed again at a moment when a signal was recorded. It would be interesting to see how strong the Rhodamine WT signal would have become.

Furthermore, the Rhodamine WT signal shows very different behaviour than KL-23-04-GPB-Ur. It is more constant than the Uranine signal of KL-23-04-GPB-Ur. The latter demonstrates high variability in the measured Uranine concentrations. However, both signals start to rise 36 hours after the injection, which significantly enhances the hypothesis that sink (KL-GPB) and source (KL-WHB) are indeed connected to each other. Moreover, KL-23-07-GFB-Ur indicates a connection between the Chammli-Griessfirn Gletscherbach and Waldhüttli Waterfall (KL-WHF). The first Uranine signal is measured at KL-WHF 28 hours after the injection on the western side of the Klausenpass. KL-23-0s4-GPB-Ur and KL-23-07-GFB-Ur flow times deviate by around 8 hours, which supports the suggestion of two different flow paths and therefore the re-emergence in two different springs. Another possibility is that the longer flow time could be caused by an underground structure which slows down the water flow through retaining water and hindering it from keep flowing.

6.2. Pressure and temperature sensors of Chlus and Waldhüttli

According to the pressure and temperature sensors, which have been installed during spring and summer 2023, the measured data supports the established hypothesis outlined previously

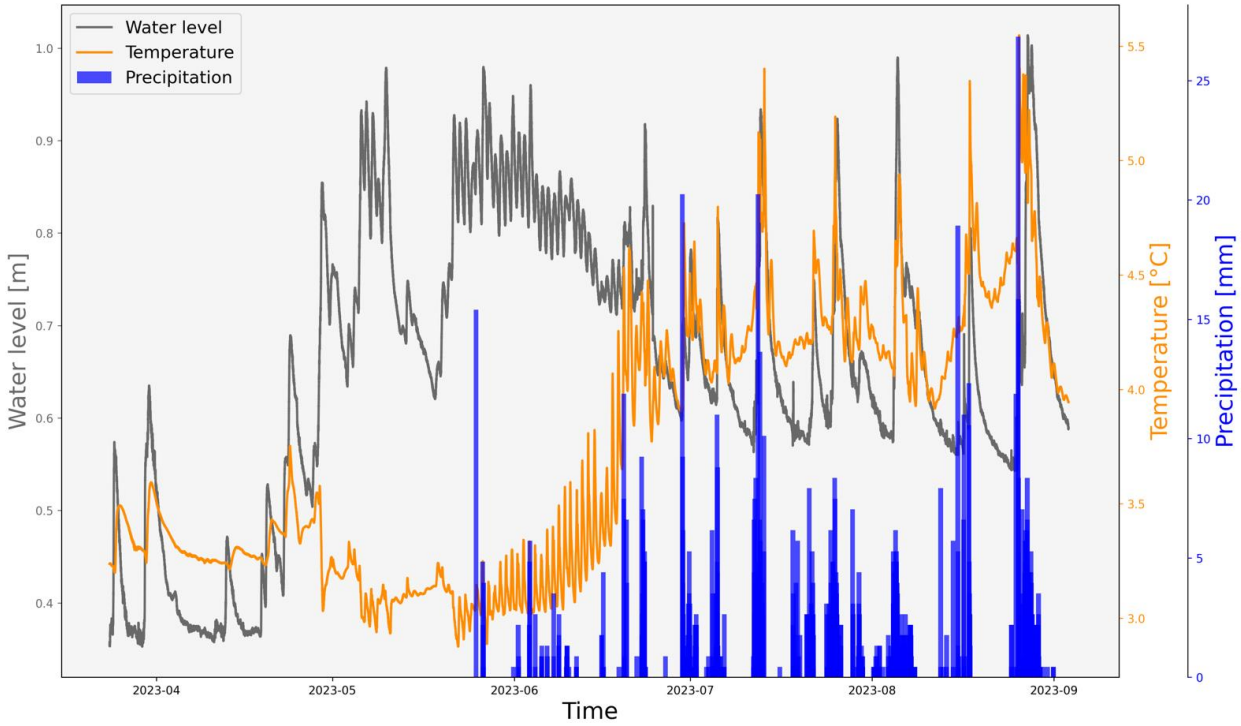

Figure 58: Data from the p&T logger at KL-CHH displaying from 27.03. to 04.09 when the sensor was removed during the OGH field camp.

in this study. The start of the highly variably phases in the Chlus (Figure 59) and Waldhüttli springs (KL-WH) indicate the beginning of the snow melt season. This snow melt's influence is clearly distinguishable in the curve (Figure 59). Interestingly, it seems like the melt water has a long-term impact on the discharge of Waldhüttli as the highly variable daily changes, which stay

active until September (Figure 60), show. Even though the daily amplitude minimizes towards the end to approximately 0.25°C, the temperature rises to around 5°C.

In contrast, the temperature curve of Chlus (KL-CHH) changes its behaviour at the end of June to a less regular variability. It features more spikes with a higher amplitude of almost 1°C staying on an average around 4.5°C. This means that the influence of snow melt came to an end, indicating that these highly inconsistent peaks originate from the precipitation's influence. This can be observed in the right half of Figure 59. Most of the major spikes of water temperature and water pressure coincide with the precipitation events. However, not all the spikes of similar size are connected to large rain events. Most KL-CHH peaks are also induced through smaller precipitation events, which suggests that the Chlus system reacts strongly and immediately to precipitation events. Less intense but longer ongoing rainfalls do have a similar effect on Kl-CHH discharge as shorter but more intense precipitation events.

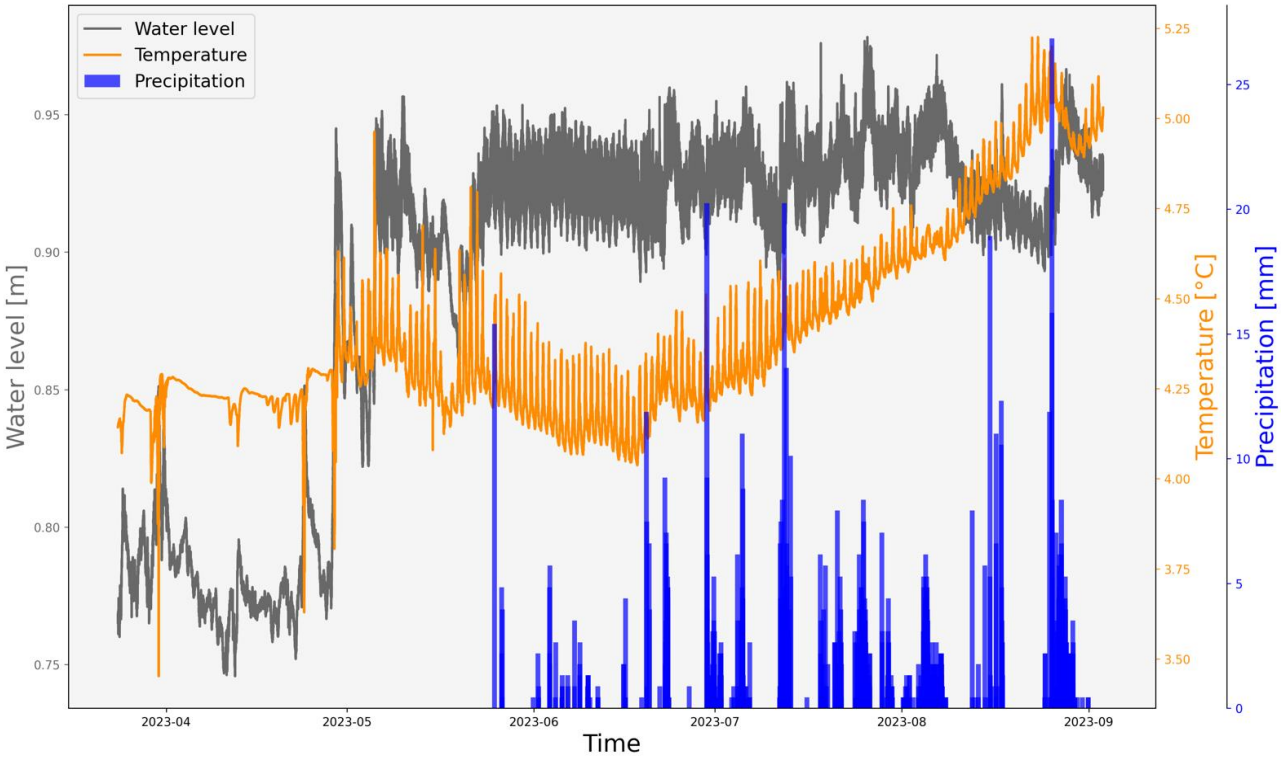

Figure 59: Temperature and pressure data recorded by the sensor placed at KL-WH during late spring and summer 2023

There are significant increases in discharge at the end of July and the beginning of August, a period where the pluviometer of KLAU does not register heavy rain events. Nevertheless, temperature and water discharge show peaks with stronger rises compared to the first half of the year. In conclusion, this finding aligns with the result of the tracer studies performed in the area. Chlus seems not directly connected to a glacier but rather to areas which are ice free and characterized by snow melt. As soon as the snow is gone, Chlus changes its discharge characteristics to a rain fed watershed as supported by the KLAU's meteo data. Furthermore, it seems that Chlus is possibly not connected to the lake according to the temperature data. A

water body of the size of the lake is too large to express temperature variations with the frequency as the KL-CHH displays. Earlier in the current paper was hypothesized that KL-CHH and Griesssee are directly linked since the Chlus' discharge and the lake level increase simultaneously. However, the comparison of temperature and pressure data rather indicate a reaction to precipitation events. It is still a possibility, that the lake is responsible for the baseflow of KL-CHH and it can therefore not completely be ruled out that any connection exists at all, but the lake as main water supplier for KL-CHH seems unlikely. The responses to precipitation events very strong. This might also imply, that the catchment of KL-CHH is very large and in the event of rain, the water gets channeled and directed to KL-CHH with high efficiency. If the precipitation water is coming very concentrated, the warmer rainwater could be able to raise the lake water temperature in the Chlus karst system through mixing of the water. Another possibility is, that the lake drain into a karstic aquifer, which releases the water at a yet unknown or unsampled karst spring, as for example the one joining Fätschbach close to Berglistüber waterfall. This spring outlet was releasing great masses of water in September, yet it was neither accessible enough nor were enough fluorometers available to also sample this karst spring (approximate coordinates: 2'717'075.8, 1'196'339.6).

Figures 59 and 60 also provide answers to several research questions. Referring to research question 8 (*For how long is the snow and ice melt observable in the water pressure and temperature data?*), the two springs KL-CHH and KL-WH show very different behaviours. Even Waldhüttli could be split up into KL-WHB and KL-WHF again, but there is no long-term time series of pressure and water temperatures available. Considering the highly variable patterns in the temperature curves indicating snow or ice melt, the spring's measurements indicate different catchments for the two springs. For KL-WH the melt behaviour starts on the 1st of May and lasts till the day the sensor was removed. As no continuous snow melt is present in fall anymore, this signal indicates the connection to a glacier. KL-CHH's snow melt signal commences on the 22nd of May and lasts until the end of June. For the rest of the experiment, the behaviour and similarities to KLAU's-precipitation data indicate that the spring is mainly rain fed because KL-CHH reacts immediately to precipitation events registered by KLAU. During the melting season, distinct daily variations are observable. On one side, KL-CHH registered temperature peaks each day between approximately 13.00 and 15.00. On the other side, KL-WH displays temperature peaks

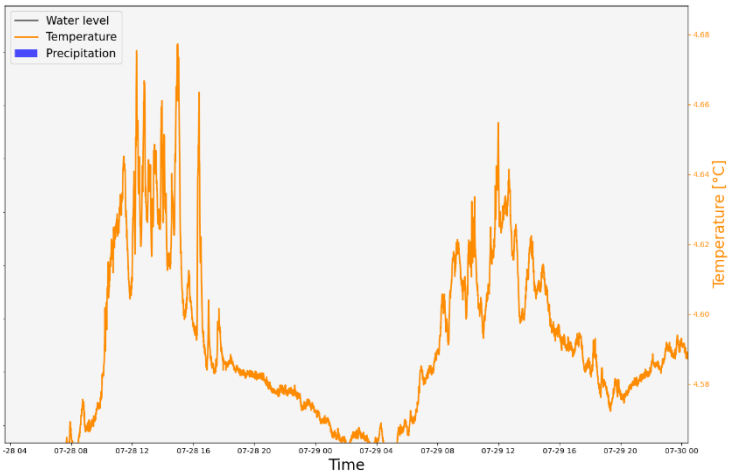

Figure 60: Zoom into the temperature curve of the data logger of KL-WH

between 11.30 and 13.00 every day. The longer the melting season was active, the more unstable the peak became and showed noisy behaviour, as the zoom-in Figure 61 illustrates. The plot shows days on which the peaks are more distinct as well as highly variable. It is striking that the temperature peaks often coincide with low water flow. Respectively, high flow times are simultaneous to low temperatures. Hence, the influence of glacial melt water is visible at this point. This is in line with the observations done by Brown et al. (2006) in the Pyrenees. They aatributed strong diurnal fluctuations in discharge and water temperature later in the melting season to water flowing over shallow open plains, exposed to solar radiation and therefore highly responsive to energy loss and gain through the atmospheric influence (Brown et al., 2006). Summarizing, the thermal heterogeneity in alpine karstic streambeds may have several different origins: variable water sources (e.g. snow or icemelt, groundwater), distance to the source (longer distances infer a damping of the signal) and hydro-climatical conditions, including 'extreme' weather events (Brown et al., 2006, p. 19) Conclusively, they measured similar temperature and discharge developments to Urnerboden over the course of the melting season. This helps to further understand the data measured at Chlus and Waldhüttli and supports assumptions made on potential origins of the karstic water measured.

Considering the tracer data, it has been established that the water takes around 36 hours to get from Chammli Griessfirn to Waldhüttli. This is in line with the temperature minima at 1.00 to 4.00. 36 hours back is the afternoon of the day before yesterday, where due to increased solar radiation, glacier melt was increased. In conclusion, when temperatures drop, the impact of melt water increases. Therefore, higher temperatures indicate the base flow, when melt water does not have a substantial share in the discharge. However, where this base flow originates exactly remains unsolved.

Daily temperature and discharge variations are the strongest in May and June. Snow still covers the slopes currently feeding creeks and streams. When the snow is gone, and the melt water is absent, a major contributor to discharge is lost. Hence, the observed variations are the most frequent during the time of snow melt. The changes are less recurring when the catchment starts to be mainly fed by rain. However, the temperature and discharge amplitudes show a significant increase. Furthermore, as KL-CHH strongly reacts to the presence of precipitation events. This is similarly described for another karst spring system in the Kashmir, where "high discharge amplitudes of the karst springs in non-glacierized basins suggest that these springs are more vulnerable to any change in the amount, timing and form of precipitation" (Jeelani et al., 2017, p. 251). This is in line with the data collected at Chlus in the second half of the summer, when the snow melt period was over. Meanwhile, KL-WH only to reacts to precipitation events on the water level curve. Additionally, the curve increases of water level and temperature are not as distinct as in KL-CHH. Especially the temperature measurements of KL-WH do not show any

signs of a precipitation impact whereas they rise and drop clearly at KL-CHH. This is remarkable since it was expected that the karst networks show at least a small response to the weather.

Research question 12 was regarding the potential connection between the Griess Glacier and Chlus, based on the ammunition remaining in the cave ('Where are the possible entrances to the cave system for the ammunition remainders and is the Chlus connected to the Griess Basin, which used to be a practise target for the Swiss Army?').

The answer to how the ammunition reached this location in the underground has yet to be discovered since the Chlus sensor did not record clear signals indicating a constant flow of melt water as KL-WH did. Therefore, there is no evidence in the current study which would indicate a connection to the glacier. The additional information on the targeted zones of the Swiss Army artillery training could have helped to limit the potential catchment of Chlus to certain areas but only if the army had used specific zones in the area. However, the information provided by ARMASUISSE (Keiser, n.d.) did not help to further minimize the area. Keiser (n.d.) stated that the Swiss Army targeted large parts of the Griesssee area, as shown on Figure 62. Therefore, every marked zone on the map is worth considering as a potential part of the Chlus spring catchment. This aligns with the results of KI-23-01-CBP-Ur at Chlaridenbödmeli, from where the only connection to KL-CHH was successfully tested. No other clear entrance to the Chlus catchment could be determined. The current study only allows to label one access for the ammunition remainders into the cave network. This particular finding is not encouraging since

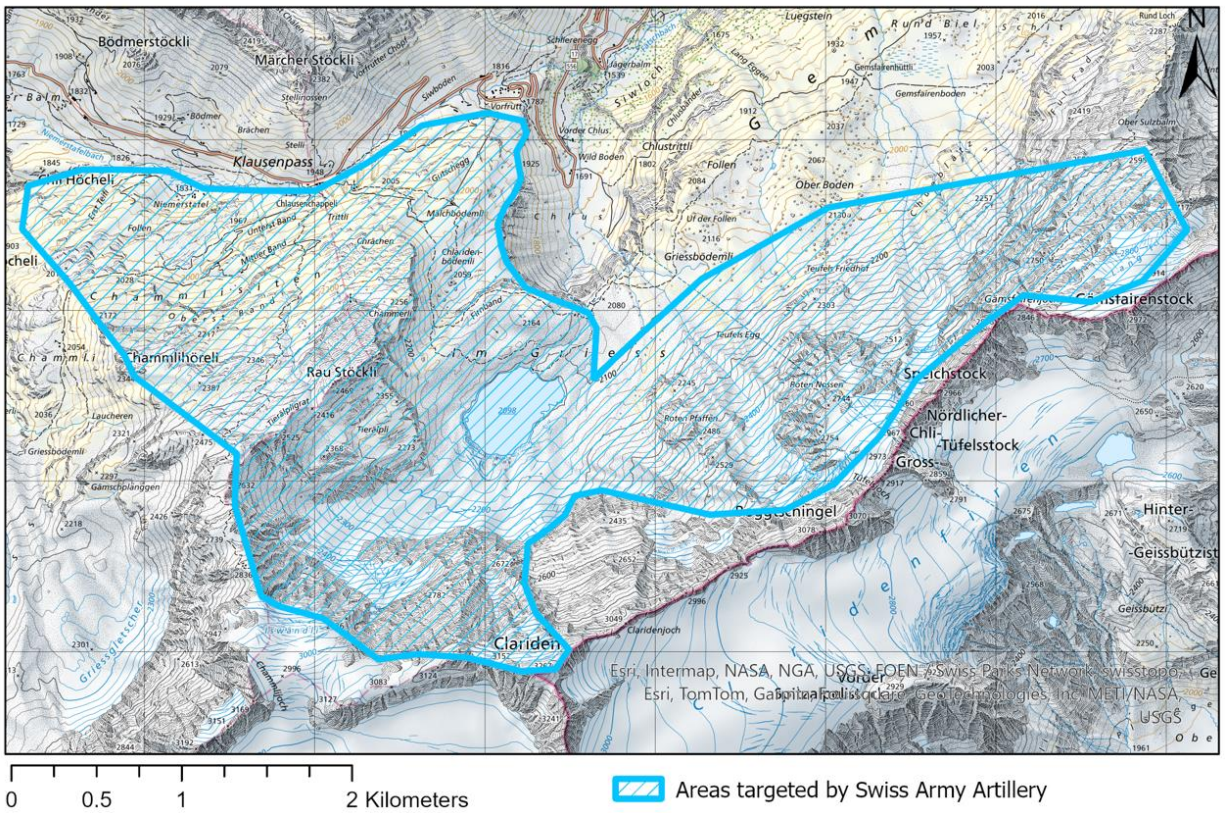

Figure 61: Zones used as former targets for artillery drills by the Swiss Army (Keiser, n.d.).

there might be countless smaller and larger cave entrances in the designated perimeter, which could be traced to KL-CHH. To answer this research question, future studies should target the search for additional water sinks and investigate them.

Moreover, the data collected by the Waldhüttli sensor does not support similar assumptions regarding the melt situation in its catchment. It shows the start of the snow melt in May but whereas KL-CHH changes its behaviour at the end of June indicating a catchment, in which the snow melts earlier due to sun exposure. KL-WH just reduces the amplitude of the temperature variations presenting continuous melt water characteristics. This implies, that Waldhüttli is connected to a glacier in its watershed. Its continuous melt water release after the snow had already melted indicates ablation water. This is successfully supported by the tracer experiment Kl-23-07 and Kl-23-08, which demonstrated a connection to the glacier on the western side of Klausenpass. However, it must be noted that the area around Griessstock in the Schächental is characterised by nappes built up by limestone. Potentially these karst cave systems from further west do also discharge towards Urnerboden.

Furthermore, another compelling detail is presented by the pressure curve of Waldhüttli. First the curve shows some variation without structure. However, once the snow melt begins to appear on the Chlus sensor, the Waldhüttli pressure records stabilize on an even level without

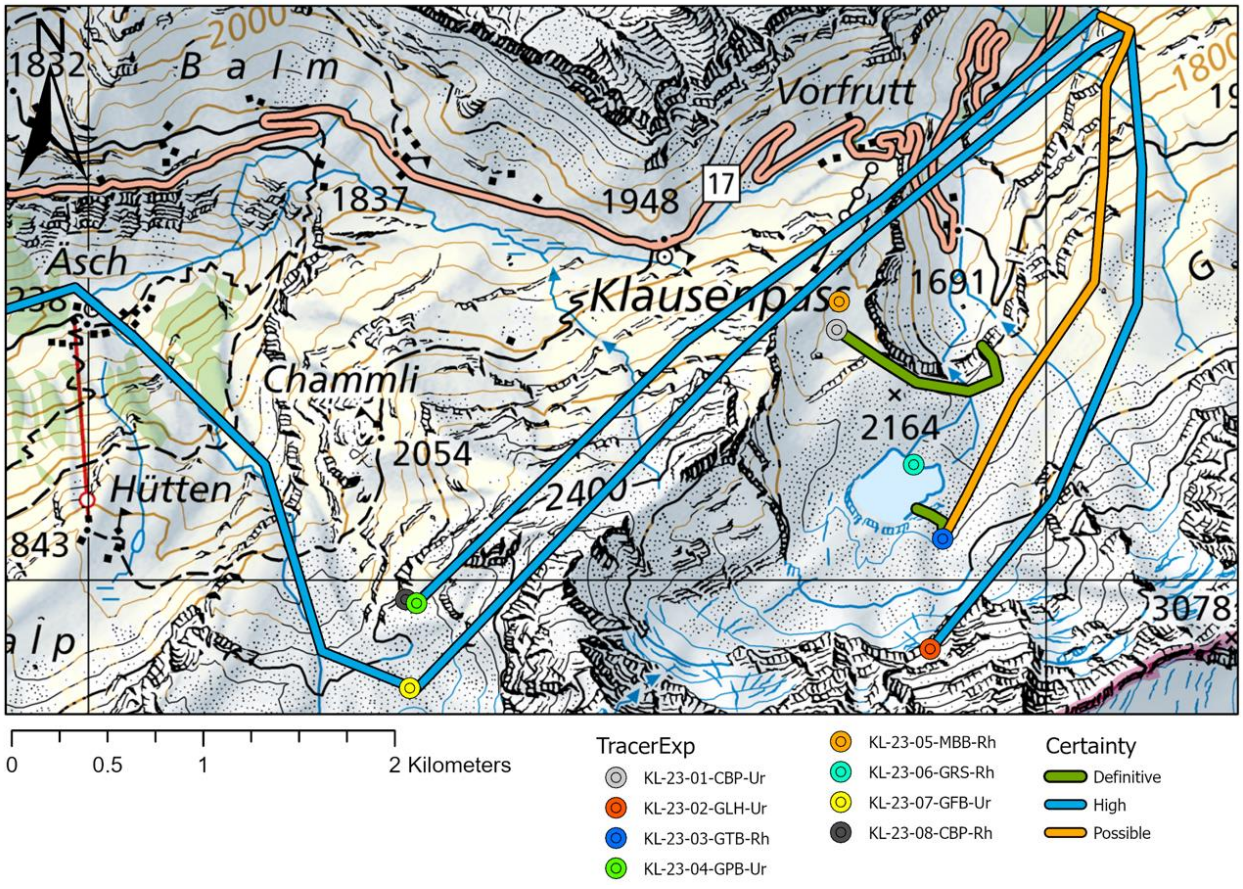

Figure 62: Connections of the subterranean karst network which were discovered during this field study. 3 different probability levels are assumed. Definitive are the ones which gave visual feedback, water which was carrying the tracer and therefore colored green or red. Connections with high certainty showed a signal and possible connections are not certain due to strange behaviour of the signal and were not clearly determinable.

larger deviations. The water level stays almost the same. This is very interesting as it is only minorly influenced by precipitation events and therefore contrasting the Chlus discharge strongly. A potential explanation for this weak signal could be the long way the water covers from its watershed. As the water is longer in the underground, the temperatures and water level can easier be buffered by the karst network. The distance which water must cover to emerge at KL-CHH is assumed to be smaller, provided that its watershed is the Griess basin. Therefore, KL-CHH reacts stronger and quicker to sudden changes in temperature and discharge than KL-WH.

To answer research question 5 and 7 all tracer studies were considered leading to the following potential connections, visually presented in Figure 63.

Definitive connections:
- Chlaridenbödmeli → Chlus
- Ice tunnel → Griesssee

High certainty:
- Griessloch → Waldhüttli Waterfall
- Gämschplanggen → Waldhüttli Bach
- Griess Glacier Chammli → Waldhüttli Waterfall
- Griess Glacier Chammli → Ribi

Possible connections:
- Ice tunnel → Waldhüttli Waterfall

These connections (see Figure 64) all possess legitimate foundation to be classified in their respective class. Based on the tracer experiment findings and the summarizing map in Figure 63, research question 5 can be addressed. Almost every experiment revealed at least one connection between injection sites and a spring on Urnerboden. Since no tracer recovery could be performed, it cannot be assured that the fluorometers positions were the only exit point of the tracers from the karst aquifer. There might be more connections to other springs, either further east on Urnerboden or even around Linthal. To get more information on potentially far reaches of the karst network, additional fluorometers could have been placed in the river Linth, before the Fätschbach joins at Linthal.

Furthermore, concluding the tracer experiments it is not clear where the lake discharges to. It remains to be seen whether there even is a subterranean drainage channel, or if water infiltrates through the sedimented debris into the karst network. However, this is a complex undertaking, as the complete lake might have to be coloured with tracer for further evidence. Additionally, this needs to be done in fall, when the lake level has fallen below the outlet level. Therefore, the current study does not provide an answer for research question 7.

Moreover, an application of a melt model, ablation and discharge information of the springs would be an appropriate way to follow up the current study. Using such a model the origins of the springs might be assessed with higher precision. The model could calculate where and when

melt occurs. In combination with the discharge data of the springs a potential catchment area could be narrowed down for Chlus.

Various results were considered in this study. For future studies the following is recommended: firstly, the Chlus spring's (KL-CHH) origins should be studied thoroughly. The Chlus is a major water supplier of the Fätschbach and therefore of great importance for the water supply of Urnerboden. Since it is seems not connected to the glacier, another part of the valley region must be feeding the cave network. Secondly, it would be interesting to further investigate the signals at both Waldhüttli springs. The connection to Schächental is evident. Although, the signal exhibits uncommon and merely explicable characteristics caused by KL-23-02-GLH-Ur, which indicates a connection from KL-WHF to KL-GLH. To further explore this behaviour, isolated tracer studies should be conducted at KL-GLH. Future studies should also address the origin of the KL-GLH's water. The results of the current study suggest that this is either in the Clariden north face or from the Claridenfirn itself. Contradictingly, geological features do not provide underground structures in favour of this theory. Considering these features, the water from Claridenfirn should be channelled southwards in accordance with the layering of the stratigraphy.

Despite the promising results of the current study, questions remain. Furthermore, several new questions were raised throughout the current study:

- Where is the discharge of the small karstscape between Alp Chammli and Klausenpass directed to?
- Where is the discharge of the big karstscape between Alp Chammli and Griessstock routed to?
- Since the spring was dry in March, where are the large masses of water of Waldhüttli Waterfall coming from?
- Where is the water of the other resourceful springs on Urnerboden coming from?
- Are there subterranean connections between the karstified limestones of the Griessstock nappe and the large springs at Berglistüber or even further down in Linthal?

Overall, the results and limitations of the current study urgently require further investigations to gain a better understanding of Klausenpass' hydrological network functioning.

6.2.1. Further use for the water level measurements

Using a melt and ablation model, in combination with other models representing the runoff and creek flow of water exiting the lake, the lake water level could be modelled. While such a procedure is off limits for the framework of this thesis, it could be tackled in further investigations of the area with attempts to model discharges of the springs on Urnerboden.

6.3. Comparison of the visually observed events and the lake pressure sensor.

Ten events were observed which could have had an influence on the wave activity on the lake. There may well have been more events than discovered on the Tikee 3 photographs. However, one goal of this part section was to confirm the visually seen events on the photographs with an increase in water level variability recorded by the pressure sensor in the lake. It is imperative to differentiate between the two types of signals visible on the plots of the lake pressure sensor. Signals starting off with a high amplitude and then slowly decreasing may indicate an event like calving or ice avalanche while signals with a slight increase and steadily high amplitudes may be due to wind and weather influences.

The calving signals were indeed recorded by the pressure sensor used in the current study. However, for future studies focussing on these events, the sampling interval needs to be smaller to deliver precise data. The chosen frequency of 30 seconds turned out to be too big. Many events forming waves on the lake surface are only symbolised by about two to three peaks in the curve. A shorter interval would lead to more precise data and help to understand the lake's reaction to certain events. Although the interval length of 30 seconds is not appropriate for high resolution analysis of calving events, the data can be used as general representation of the lake water level fluctuations in this study.

It can be seen in Figure 64, the sections of high variability, quick changes of lake level but not of high amplitudes, indicate higher activity on the lake surface and may therefore represent waves on the lake surface. Unfortunately, an anemometer has not been part of the meteo station. Therefore, these increased variability periods cannot be matched to wind measurements.

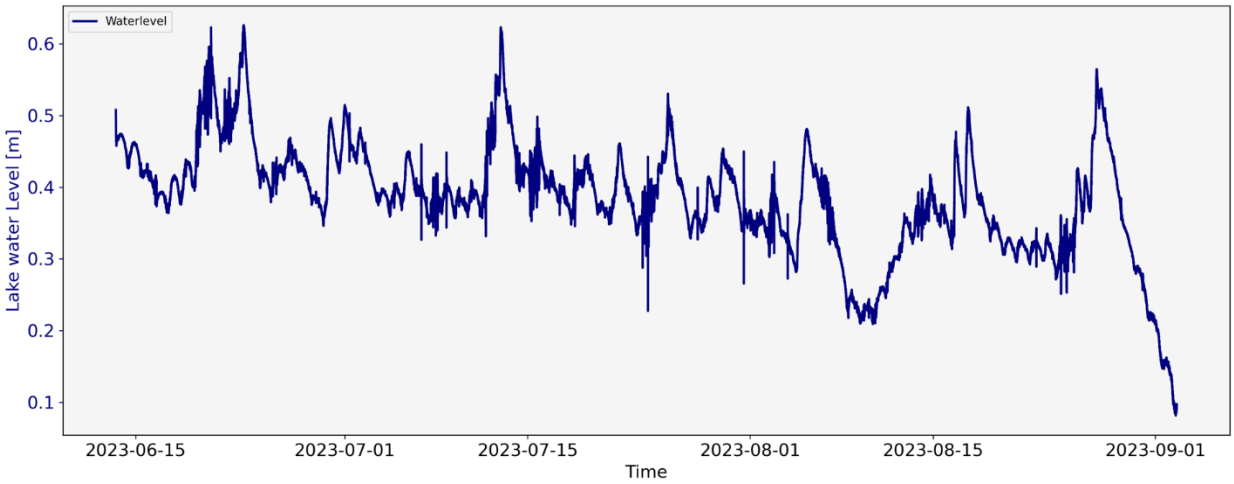

Figure 63: Illustration of the lake surface level variability from middle of June 2023 until the beginning of September 2023. The water level of the Griesssee is steady over the whole measuring period, only decreasing at the beginning of September.

As displayed on Figure 64, the lake level starts to decrease in September, right before the removal of the sensor. However, leaving the sensor slightly longer in place would not have had significant consequences. On the last drone missions on the 1st of October the sensors location was more than one meter above the lake water level. Therefore the sensor's recording would have stopped anyways soon after the removal. Based on the current measurements, the ablation has decreased in September. Additionally, there were only three days with more than 5mm of precipitation in the area and in total fewer rain events than in the surveyed months before. Conclusively, this combination leaves not enough water resources available to sustain the lake water level in October.

As indicated by Figure 64 the lake surface varied continuously over the summer. However, this is also true for the Griesssee's surface area. To answer research question 4 visual observations and the ortho photos from the terminus were taken into account as the whole lake surface area was not covered by this study. It has been stated that the lake surface varied as well as retreated laterally with the reduction of the water level. As some parts of the shoreline are shallow, a lake level decrease causes an expansion of the shore area into the lake area. In conclusion to answer research question 4, the lake level and surrounding area are causally connected and develop accordingly.

The following limitations were determined for the hydrological part.

- Since the origin of the water is unknown and many sinks in the area are either not easily accessible or have not been discovered yet. The origin of the water remains largely unknown and therefore not every connection could be retraced.
- Not all connections could be sampled with the prevailing low water flow in September.
- It would be helpful when creeks and streams carried more water. Therefore, it us suggested that similar experiments should be conducted during the snow melt season, when more water is displaced.
- The number of sensors at hand limited a thorough investigation. It would have been possible to observe more springs at the same time with more fluorometers. Conclusively, the data would have been more diverse since every location and spring itself would have been eligible for the study leading to a higher precision in assessing the network.
- The pressure and temperature sensor at Waldhüttli was not positioned well enough. The sensor was installed during winter and Waldhüttli waterfall spring was still covered by snow and was releasing no water. Therefore, the exact position of the spring could not be found. The measured signal suggests two options. Either as soon as the waterfall began running, the sensor was influenced by both springs, or that there is even a third outlet releasing water from third origin. Conclusively, the recorded data possibly is a mixture of both springs. This is problematic because the data cannot give clear indices on the origin of the water. For future studies, every spring outlet should be considered

and sampled individually. Also as the temperature data proposes that the KL-WH spring outlet was independent of the others, it should be sampled in a next tracer study separately.

- Usually, the tracer data gives valid information about a link between sink and spring. However, the current measurements show uncommon behaviour. This must be considered leading to an increased uncertainty of the signal's accuracy.

6.4. Glaciological analysis

The ground targets (GTs) were installed to be able to retrace surface movement of the glacier. In hindsight, they did not fulfil the intended purpose. Some downstream movement over the summer was expected. However, this cannot be seen on the ortho photos due to very jumpy data points. Based on the collected data, no clear signal of movement could be detected, only some GTs indicate that there might be some minor flow present. As mentioned earlier, the GTs came to lie within a square meter, with barely a sign of a one-direction flow. Contradictory, they moved up and down the glacier flow line and even show movements to the left and right. GT1 is even showing movement to the northwest. If there was movement, it was assumed to indicate different directions towards east northeast.

Several significant challenges rose during this data collection. Unfortunately, three of the five GTs got moved unnaturally at least once. GT 3 was blown away on one day. Luckily, it could be retrieved, but only after the drone surveys were already conducted. A similar thing happened to GT 1, which has been moved but refixed on to the boulder by a stranger, using several rocks as weights. Unfortunately, it was about one meter off the original position. This was only detected at the end of an investigation when noticing, that the bolt was sticking out too much, for that there should have been a drilled hole underneath it where the bolt would have reached into. Moreover, GT5 was lost for most of the summer. It was probably blown away by the wind as well, as the GTs have not been fixed permanently into the rock. For future investigations on the Griess Glacier using GTs larger bolts should be used to screw the GTs onto the carrier rock.

Generally, the GT data did not produce the results as expected. The outcome is very diverse. Whereas some GTs indicate the possibility of present ice flow, others further down in the flow line only indicate minimal or unrecognisable basal flow. These findings may be limited by the quality of the aerial images and the temporal resolution applied. GTs measuring technisues might reveal more promising results when used over more than one summer. Additionally, reference points off the glacier on bedrock should be installed. Hence, the relative position of the GTs on the ice could be set into perspective and movements would be visualized with less uncertainty. In general, the method of ground control points (GCPs) on bedrock improves the

precision of the ortho photos significantly, as distinct locations could have been used for geo-referencing the images.

It seems that the problem with the satellite reception influenced the data precision not only for ortho photos but also for the digital elevation models (DEMs) leading to differences within the produced elevation models. For example, there were two bedrock areas off the glacier (north towards Tieralpli). Areas on bedrock do not move in any direction. However the designated zones showed motions. While Point A was at a difference of 0cm between two elevation models, point B exhibited an elevation difference of 69 centimetres. This variation within the DEM is not possible and therefore, must be a distortion of the drone data and the photos taken.

This error was determined to be the random error, because no clear trend of the error is visible. The mean equals 3 cm and the distribution of error shown in the histogram (Figure 38) displays a neat bell-shaped curve, indicating a even variation of the vertical shift and therefore a low systematic bias in the data. The standard deviation was calculated to be 0.07m and 0.06m. This is a low value and indicates high precision with a low bias.

Furthermore, there was a discrepancy of the drone images taken and the data provided by Swisstopo (Federal Office of Topography Swisstopo, 2023). The DEMs produced for this study seemed were 50 meters higher than the ones of Swisstopo. The origin of this inconsistency most certainly lies in the triangulation of the base station used for the referencing process. The base station calculated its position according to the satellite data it received in the beginning. For the following experiment conduction, always the same settings were used. However, it was noticed after post-processing that the elevation above sea level of the base station and the elevation data of Swisstopo for the exact same coordinates, were about 50 metres off. Despite this offset, the drone data produced in this thesis can be used for internal comparison without hesitation, since the reference point was always the same. However, when comparing to external data this must be taken into account.

6.4.1. Ablation stakes and PDDF

As well as the GTs, the stakes measurements were also not as precise as anticipated. Most of the ablation stakes melted out of the ice. Hence, data was lost. The hole had to be redrilled to reintroduce the ablation stakes into the ice again. Therefore, all apart from one stake timelines contained gaps, which are not to be filled. However, they still they registered ice loss, presenting minimal ablation which has occurred at the specific location.

Being more specific, the ablation stakes have recorded a diverse loss of ice spreaded over the glacier. For example, stake 5 has a melt rate of 2.09 cm/d in period 1 whereas the registered ablation rate in the 5th period was about 1.09 cm/d, which is a difference of one centimetre per day. Compared to the ablation difference for stake 1 (0.038 cm/d) between the same periods,

the difference for stake 5 is enormous. 5. The uncertainty assessment resulted in an error of ±41cm of ice loss which equals to ±0.37 m w.e. for summer 2023. This error margin seems high for measurements which span between 1m and 2m in three months, but is similar to the uncertainty presented by Romshoo et al. (2023) for Kolahoi Glacier in the Kashmir with ±0.34m.

The differences between may be explained by the different debris cover thickness. However, the variation within their measurements must be due to some other reasons. A possible factor influencing the melt might be the exposure to sunlight. Several changing circumstances occure during the experiment. The sun changes its path across the sky throughout the summer, lowering its orbit in fall. The to the shadow provided by the Clariden, the shaded times on the glacier are lengthened and less radiation reaches the glacier. Sunshine duration is significantly influenced by that process. It seems quite possible that, for example, stake 1 was exposed to more sunlight at the beginning of summer compared to fall since the sun was increasingly hidden behind the mountain range.

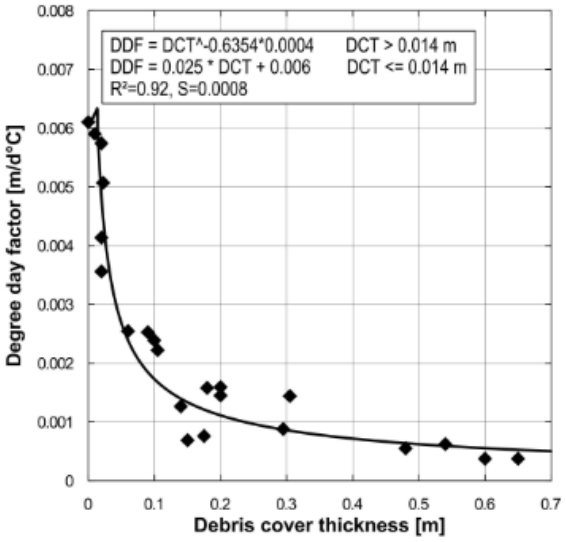

Figure 64: Relationship of PDDF and the debris cover thickness as it has been retrieved by Juen et al. (2014).

Countering the gaps in the stake measurements, two measures were taken. Firstly, it was assumed, that the melt is always proportional at every stake. Therefore, the proportionality factor of each stake relative to stake 3 was taken to extrapolate each stake for the complete measurement period. It was considered that these extrapolated stake measurements do not represent reality. However, they model the potential ice loss at each location. Note that this method has its limitation since it does not include any specific influences this site might have experienced.

Secondly, the extrapolation method was conducted, which relies on the positive degree day factor (PDDF). Applying the PDDF the stake measurements were newly arranged resulting in more precise ablation at the stakes over the whole summer than the actually measured ablation stake data.

The displayed PDDF and debris cover map (Figure 46 and Figure 44) visualize the potential ablation differences over the glacier surface. The calculations for this map were performed based on Juen et al. (2014) and Fyffe et al. (2014) who have conducted similar studies. Comparing the PDDF and the corresponding debris cover thickness (DCT), a regression line

was derived. Based on that relation, the PDDF for every debris cover thickness was estimated (Figure 65).

However, Juen et al. (2014) deduced a regression relation which compares the debris thickness to the PDDF and performed a brief statistical analysis of correlation. Their correlation factor was $R^2 = 0.92$ with a $SD = 0.0008$ for the regression function:

$$DDF = DCT^{-0.6354} * 0.0004 \; for \; DCT > 0.014m$$

For this study the curves produced from the data were

$$DDF = 0.0027^{-3.44DCT}$$

$$DDF = -0.0054\, DCT + 0.0025$$

With correlation factors of $R^2 = 0.8498$ for the exponential and $R^2 = 0.8439$ fo r the linear regression respectively, they presented a good correlation (Figure 65). Even though both regression factors are almost equal, the exponential regression fits the current data better. This

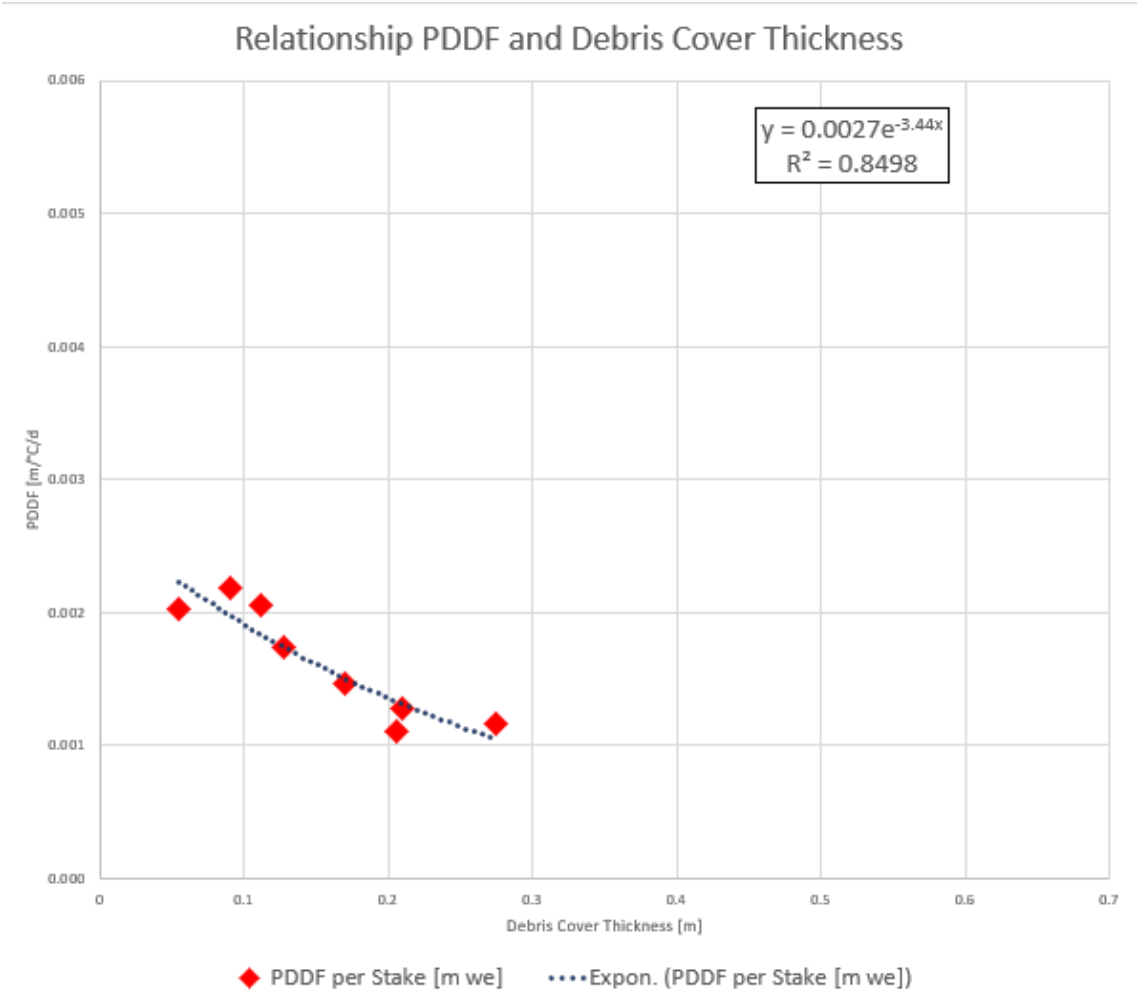

Figure 65: Relationship between PDDF and the debris cover thickness depicted with the exponential line of best fit. The plot set up in a comparable manner as Figure 64, the same relationship presented by Juen et al. (2014).

In Appendix 27, the same scatter plot with the linear fit is presented.

is in line with Juen et al. (2014), as for their ablation stake data an exponential curve is also the better choice. Generally, the relationship between debris cover thickness and ablation has been described as non-linear before (Fyffe et al., 2014) as confirmed by Juen et al. (2014) and also shown in this thesis (Figure 66).

All curves in one plot (Figure 67) show a similarity in the areas where the data of this study was situated. However, it is also displayed deviations below 0.1m and above 0.4m. Most certainly these heavy deviations originate in the lack of data points within the performed study on Griess Glacier. Adding more data of ablation stakes measurements would have increased the precision and robustness of the regression. One significant difference between the current study and Juen et al. (2014) is the lack of a complete measurement series of a glacier area with a debris cover thickness of five or less centimetres. In this study, Stake 7 was in a zone where the debris cover thickness was the thinnest with only 5.5 cm. Unfortunately, this is exactly one of the stakes which lacks the most data since the stake melted out after the first period.

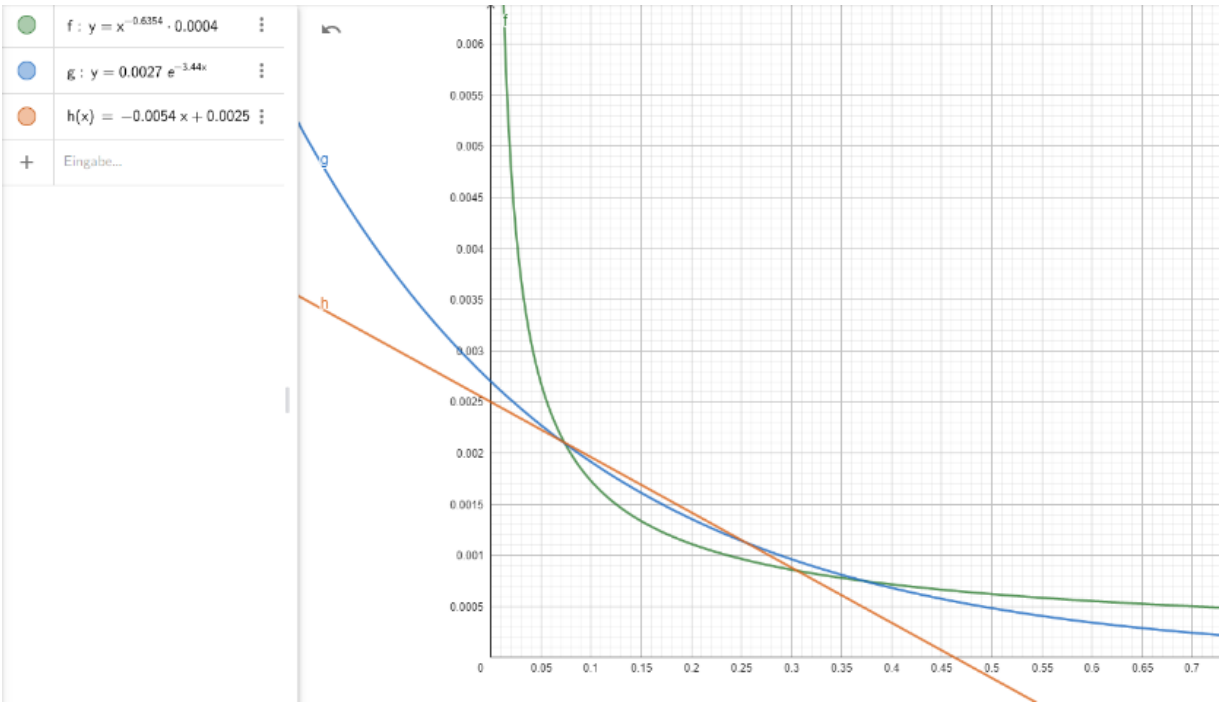

Figure 66: Plot of the 3 different curves, green is the curve found by Juen et al. (2014), while blue (exponential) and orange (linear) are the two suggested curves from this study. At a debris cover thickness between 0.05m and 0.35m they all show similar PDDFs, but outside of that range, the curves differ strongly.

There was considerable difference observed between the measured stake data and the ablation measured by the drone. Additionally, these dissimilarities were not consistent with each other either, some of them differencing negatively, others positively. Therefore, a general deviation (systematic error) could not be assumed. There might be the possibility, that the difference between stake-measured and drone-sensed height loss was due to glacier movement. In this case, the ablation stake measurement would have been relative to the point on the ice (Scenario 1, Figure 68) while the sensed ablation would have measured the change of surface elevation at the specific coordinates (Scenario 2, Figure 68). If there was ice flow present, these two types

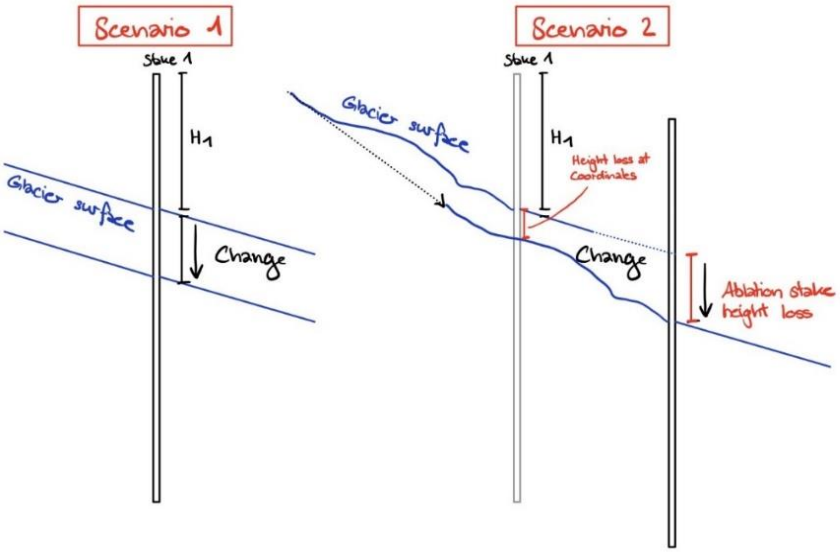

Figure 67: Illustration of how the different measurements of ablation with the drone could have come into place. Scenario 1 and Scenario 2 are a differentiation of surface elevation which has changed in combination with a coordinate change of the ablation stake.

of elevation change would differ, whereas without ice flow, this difference could originate in data inprecision.

The PDDFs acquired for this glacier depend strongly on the debris cover thickness. It varies between 0.5 and $2.5\,\frac{mm}{°C*d}$, with a mean PDDF over the whole glacier at $1.8\,\frac{mm}{°C*d}$. As for the PDDFs of Brook et al. (2013). This PDDF of Griess Glacier was comparibly low. The PDDFs measured on Franz Josef glacier in New Zealand varis between $1.1\,\frac{mm}{°C*d}$ under 43cm of debris and $8.1\,\frac{mm}{°C*d}$ on bare ice. The mean PDDF is $4.4\,\frac{mm}{°C*d}$ (Brook et al., 2013). However, these differences are probably due to different site conditions. The Franz Josef Glacier is a temperate glacier reaching down to only 280 meters above sea level. Additionally, it is situated at the West Coast of New Zealands South Island, which is known for heavy precipitation. The precipitation on the terminus was measured to be 7 m/a which is around three times the precipitation a Swiss glacier experiences in a year (MeteoSwiss, 2024). Precipitation can influence melt below debris. However, Anderson et al. (2006) argue that temperatures have a stronger influence on the ice melt than precipitation.

Juen et al. (2014) present PDDFs in combination with ice cliff backwasting as this was analysed in this thesis. They measured $4.3\,\frac{mm}{°C*d}$ on north facing and $5.2\,\frac{mm}{°C*d}$ on east and west facing cliffs. These PDDFs are lower than the ones calculated for Griess Glacier The northwest facing cliff showed a PDDF of $7.8\,\frac{mm}{°C*d}$ and the eastern facing terminus $9.9\,\frac{mm}{°C*d}$. This can be explained by elevation differences. The lowest point of Koxkar Glacier (Juen et al., 2014) is at 3060 meter a.s.l., Griess Glacier's highest elevation is approximately 400 meters lower at 2650 meters a.s.l.

In conclusion to answer research question 1, the Griess Glaciers surface was reduced on average by 1.8 meters of ice loss. The several larger ponors and ice cliffs recorded strong mean edge retreats of 3.7m to 9.5m. There were zones with higher horizontal retreats, up to 19.5m at the terminus. The mean ice height loss of summer 2023 during the drone missions is line with

the pre-study performed with the DEM differentiation for 2015 and 2022. The results differ in the one-digit centimetre area. Extrapolating the ablation using the PDD derived from KLAU for a longer period of summer 2023 (May 25 – October 1) the melt can be estimated higher at approximately 2.37m. However, this estimation of the ablation for 2023 is 0.6m higher than the mean melt from the years before. A year-to-year resolution of the years before does not exist, therefore the ablation trend in the last seven years could not be retraced. Maybe the ablation of 2022 was also around 2.3m and would be more like 2023. Best option to validate this data in 2024 is to set up the measurement installations again and compare how it develops and potentially differs from the 2023 results. Comparing them might reveal lack of precision in this study's results or it possibly confirms the measured melt. Yet still not the complete year 2023 has been considered in this survey, but since at the end of May snow was still covering the Griess Basin, it can be considered representative for the year 2023.

The study had some limitations in all fields of research.

- Firstly, due to the topographical set up of the area, being surrounded by mountain ridges and rock faces on three sides, the satellite service was not enough for the application of preprogrammed drone missions, which rely on satellites for high precision data on the images. This possibly influenced the coordinate's precision of the drone and the images, as well as the precision of the elevation models, as seen in the comparison of the two supposedly stable bedrock areas. The poor signal reception also caused troubles while flying the drone, the autopilot was turned off every 5 meters and had to be activated again manually on the remote.
- Secondly, the error in the elevation models and the program for ortho photos from the point clouds challenged the analysis. A systematic error was present on every image, on the XY-axis, but also on the Z-axis.
- Thirdly, the debris thickness at the stake's locations was inconsistent, which is a general limitation in the field of the glaciological methods. The stake's holes in the debris cover were always closed by hand again. However the thickness of the newly covered areas was still impacting this data collection, as it was never the same as before the measurement. This is also a source for a random error in the ablation stakes measurements. Additionally, each uncovering and closing shifted the rock composition leading to different thermic characteristics and influencing the sub debris melt.

In further research, the residual volume of Griess Glacier ice could be investigated using ground penetrating radar methods. From there the water stored in the glacier in can be estimated. Applying melt models with different climate scenarios to it, future water availability can be estimated and possibly determine for how long Griess Glacier will be feeding Urnerboden with melt water before it is gone.

7. Conclusion

This study set out to gain a better understanding of the hydrological functioning of the Klausenpass and Urnerboden area. Applying thorough research methods in the fields of alpine hydrology and glaciology, the relationships between the karst network and the glacier were examined.

This study has produced a plausible PDDF of the glacier and identified zones of higher ablation and horizontal retreat on the different ice cliffs and terminus. Being limited to the survey perimeters and the number and distribution of the ice stakes, this glaciological study lacks the precision and wholeness for validation and calibration of a complete mass balance of the ablation season. For further research, the surveyed extents should be expanded to cover more glacier area, and ground control points of the glacier should be established to make proper geo-referencing possible. As the PDDF method has been subsequently applied for ablation estimation of the glacier, an acceptable approximation of the ice melt on Griess Glacier could be determined. The ablation of summer 2023 is in line with the ablation per year of the previous years. On average the ablation rate was -1.8m (-1.64m w.e.) for 2015-2022 and for 2023 between 27th of June and 1st of October the ablation was -1.8m as well. Though, it has to be kept in mind, that before the first drone survey, some ablation already happened and thus it has to be assumed that the effective ablation of 2023 is slightly higher. One way to compensate for that, would be extrapolating the melt according to the positive degree days measured before the first drone flights.

While the drone survey findings partially confirm hypotheses 1, nuances in the GTs data suggest that there might be partial ice flow present but not at every GT location, the ortho photos georeferencing is not precise enough to let definitive conclusions be drawn. Despite these vague variations, it can be stated, that at two locations at least some movement in the centimetre area is present.

The research has also shown how the karst network is structured and revealed subterranean connections between different points in the area. It has also further shown that even if spring outlets are directly beside each other, they may show significant differences in discharge and temperature characteristics and therefore suggest different karst networks. This highlights the importance of knowing where the water feeding the springs is originating from, as they are essential water suppliers of Urnerboden. Serious challenges would be brought to the ecological functioning of Urnerboden if these springs would not feed Fätschbach anymore. The most important findings are that both Waldhüttli springs are fed at least partially by water from the western side of Klausenpass, KL-WHF even by glacial melt water. Additionally, KL-WHF is fed by water coming from Clariden, as the Uranine signals from the injection at Griessloch KL-23-

02-GLB-Ur were picked up at KL-WHF. The precise mechanism of the oscillating Uranine signal at KL-WHF from Griessloch remains to be elucidated in future research to reveal whether this signal is indeed caused by a siphon. Meanwhile snow melt and precipitation recharge from the Griess basin controls the discharge of the Chlus spring (KL-CHH), as indicated by tracer test KL-23-01-CBP-Ur as well as pressure and temperature data registered for spring and summer of 2023. That KL-CHH is directly fed by glacial melt water can be ruled out due to the temperature profile of the p&T logger in the spring, but a potential connection to the lake can neither be confirmed nor denied. '*Most of the water discharge takes place underground through the karst conduits'*, strong evidence is provided to accept this hypothesis (H2), as it has been observed that the lake water level has lowered, even though the outlet ran dry, and no other surface drain has been observed. Also, the tracer test KL-23-06-GRS-Rh did not provide clear and distinct results. To accept this hypothesis, further tracer analyses would have be to performed, focussing more closely on the Griesssee itself. In the absence of any alternative lake outlet or site with water clearly permeating the terrain, hypothesis 3 and hypothesis 4 can neither be accepted nor rejected. A determined response would necessitate the revelation of at least one additional lake drain. Yet it cannot be ruled out based on the obtained data. Potentially the main karst aquifer spring discharging the water of Griesssee has not been found yet, as this spring has not been sampled during this thesis.

The results of the tracer experiments fully support hypothesis 5. All tracer experiments conducted have routed the tracer in direction of Urnerboden. In line with the incline of the Griessstock nappe, it might even be possible that parts of the water are directed southwards and leaves the karst network in somewhere around 'Vorder Sand' or 'Hinter Sand'. But as no fluorometer had been placed outside of Urnerboden this could not be confirmed.

While most of the hypotheses could not be fully confirmed, the insights gained from this study offer valuable directions for future tracer experiments in the area which are already in the planning stage.

Some further studies which could be initiated would be a tracer injection on the glacier in several different moulins, preferably with different tracers and then test, whether the tracers are only recorded in the lake or whether a spring on Urnerboden records the signals. This way the connection of the Griess basin to Urnerboden could further be evaluated.

8. Acknowledgements

A project of the size of a Master's thesis is not possible to do without the help of other people. Writing a thesis on my own, I had to face some ups and downs, which were overcome with the help of my supporters.

First of all, I want to thank my supervisor, Dr. Martin Lüthi, who has supported me from start to finish line and helped me get this project on the right track. With extensive knowledge and passion for Alpine environments and deep interest in cave exploration, this project was an affair of the heart and with his enthusiasm he has pulled me in deeply. I'm immensely grateful for the support and the talks on possible explanations for the data. And of course, thank you for taking me on my first to ski tours around the Griess Basin and to Raustöckli.

Second, I want to thank my co-supervisor Boris Ouvry for the support regarding everything that had to do with the drone, remote sensing analysis and data evaluation. Also, for assisting me in the field and acting as a remote consultant when technical issues with the drone occurred, the first time you were not accompanying me in the field.

Further, I want to express my gratitude to the following:

- To Yvo Weidmann for initiating this research topic and the hospitality during the caving field camp at Urnerboden in September. Additionally, thanks to all the OGH members supporting the thesis in any possible way, especially Res, Fabian, and Yannick, for the introduction of the tracer Uranine at Griessloch.
- To Tobias Ibele for the support in geological-related matters.
- To Oliver Indergand, Lukas Eggimann of the Canton of Uri.
- To Marco Baggio of AXPO KLL, for the provision of information on the power plant in context to the water captures.
- To the GIUZ for providing me with various materials and tools needed for the fieldwork, drills, ablation stakes, DJI drone, ground targets, fluorometers, and p&T data loggers.
- To the WSL for providing further fluorometers needed for the tracer studies.
- To my fieldwork buddies Dale, Pepsi, and Gisela, for accompanying me for a day on the glacier and assisting reading out data and flying with the drone.
- To my fellow peers, of whom are some also finishing their Master's degree currently and are always open for interesting discussions on different topics and made my studies an even more lasting experience.
- To Norina, Aakash, Gisela, and Thomas for correcting and proofreading my thesis.
- And last but not least, to my girlfriend Hanna, who supported me during every second of this thesis, listened to me even when occupied with her own challenges and always cheered me up in exhausting moments.

Literature

AgEagle Aerial Systems Inc. (2024, January 6). *High-performance fixed-wing mapping drones*. https://ageagle.com

Albillia Fluorometers. (2023). *GGUN FL-30*. https://albillia.com/

Anderson, B., Lawson, W., Owens, I., & Goodsell, B. (2006). Past and future mass balance of 'Ka Roimata o Hine Hukatere' Franz Josef Glacier, New Zealand. *Journal of Glaciology*, *52*(179), 597–607. https://doi.org/10.3189/172756506781828449

Appenzeller Kalender. (1967). Das Kraftwerk Linth-Limmern im Kanton Glarus. *Appenzeller Kalender*, *246*. https://doi.org/10.5169/seals-375874

Arnold, K. C., & MacKay, D. K. (1964). *Different methods of calculating mean daily temperatures, their effects on degree-day totals in the high Arctic and their significance to glaciology*. https://doi.org/10.4095/331217

Baggio, M. (2023). *Information about the AXPOs activities on Urnerboden and Klausenpass*.

Bastiancich, L., Lasagna, M., Mancini, S., Falco, M., & De Luca, D. A. (2022). Temperature and discharge variations in natural mineral water springs due to climate variability: a case study in the Piedmont Alps (NW Italy). *Environmental Gechemical Health*, *44*, 1971–1994. https://doi.org/10.1007/s10653-021-00864-8

Benischke, R. (2021). Review: Advances in the methodology and application of tracing in karst aquifers. *Hydrogeology Journal*, *29*(1), 67–88. https://doi.org/10.1007/S10040-020-02278-9/FIGURES/6

Benn, D. I., Bolch, T., Hands, K., Gulley, J., Luckman, A., Nicholson, L. I., Quincey, D., Thompson, S., Toumi, R., & Wiseman, S. (2012). Response of debris-covered glaciers in the Mount Everest region to recent warming, and implications for outburst flood hazards. *Earth-Science Reviews*, *114*(1–2), 156–174. https://doi.org/10.1016/J.EARSCIREV.2012.03.008

Bhardwaj, A., Sam, L., Javier Martín-Torres, F., & Kumar, R. (2016). UAVs as remote sensing platform in glaciology: Present applications and future prospects. *Remote Sensing of Environment*, *175*, 196–204. https://doi.org/10.1016/j.rse.2015.12.029

Biemans, H., Siderius, C., Lutz, A. F., Nepal, S., Ahmad, B., Hassan, T., von Bloh, W., Wijngaard, R. R., Wester, P., Shrestha, A. B., & Immerzeel, W. W. (2019). Importance of snow and glacier meltwater for agriculture on the Indo-Gangetic Plain. *Nature Sustainability*, *2*, 594–601. https://doi.org/10.1038/s41893-019-0305-3

Bolch, T., Buchroithner, M. F., Peters, J., Baessler, M., & Bajracharya, S. (2008). Identification of glacier motion and potentially dangerous glacial lakes in the Mt. Everest region/Nepal using spaceborne imagery. *Natural Hazards and Earth System Sciences*, *8*(6), 1329–1340. https://doi.org/10.5194/NHESS-8-1329-2008

Bolch, T., Pieczonka, T., & Benn, D. I. (2011). Multi-decadal mass loss of glaciers in the Everest area (Nepal Himalaya) derived from stereo imagery. *Cryosphere*, *5*(2), 349–358. https://doi.org/10.5194/TC-5-349-2011

Braithwaite, R. J. (1995). Positive degree-day factors for ablation on the Greenland ice sheet studied by energy-balance modelling. *Journal of Glaciology*, *41*(137), 153–160. https://doi.org/10.3189/S0022143000017846

Braithwaite, R. J., & Olesen, O. B. (1989). Calculation of Glacier Ablation from Air Temperature, West Greenland. In J. Oerlemans (Ed.), *Glacier Fluctuations and Climatic Change. Glaciology and quarternary geology* (Vol. 6). Springer. https://doi.org/https://doi.org/10.1007/978-94-015-7823-3_15

Brook, M. S., Hagg, W., & Winkler, S. (2013). Debris cover and surface melt at a temperate maritime alpine glacier: Franz Josef Glacier, New Zealand. *New Zealand Journal of Geology and Geophysics*, *56*(1), 27–38. https://doi.org/10.1080/00288306.2012.736391

Brown, L. E., Hannah, D. M., & Milner, A. M. (2006). Hydroclimatological influences on water column and streambed thermal dynamics in an alpine river system. *Journal of Hydrology*, *325*, 1–20. https://doi.org/10.1016/j.jhydrol.2005.09.025

Buri, P., Fischer, M., Huss, M., & Epp, M. (n.d.). Data on Clariden Lake. In *unpublished*.

Carrivick, J. L., & Tweed, F. S. (2013). Proglacial lakes: character, behaviour and geological importance. *Quaternary Science Reviews*, *78*, 34–52. https://doi.org/10.1016/J.QUASCIREV.2013.07.028

Central Intelligence Agency. (2011). Switzerland. *The World Factbook / Central Intelligence Agency*. https://www.cia.gov

Cogley, J. G. (2021). Mass Balance of Glaciers. *Reference Module in Earth Systems and Environmental Sciences*, *50*(50), 96–100. https://doi.org/10.3189/172756409787769744

Cogley, J. G., Arendt, A. A., Bauder, A., Braithwaite, R. J., Hock, R., Jansson, P., Kaser, G., Moller, M., Nicholson, L., Rasmussen, L. A., & Zemp, M. (2010). *Glossary of glacier mass balance and related terms*. International Hydrological Programme. https://research.manchester.ac.uk/en/publications/glossary-of-glacier-mass-balance-and-related-terms

Cox, L. H., & March, R. S. (2004). Comparison of geodetic and glaciological mass-balance techniques. *Journal of Glaciology*, *50*, 363–370. https://doi.org/10.3189/172756504781829855

DJI. (2024, January 6). *Phantom 4 RTK*. https://www.dji.com

EMLID LTD. (2024). *REACH RS2+*. https://emlid.com/

Federal Office of Meteorology and Climatology MeteoSwiss. (2023, November 26). *Decreases in temperature with altitude*. https://www.meteoswiss.admin.ch/

Federal Office of Topography Swisstopo. (2023). *Map of Switzerland*. https://www.swisstopo.admin.ch/

Finsterwalder, S., & Schunk, H. (1887). Der Suldenferner. *Zeitschrift Des Deutschen Und Österreichischen Alpenvereins 18*, 72–89.

Fyffe, C. L., Reid, T. D., Brock, B. W., Kirkbride, M. P., Diolaiuti, G., Smiraglia, C., & Diotri, F. (2014). A distributed energy-balance melt model of an alpine debris-covered glacier. *Journal of Glaciology*, *60*(221), 587–602. https://doi.org/10.3189/2014JOG13J148

Goldscheider, N., Meiman, J., Pronk, M., & Smart, C. (2008). Tracer tests in karst hydrogeology and speleology. *International Journal of Speleology*, *37*(1), 27–40. www.ijs.speleo.it

Grabovšek, F., & Turk, J. (2010). Observations of stage and temperature dynamics in the epiphreatic caves within the catchment area of the Ljubljanica river (Slovenia). *Geologia Croatica*, *63*, 187–193.

Gremaud, V., & Goldscheider, N. (2010). Geometry and drainage of a retreating glacier overlying and recharging a karst aquifer, Tsanfleuron-Sanetsch, Swiss Alps. *Acta Carsologica*, *39*(2), 289–300. https://doi.org/10.3986/AC.V39I2.100

Gunn, J. (2003). Encyclopedia of Caves and Karst Science. In John Gunn (Ed.), *Encyclopedia of Caves and Karst Science*. Fitzroy Dearborn.

https://doi.org/10.4324/9780203483855/ENCYCLOPEDIA-CAVES-KARST-SCIENCE-JOHN-GUNN

Haeberli, W., Cihlar, J., & Barry, R. G. (2000). Glacier monitoring within the Global Climate Observing System*. *Annals of Glaciology*, *31*, 241–246. https://doi.org/10.3189/172756400781820192

Han, H., Liu, S., Ding, Y., Deng, X., Wang, Q., Xie, C., Wang, J., Zhang, Y., Li, J., Shangguan, D., Zhang, P., Zhao, J., Niu, L., & Chen, C. (2008). Near-Surface Meteorological Characteristics on the Koxkar Baxi Glacier, Tianshan. *Journal of Glaciology and Geocryology*, *30*, 967–975.

Heim, A. (1871). Notizen aus den geologischen Untersuchungen für Blatt XIV der eidg. Karte. In R. Wolf (Ed.), *Vierteljahrsschrift der Naturforschenden Gesellschaft in Zürich: Vol. 16 (3)* (pp. 241–262). In Commission bei S. Höhr.

Herreid, S., & Pellicciotti, F. (2020). The state of rock debris covering Earth's glaciers. *Nature Geoscience 2020 13:9*, *13*(9), 621–627. https://doi.org/10.1038/s41561-020-0615-0

Hock, R. (2003). Temperature index melt modelling in mountain areas. *Journal of Hydrology*, *282*(1–4), 104–115. https://doi.org/10.1016/S0022-1694(03)00257-9

Hock, R., Rees, G., Williams, M. W., & Ramirez, E. (2006). Contribution from glaciers and snow cover to runoff from mountains in different climates. *Hydrological Processes*, *20*(10), 2089–2090. https://doi.org/10.1002/HYP.6206

Huo, D., Bishop, M. P., & Bush, A. B. G. (2021). Understanding Complex Debris-Covered Glaciers: Concepts, Issues, and Research Directions. *Frontiers in Earth Science*, *9*, 652279. https://doi.org/10.3389/FEART.2021.652279/BIBTEX

Huss, M., & Hock, R. (2018). Global-scale hydrological response to future glacier mass loss. *Nature Climate Change 2018 8:2*, *8*(2), 135–140. https://doi.org/10.1038/s41558-017-0049-x

Ibele, T. (n.d.). Verifications on geological Information. In *unpublished*.

IPCC. (2023). *Summary for Policymakers. In: Climate Change 2023: Synthesis Report.Contribution of Working Groups I, II and III to the Sixth Assessment Report of the Intergovernmental Panel on Climate Change [Core Writing Team, H. Lee and J. Romero (eds.)].* https://doi.org/10.59327/IPCC/AR6-9789291691647

Jeelani, G., Shah, R. A., Deshpande, R. D., Fryar, A. E., Perrin, J., & Mukherjee, A. (2017). Distinguishing and estimating recharge to karst springs in snow and glacier dominated mountainous basins of the western Himalaya, India. *Journal of Hydrology*, *550*, 239–252. https://doi.org/10.1016/J.JHYDROL.2017.05.001

Johnston, R. J. (2024). *ecosystem services*. Encyclopedia Britannica, Inc. https://www.britannica.com/

Juen, M., Mayer, C., Lambrecht, A., Han, H., & Liu, S. (2014). Impact of varying debris cover thickness on ablation: A case study for Koxkar Glacier in the Tien Shan. *Cryosphere*, *8*(2), 377–386. https://doi.org/10.5194/tc-8-377-2014

Kääb, A., Berthier, E., Nuth, C., Gardelle, J., & Arnaud, Y. (2012). Contrasting patterns of early twenty-first-century glacier mass change in the Himalayas. *Nature 2012 488:7412*, *488*(7412), 495–498. https://doi.org/10.1038/nature11324

Keiser, R. (n.d.). Information by ARMASUISSE. In *unpublished*.

Kovacs Enterprise. (2023). *About Kovacs Ice Auger Drills*. https://kovacsicedrillingequipment.com/

Lang, H., Schadler, B., & Davidson, G. (1976). Hydroglaciological investigations on the Ewigschneefeld - Gr. Aletschgletscher. *Zeitschrift Für Gletscherkunde Und Glazialgeologie*, *12*(2), 109–124.

Lauber, U., Ufrecht, W., & Goldscheider, N. (2014). Spatially resolved information on karst conduit flow from in-cave dye tracing. *Hydrol. Earth Syst. Sci*, *18*, 435–445. https://doi.org/10.5194/hess-18-435-2014

Lawson, D. E. (1982). Mobilization, movement and deposition of active subaerial sediment flows, Matanuska Glacier, Alaska. *The Hournal of Geology*, *90*, 279–300.

Leibundgut, C., & Seibert, J. (2011). Tracer Hydrology. In *Treatise on Water Science* (pp. 215–236). Elsevier. https://doi.org/10.1016/B978-0-444-53199-5.00036-1

Leupold, W. (1948). *Bericht über den I. und II. Färbungsversuch am Fätschbach*.

Linsbauer, A., Huss, M., Hodel, E., Bauder, A., Fischer, M., Weidmann, Y., Bärtschi, H., & Schmassmann, E. (2021). The New Swiss Glacier Inventory SGI2016: From a Topographical to a Glaciological Dataset. *Frontiers in Earth Science*, *9*. https://doi.org/10.3389/FEART.2021.704189

Lisag AG. (2023). *Geodienste des GIS Uri*. Geodaten Des Kantons Uri. https://www.lisag.ch/

Liu, W., & Brancelj, A. (2014). Hydrochemical response of cave drip water to snowmelt water, a case study from Velika Pasica Cave, Central Slovenia. *Acta Carsologica*, *43*(1), 65–74. https://doi.org/10.3986/AC.V43I1.613

MeteoSchweiz. (2023). *Klimabulletin Sommer 2023*.

MeteoSwiss. (2024). *The climate of Switzerland*. https://www.meteoswiss.admin.ch/

Mihalcea, C., Mayer, C., Diolaiuti, G., Lambrecht, A., Smiraglia, C., & Tartari, G. (2006). Ice ablation and meteorological conditions on the debris-covered area of Baltoro glacier, Karakoram, Pakistan. *Annals of Glaciology*, *43*, 292–300. https://doi.org/10.3189/172756406781812104

Mölg, N., Ferguson, J., Bolch, T., & Vieli, A. (2020). On the influence of debris cover on glacier morphology: How high-relief structures evolve from smooth surfaces. *Geomorphology*, *357*, 107092. https://doi.org/10.1016/J.GEOMORPH.2020.107092

Moore, P. L. (2018). Stability of supraglacial debris. *Earth Surface Processes and Landforms*, *43*(1), 285–297. https://doi.org/10.1002/ESP.4244

Müller-Lemans, H., Aellen, M., Braun, L. N., Kappenberger, G., & Steinegger, U. (1997). Niederschlagsverteilung im Tödigebiet: Messungen und Überprüfung mit der Wasserhaushaltsgleichung. In U. Moser (Ed.), *Beiträge zur Hydrologie der Schweiz: Niederschlag und Wasserhaushalt im Hochgebirge der Glarner Alpen: Vol. Nr. 36* (pp. 7–43). Schweizerische Gesellschaft für Hydrologie und Limnologie.

Nicholson, L., & Benn, D. I. (2006). Calculating ice melt beneath a debris layer using meteorological data. *Journal of Glaciology*, *52*(178), 463–470. https://doi.org/10.3189/172756506781828584

Østrem, G. (1959). Ice Melting under a Thin Layer of Moraine, and the Existence of Ice Cores in Moraine Ridges. *Geografiska Annaler*, *41*(4), 228–230. https://doi.org/10.1080/20014422.1959.11907953

Pfau, D. (2023). *Wanderung zum Gletschersee am Klausenpass*. https://www.2coinstravel.ch/

Romshoo, S. A., Abdullah, T., Murtaza, K. O., & Bhat, M. H. (2023). Direct, geodetic and simulated mass balance studies of the Kolahoi Glacier in the Kashmir Himalaya, India. *Journal of Hydrology*, *617*, 129019. https://doi.org/10.1016/J.JHYDROL.2022.129019

Rossini, M., Di Mauro, B., Garzonio, R., Baccolo, G., Cavallini, G., Mattavelli, M., De Amicis, M., & Colombo, R. (2018). Rapid melting dynamics of an alpine glacier with repeated UAV photogrammetry. *Geomorphology*, *304*, 159–172. https://doi.org/10.1016/J.GEOMORPH.2017.12.039

Scherler, D., Bookhagen, B., & Strecker, M. R. (2011). Spatially variable response of Himalayan glaciers to climate change affected by debris cover. *Nature Geoscience 2011 4:3*, *4*(3), 156–159. https://doi.org/10.1038/ngeo1068

Singh, P., Kumar, N., & Arora, M. (2000). Degree-day factors for snow and ice for Dokriani Glacier, Garhwal Himalayas. *Journal of Hydrology*, *235*, 1–11. www.elsevier.com/locate/jhydrol

Tam, V. T., Trung, N. D., Ke, D. T., & Batelaan, O. (2004). *Interpretation of a cave system based on tracer experiment, geostructure and cave development analysis*. Trans-KARST 2004, Proceedings of the International Transdisciplinary Conference on Development and Conservation of Karst Regions, Hanoi, Vietnam. https://doi.org/10.13140/2.1.2495.5840

Thibert, E., Blanc, R., Vincent, C., & Eckert, N. (2008). Glaciological and volumetric mass-balance measurements: error analysis over 51 years for Glacier de Sarennes, French Alps. *Journal of Glaciology*, *54*(186), 522–532. https://doi.org/10.3189/002214308785837093

Turner Designs, Inc. (2023). *Submersible Fluorometers & Sensors*. https://www.turnerdesigns.com/

Verkehrsverein Urnerboden. (n.d.). *Geschichte*. Retrieved January 31, 2024, from https://urnerboden.ch

Weidmann, Y. (n.d.). Information of specific locations on Urnerboden UR. In *unpublished*.

WGMS. (2024, January). *Global glacier state*. World Glacier Monitoring Service.

Wingtra AG. (2020, January 16). *What's the difference between PPK and RTK drones, and which one is better?* Drone Know-How. https://wingtra.com/

Wu, L., Li, H., & Wang, L. (2011). Application of a Degree-Day Model for Determination of Mass Balance of Urumqi Glacier No. 1, Eastern Tianshan, China. *Journal of Earth Science*, *22*(4), 470–481. https://doi.org/10.1007/s12583-011-0201-x

Wyss, M., & Hermann, J. (2021). Region Klausenpass (Kla). In *CSI Alps – Die geologische Spurensuche*. CSI Alps. www.csi-alps.unibe.ch

Zemp, M., Huss, M., Thibert, E., Eckert, N., McNabb, R., Huber, J., Barandun, M., Machguth, H., Nussbaumer, S. U., Gärtner-Roer, I., Thomson, L., Paul, F., Maussion, F., Kutuzov, S., & Cogley, J. G. (2019). Global glacier mass changes and their contributions to sea-level rise from 1961 to 2016. *Nature 2019 568:7752*, *568*(7752), 382–386. https://doi.org/10.1038/s41586-019-1071-0

Zemp, M., Thibert, E., Huss, M., Stumm, D., Rolstad Denby, C., Nuth, C., Nussbaumer, S. U., Moholdt, G., Mercer, A., Mayer, C., Joerg, P. C., Jansson, P., Hynek, B., Fischer, A., Escher-Vetter, H., Elvehøy, H., & Andreassen, L. M. (2013). Reanalysing glacier mass balance measurement series. *Cryosphere*, *7*(4), 1227–1245. https://doi.org/10.5194/TC-7-1227-2013

Zepp, H. (2011). *Geomorphologie: Eine Einführung* (5th ed.) [Book]. utb GmbH.

Appendix

Appendix 1: Fieldwork protocol of summer 2023 in the area of Urnerboden, Griessbasin, Griess Glacier, Klausenpass and Chammli. Additionally in the right column, who was part of this work step.

Date	Fieldwork	People
23.03	Inst. p,T-datalogger Chlus-spring	AH, TL
	Inst. p,T-datalogger Waldhüttli-springs	AH, TL
25.05	Inst. Tikee3-camera on Raustöckli	AH, TL
	Inst. Meteostation KLAU on Mälchbödmeli	AH, TL
13.06	Inst. Fluorometer Chlus	AH, TL
	Tracer Kl-23-01 Ur Mälchbödmeli	AH, TL
	Inst. p-datalogger Griess-See	AH, TL
14.06	Removal Fluorometer Chlus	AH
19.06	Inspection visits stream dwindles	TL
20.06	Inst. GTs (no drone flights due to wind)	AH, BO
	Inst. PPK base station for drone flights	AH, BO
22.06	Flight around the hanging glacier, Griess Glacier Schächental	TL
27.06	Drilling of the ablation stakes Griess Glacier	AH, BO
	1. drone flight Griess Glacier (GG)	AH, BO
10.08	2. drone flight Griess Glacier (TP*)	AH
	Ablation stakes measurements Griess Glacier	AH
16.08	3. drone flight Griess Glacier	AH
	Ablation stakes measurements Griess Glacier	AH
02.09	Inspection visit Griess Glacier	AH, TL
03.09	Inspection visit, Stakes Griess Glacier	AH, TL
04.09	Tracer Kl-23-02 Ur Griess-Loch	AL
	Tracer Kl-23-03 Rh Griess Glacier Ice tunnel	AH, TL
	Tracer Kl-23-06 Rh Griess-See	AH, TL
	4. drone flight Griess Glacier	AH,
	Ablation stakes measurements Griess Glacier	TL
05.09	Removal p,T-datalogger Chlus-spring	AH, TL
	Tracer Kl-23-04 Ur Gämschplanggen-Bach	AH, TL
	Tracer Kl-23-05 Rh Mälchbödmeli-Bächli N	AH, TL
06.09	Removal fluorometer	TL, AM
07.09	Removal fluorometer	TL
	Removal Tikee3 camera Raustöckli	YW
27.09	Inst. of 5 fluorometer	TL
	Exchange p,T-Logger Waldhüttli	TL
	Tracer Kl-23-07 Ur Chammli-Griess Glacier	TL
	Tracer Kl-23-08 Rh Gämschplanggen-Bach	TL
	removal meteostation KLAU	TL
01.10	Ablation stakes measurements Griess Glacier	AH

	Removal ablation stakes Griess Glacier	AH
	5. drone flight Griess Glacier	AH
	removal fluorometer	
Explanations:	TP = technical issues	ML = Martin (Tinu) Lüthi (OGH, GIUZ) AH = Andrin Hauser (GIUZ) BO = Boris Ouvry (GIUZ) AL = Andreas (Res) Link (OGH) AM = Andreas Münger (OGH) YW = Yvo Weidmann (OGH)

Appendix 2: Chlus Spring in March 2023, when the water froze to an ice fall.

Appendix 3: Chlus cliff in March 2023

Appendix 4: p&T logger at Waldhüttli, with the creek emerging from underneath the rock. In fall, the water was flowing over the rock.

Appendix 5: p&T logger installed in the entrance of the Chlus cave in March 2023.

Appendix 6: Fluorometer placed at KL-WHQ during KL-23-01-CBP-Ur.

Appendix 7: Uranine injection at KL-CBP for KL-23-01-CBP-Ur.

Appendix 8: Tracer injection at Griessloch (KL-GLH) for KL-23-02-GLH-Ur (On the picture: Res Link, OGH)

Appendix 9: Tracer injection at KL-GTB for KL-23-03-Rh.

Appendix 10: Tracer injection at the shore of Griesssee for KL-23-06-GRS-Rh

Appendix 11: Ablation stakes drilled into the ice of Griess Glacier.

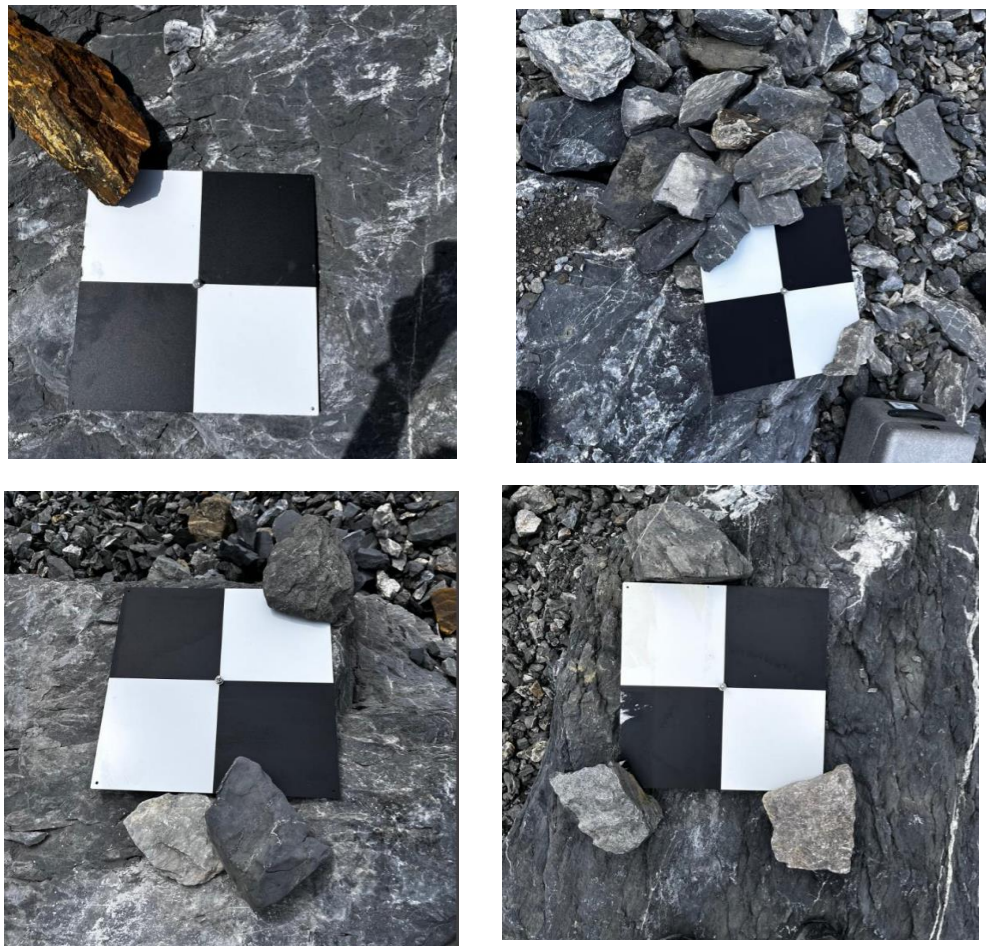

Appendix 12:GTs 2,3,4 and 5 installed on large boulders on Griess Glacier.

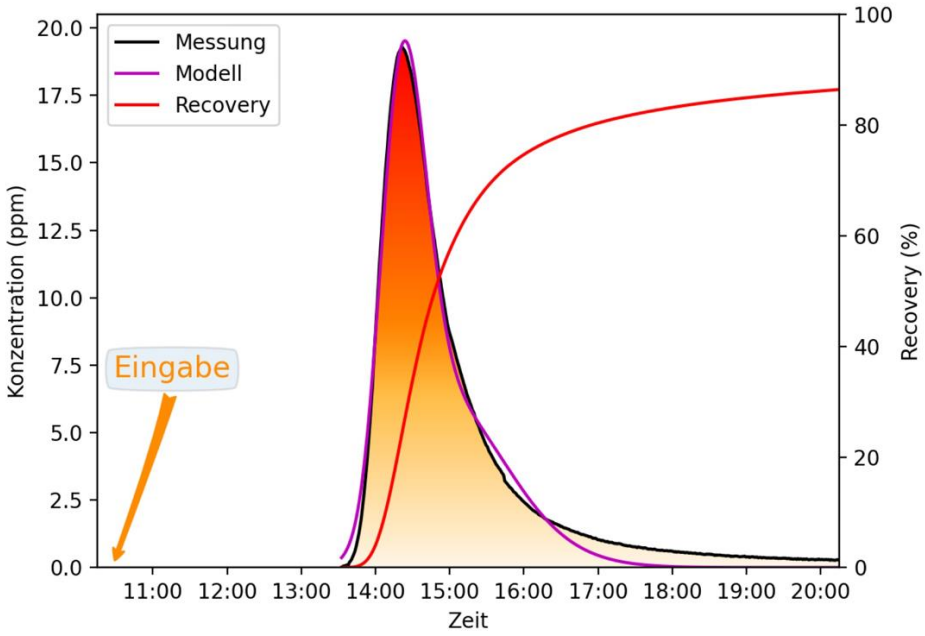

Appendix 13: Breakthrough curve of the Fluorometer at KL-CHH during KL-23-01-CBP-Ur.

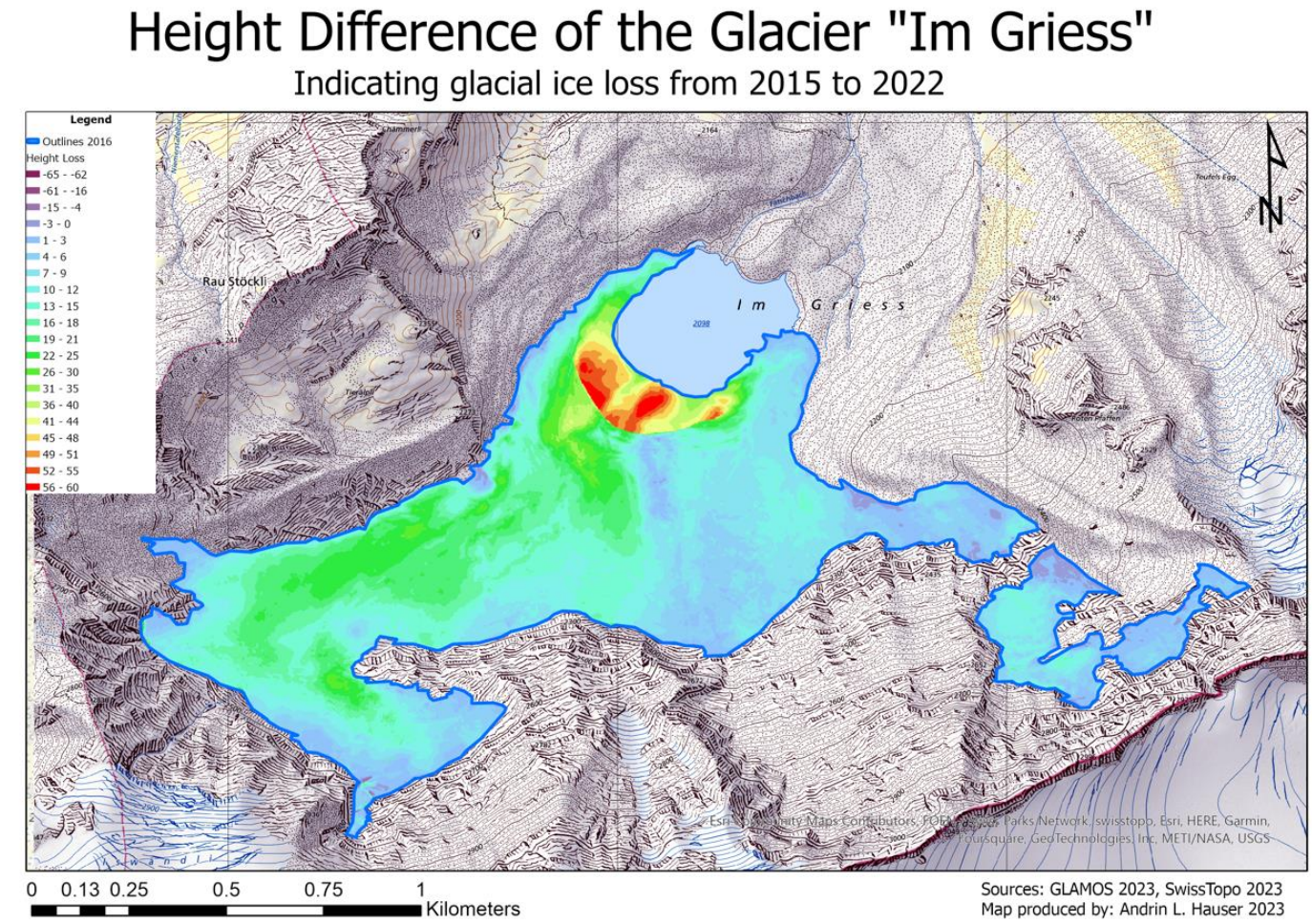

Appendix 14: DEM Differentiation between 2015 and 2022.

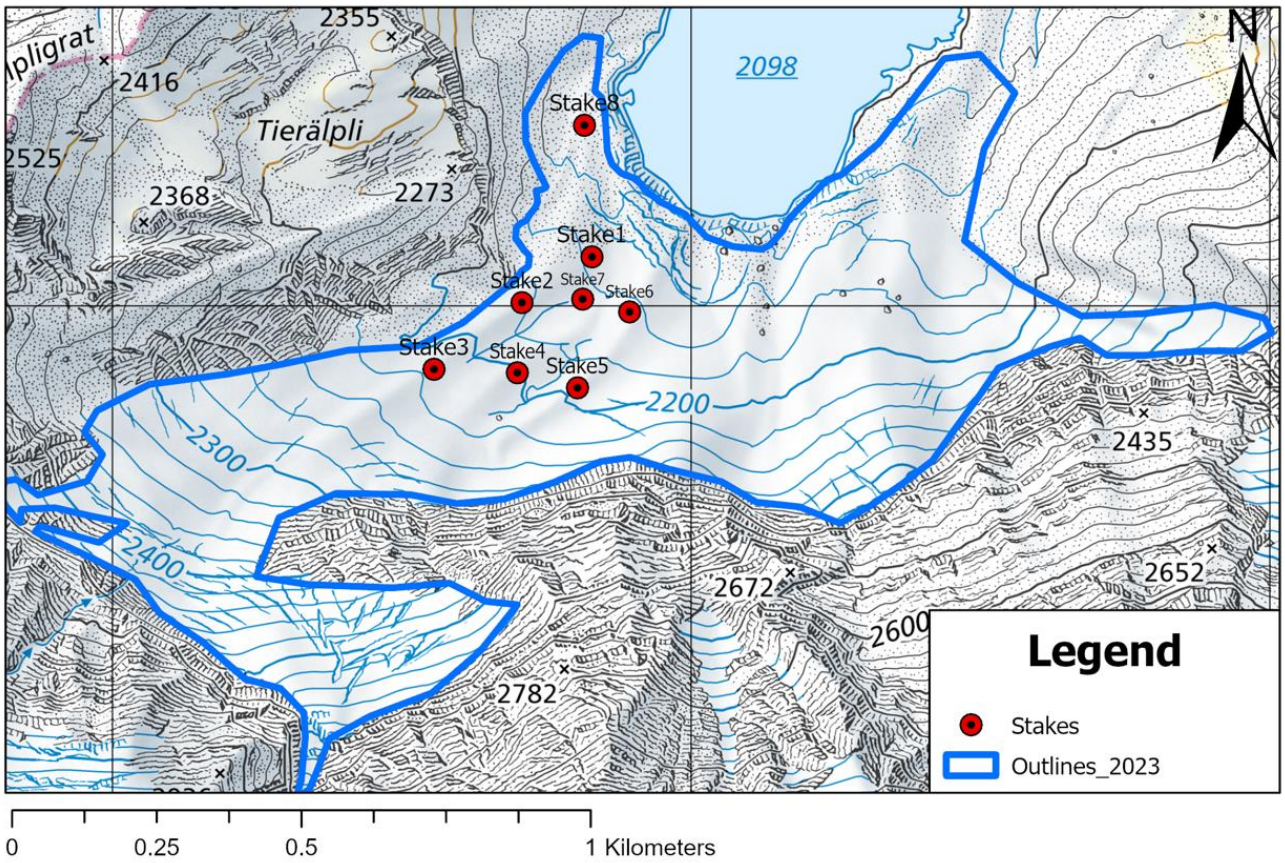

Appendix 15: Map of the ablation stake distribution on Griess Glacier.

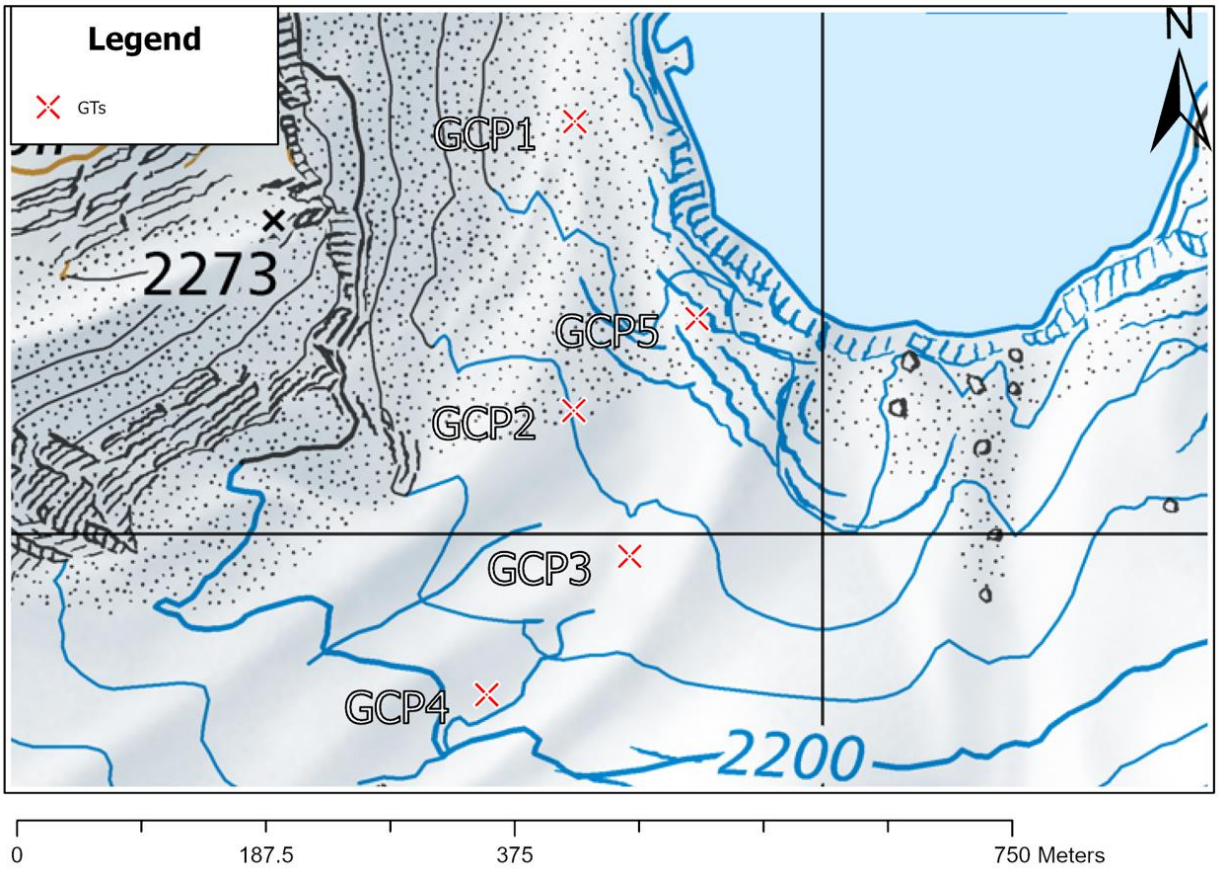

Appendix 16: Glacier-wide distribution of the five Ground Target Panels shown in Appendix 11.

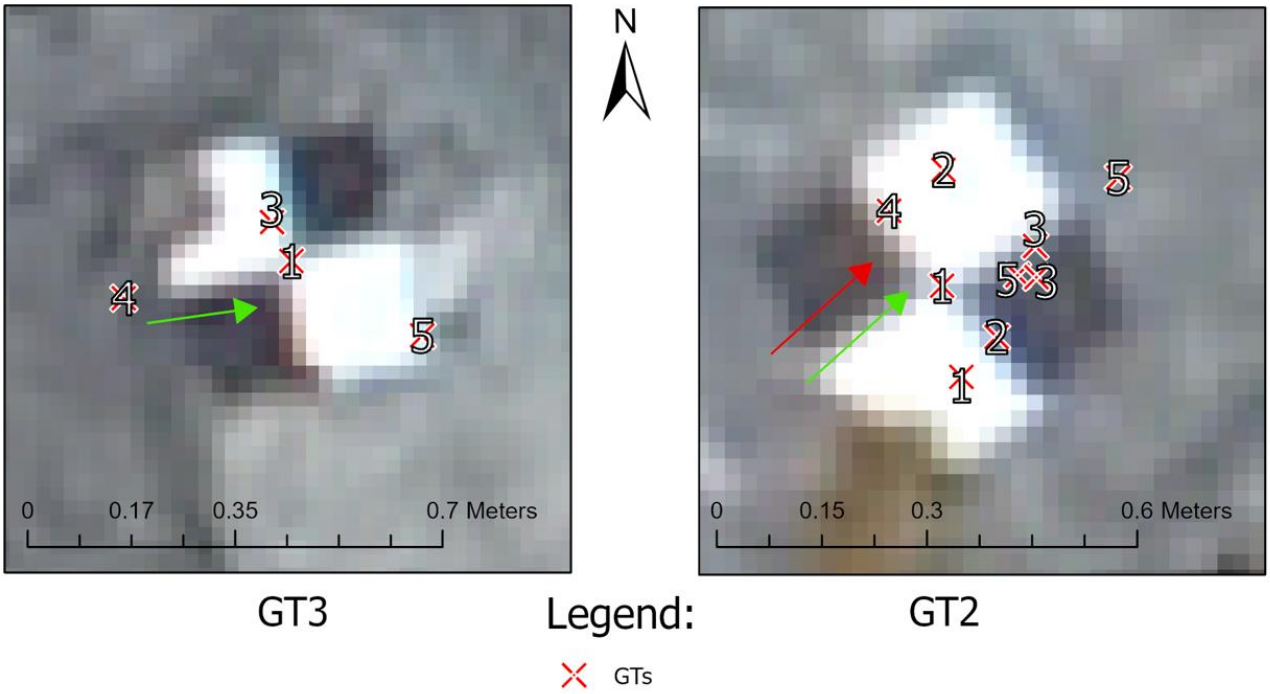

Appendix 17: Distribution and variation of the other two GTs assessed.

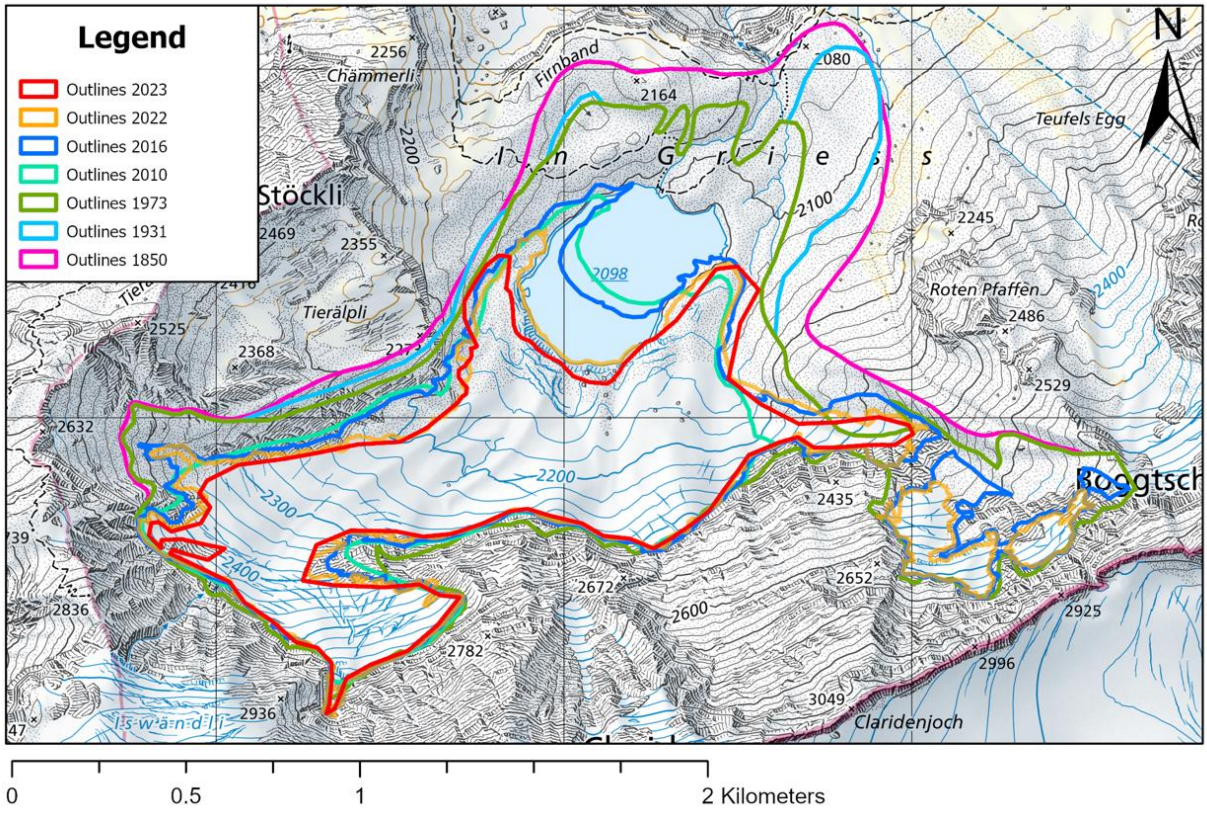

Appendix 18: Development of the glacier outlines over the past 170 years.

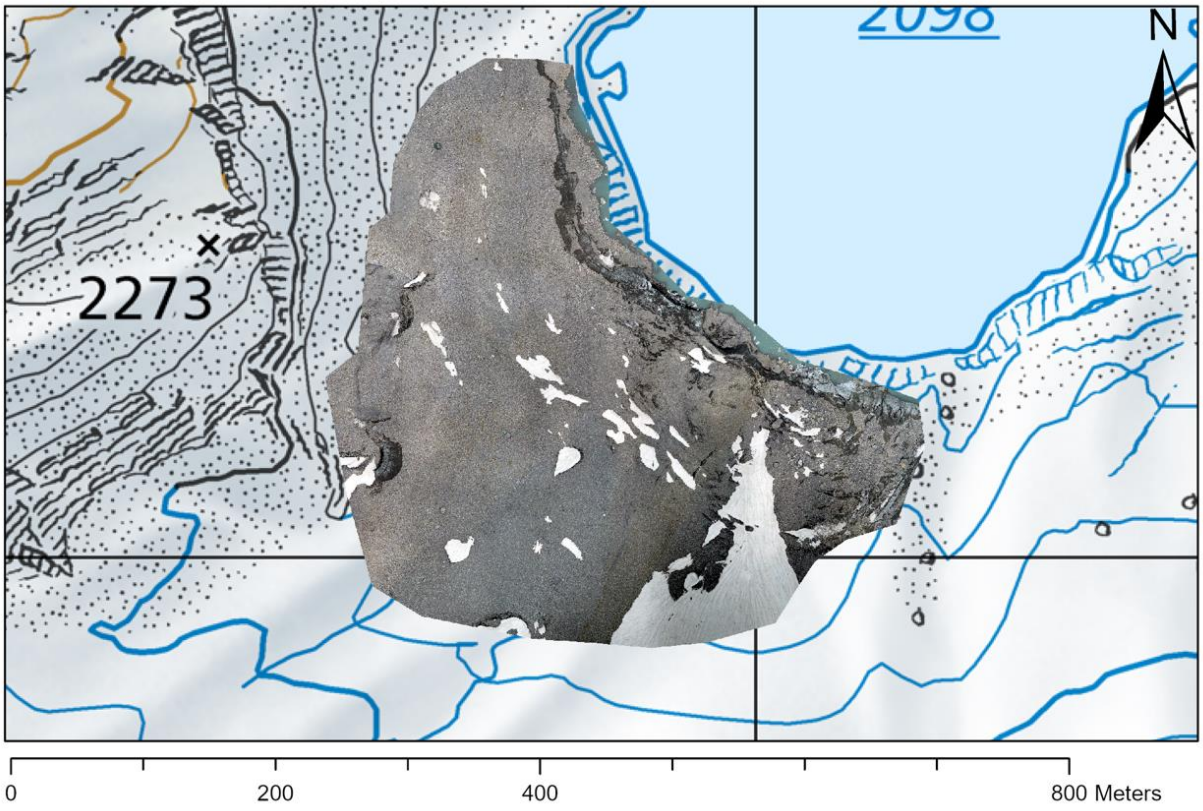

Appendix 19: Orto photo of the lower glacier part. This is the image taken on the first drone flight (Mission day1, flight 1)

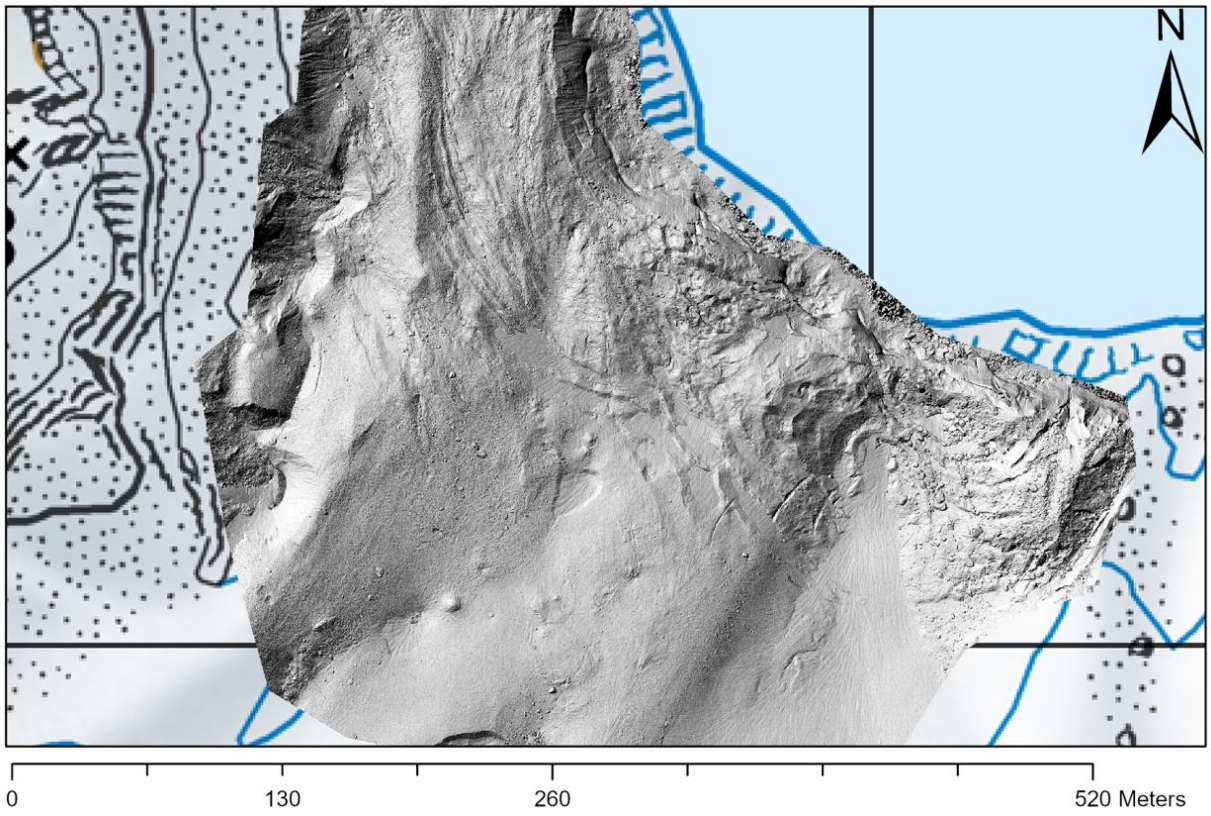

Appendix 20: Hillshade of mission day 1, flight 1

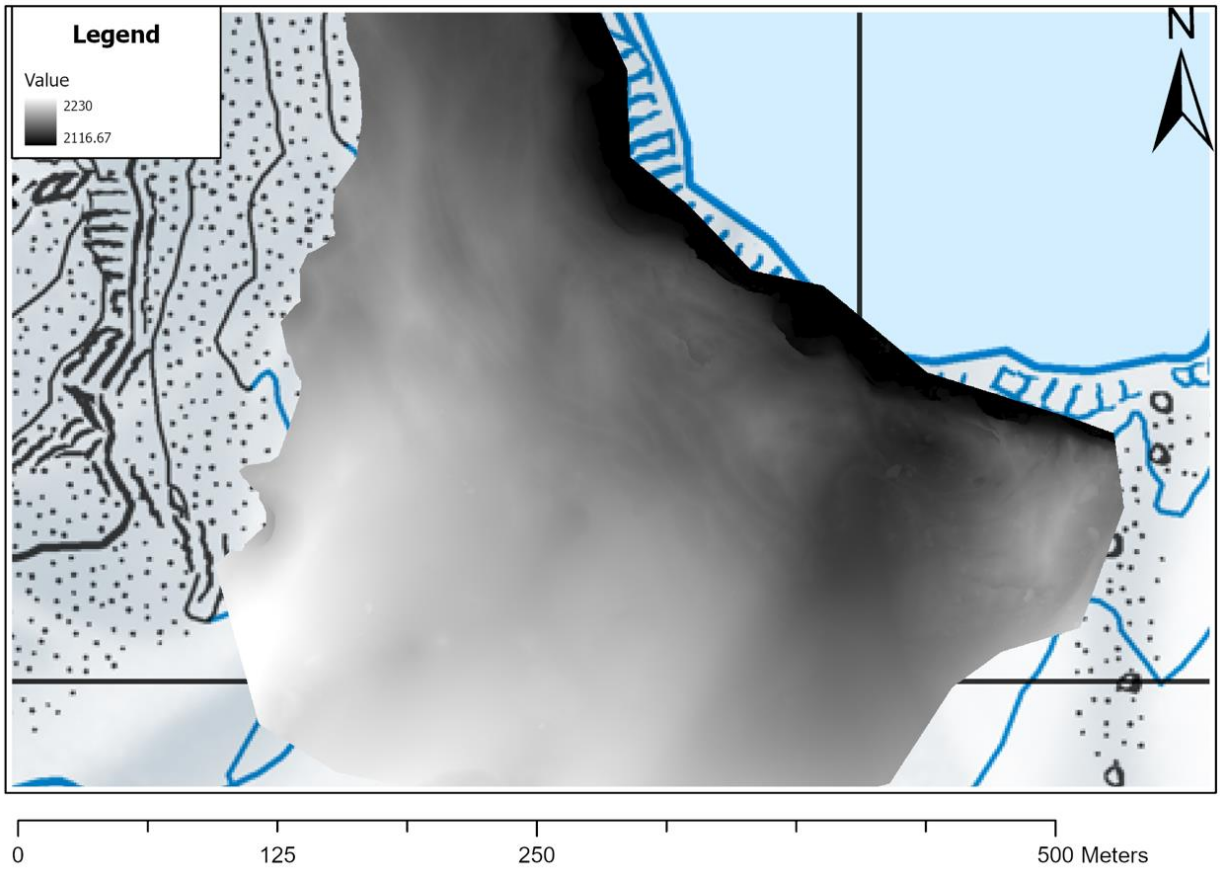

Appendix 21: DEM of mission day 1, flight 1.

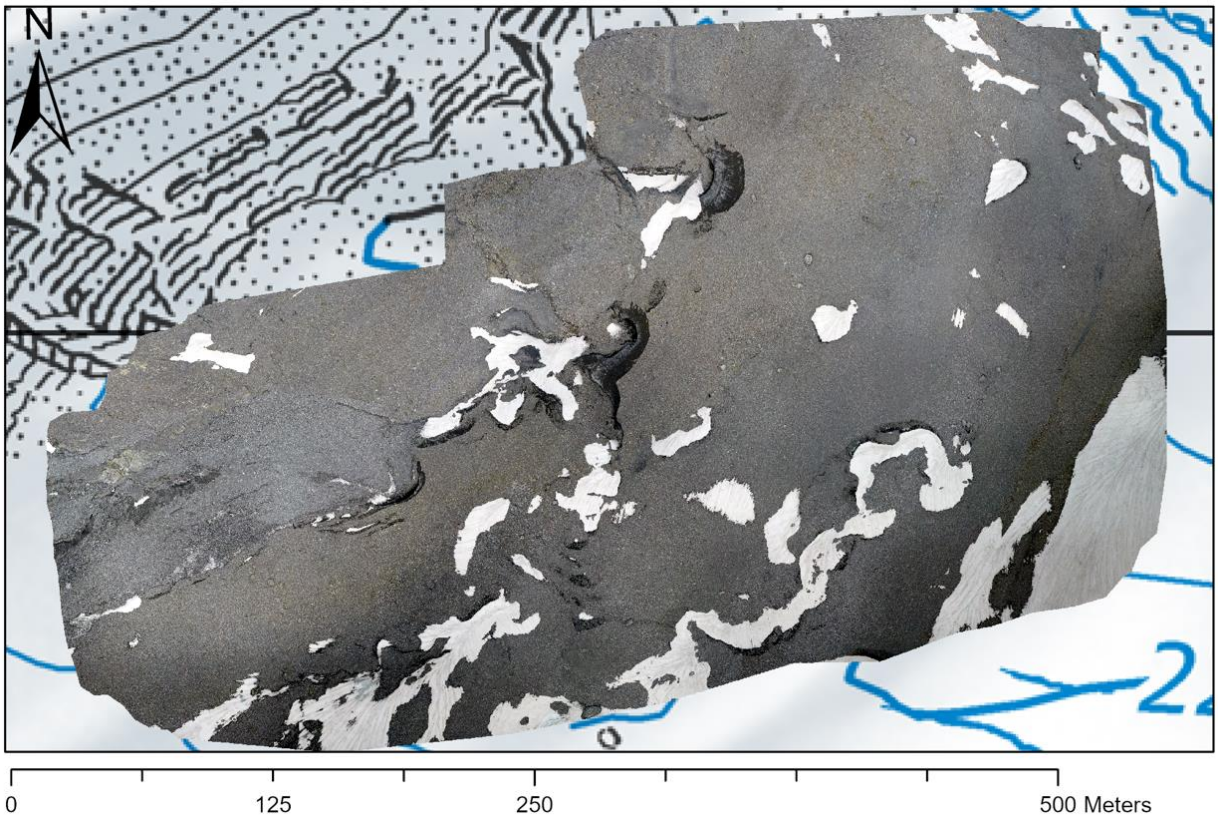

Appendix 22: Orto photo of the upper glacier perimeter, MD1, F3.

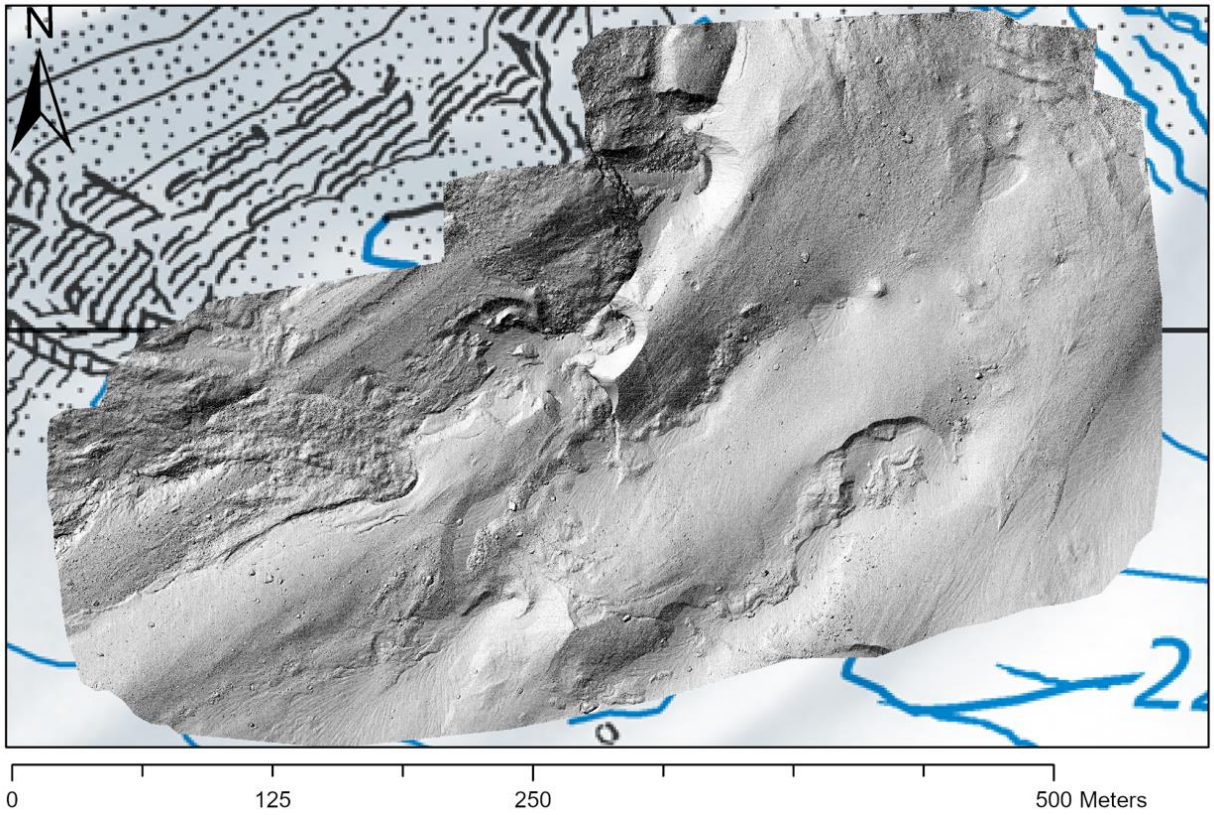

Appendix 23: Hillshade of mission day 1 flight 3.

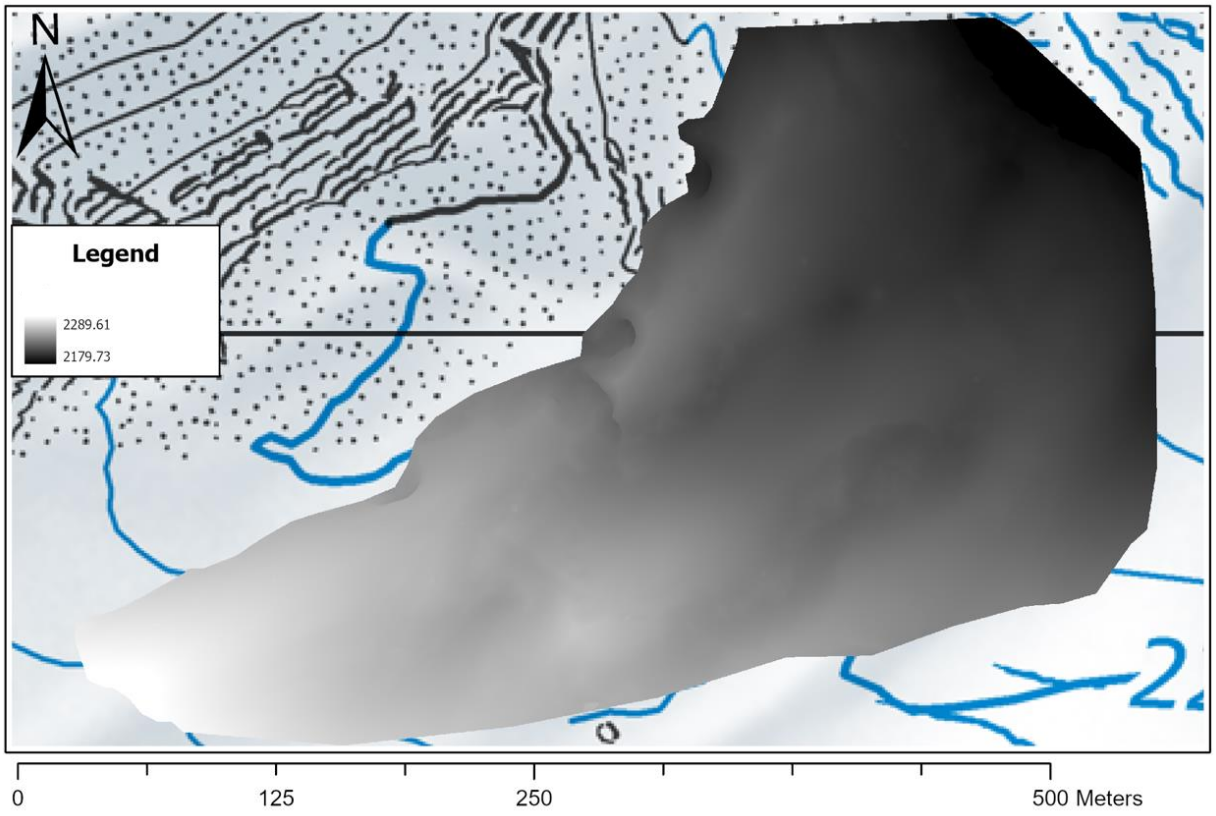

Appendix 24: DEM of the upper perimeter of mission day 1, flight 3.

For further data please contact the author, Andrin Hauser (andrinksz@gmail.com).

Available:

- DEM differencing of every mission day, step by step.
- Every DEM, Hillshade and Ortho photo produced

	TF	27.06-10.8	10.08-16.08	16.08-02.09	02.09-04.09	04.09-01.10
	Number of days	44	6	17	2	27
Stake 1	Melt in cm per TF	49.6	0	0	2.4	29.4
	Melt per day in cm	1.1272727	0	0	1.2	1.0888889
Stake 2	Melt in cm per TF	62.5	9.7	0	-0.4	28.3
	Melt per day in cm	1.4204545	1.6166667	0	-0.2	1.0481481
Stake 3	Melt in cm per TF	110.5	18.6	40.2	5.05	43.95
	Melt per day in cm	2.5113636	3.1	2.3647059	2.525	1.6277778
Stake 4	Melt in cm per TF	91.8	18.2	38.8	4.6	31
	Melt per day in cm	2.0863636	3.0333333	2.2823529	2.3	1.1481481
Stake 5	Melt in cm per TF	92.1		0	0.2	29.3
	Melt per day in cm	2.0931818	0	0	0.1	1.0851852
Stake 6	Melt in cm per TF	75.4	16.8	0	5.2	25.8
	Melt per day in cm	1.7136364	2.8	0	2.6	0.9555556
Stake 7	Melt in cm per TF	103.2		0	1.8	40.6
	Melt per day in cm	2.3454545	0	0	0.9	1.5037037
Stake 8	Melt in cm per TF	57.5	9.8	0	0	27.5
	Melt per day in cm	1.3068182	1.6333333	0	0	1.0185185

Appendix 25: Summarized ablation stake protocol, presenting the melt that happened at each ablation stake in the measurement period of 2023.

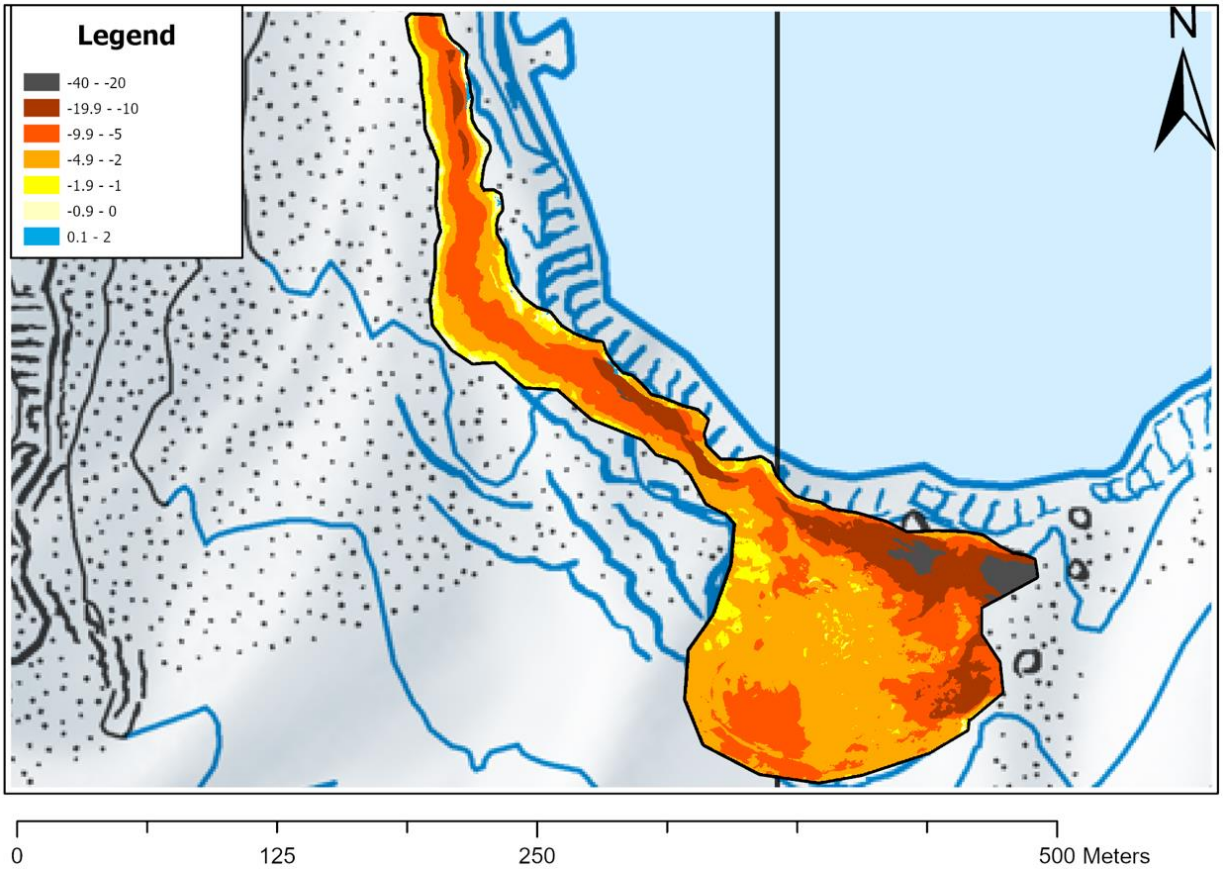

Appendix 27: Illustration of the ablation showing the isolated terminus area and the cliff front.

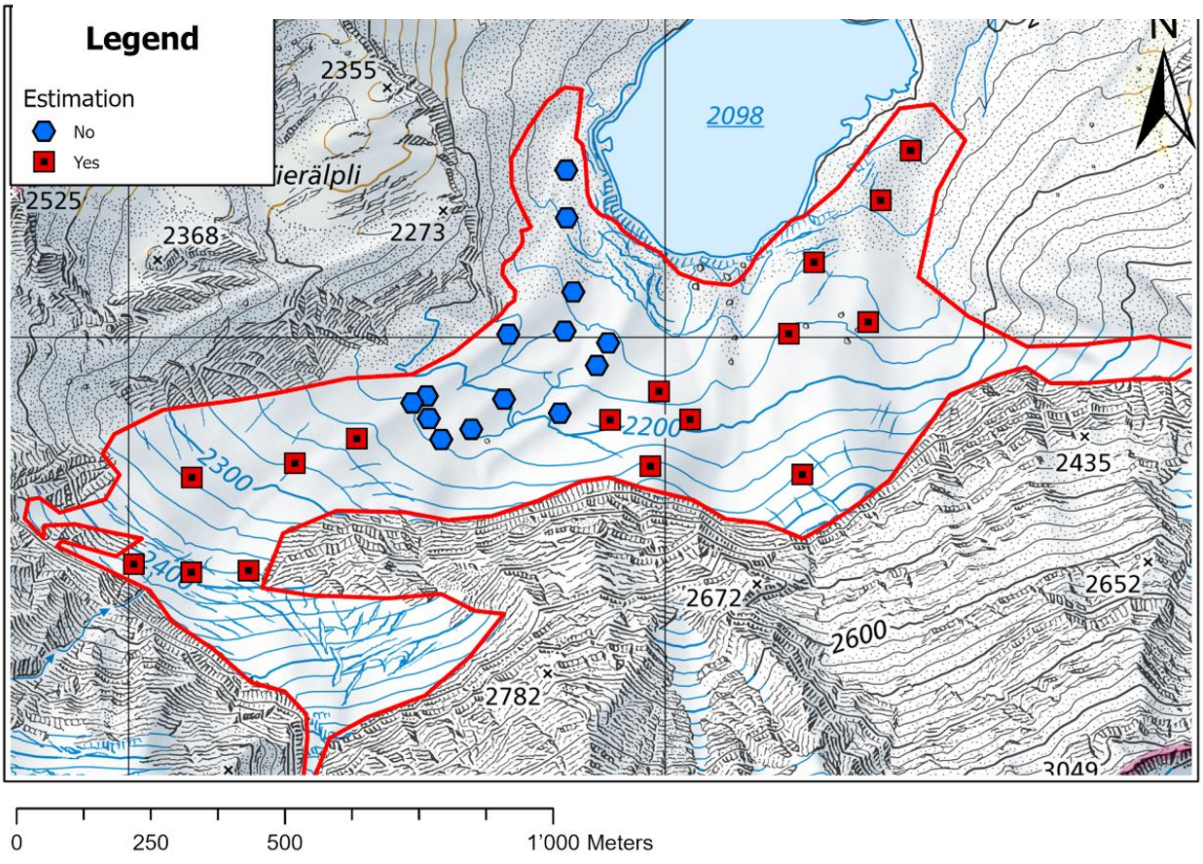

Appendix 26: Map showing the debris thickness measurements on Griess Glacier. The red squares are thickness estimation, as these locations were not sampled. From this data, the inter- and extrapolated debris cover thickness map was derived.

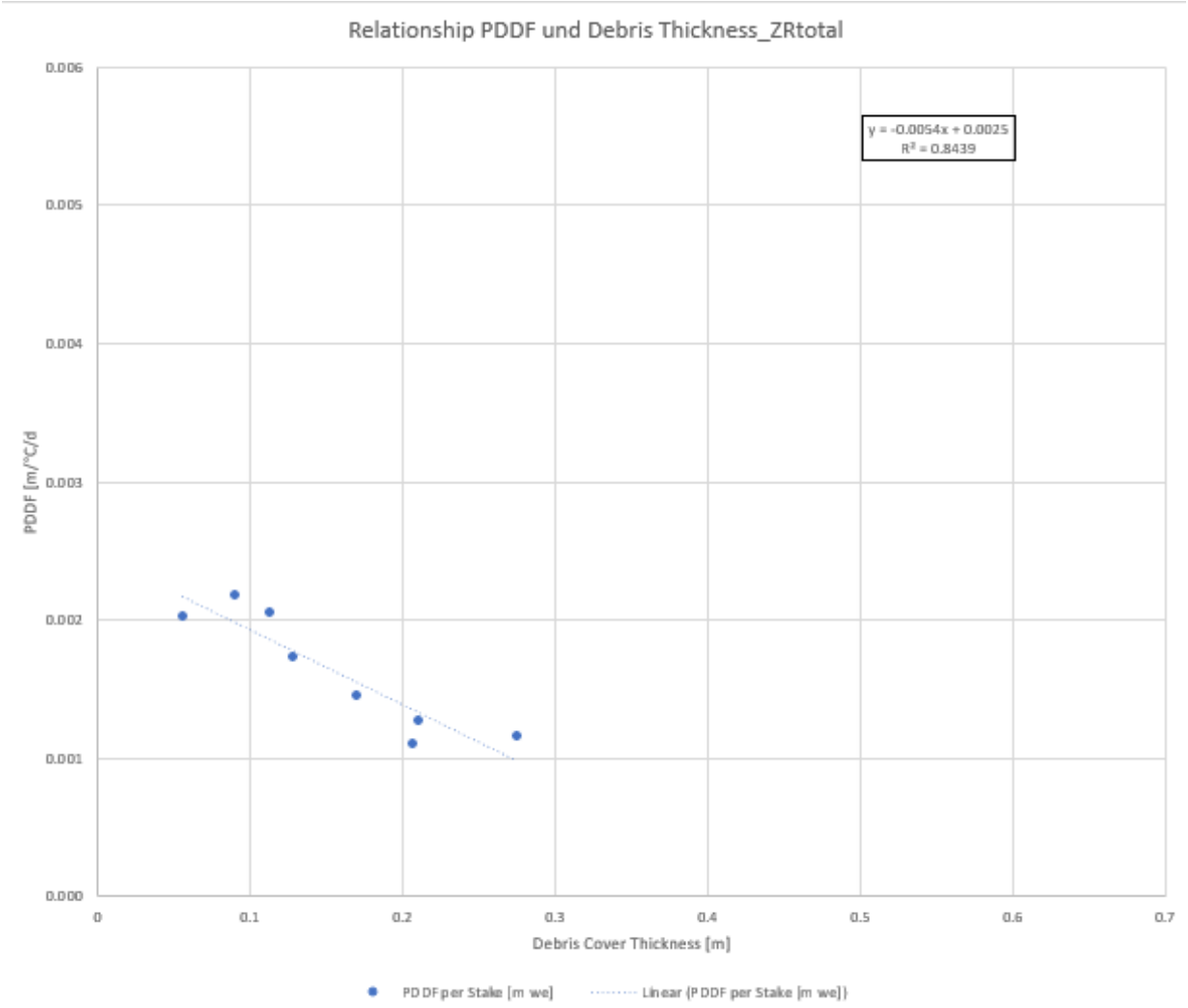

Appendix 28: Relationship of PDDF and debris cover thickness, illustrated with a linear regression line.

Personal declaration: I hereby declare that the submitted thesis is the result of my own, independent work. All external sources are explicitly acknowledged in the thesis.

Zug, 31.01.2024

Andrin Livio Hauser